University of Alberta

Interfacial Rheology at Oil-Water Interface

by

Emmanuel Kweku Ewusie

A thesis submitted to the Faculty of Graduate Studies and Research in partial fulfilment of the requirements for the degree of Master of Science

in

Chemical Engineering

Department of Chemical and Materials Engineering

Edmonton, Alberta
Spring 2005

Library and Archives Canada
Published Heritage Branch
395 Wellington Street
Ottawa ON K1A 0N4
Canada

Bibliothèque et Archives Canada
Direction du Patrimoine de l'édition
395, rue Wellington
Ottawa ON K1A 0N4
Canada

0-494-08052-3

Your file *Votre référence*
ISBN:
Our file *Notre reference*
ISBN:

NOTICE:
The author has granted a non-exclusive license allowing Library and Archives Canada to reproduce, publish, archive, preserve, conserve, communicate to the public by telecommunication or on the Internet, loan, distribute and sell theses worldwide, for commercial or non-commercial purposes, in microform, paper, electronic and/or any other formats.

The author retains copyright ownership and moral rights in this thesis. Neither the thesis nor substantial extracts from it may be printed or otherwise reproduced without the author's permission.

AVIS:
L'auteur a accordé une licence non exclusive permettant à la Bibliothèque et Archives Canada de reproduire, publier, archiver, sauvegarder, conserver, transmettre au public par télécommunication ou par l'Internet, prêter, distribuer et vendre des thèses partout dans le monde, à des fins commerciales ou autres, sur support microforme, papier, électronique et/ou autres formats.

L'auteur conserve la propriété du droit d'auteur et des droits moraux qui protège cette thèse. Ni la thèse ni des extraits substantiels de celle-ci ne doivent être imprimés ou autrement reproduits sans son autorisation.

In compliance with the Canadian Privacy Act some supporting forms may have been removed from this thesis.

While these forms may be included in the document page count, their removal does not represent any loss of content from the thesis.

Conformément à la loi canadienne sur la protection de la vie privée, quelques formulaires secondaires ont été enlevés de cette thèse.

Bien que ces formulaires aient inclus dans la pagination, il n'y aura aucun contenu manquant.

Canada

Dedication

I dedicate this work to my lovely mother and octogenarian grandmother as a way of paying homage to their tremendous effort in my upbringing. Mother, I appreciate inculcating in me self discipline and respect for one another.

I love you all.

Abstract

Surface rheology, using oscillating pendant drop technique, has been used to probe qualitatively and quantitatively the mechanical strength of interfacial films formed when a droplet of model oil (de-asphalted bitumen also known as DAB, asphaltene, and bitumen all diluted with toluene) is in the vicinity of pre-contacted water.

For three concentrations and four frequencies of the sinusoidal excitations on the interfacial area studied for each sample, it is concluded that: the complex dilatational modulus increases with ageing of interfacial film but decreases with increasing bulk concentration.

There is no detectable phase shift between sinusoidal area input and interfacial tension (IFT) response for de-asphalted bitumen. There is, however, obvious phase shift between sinusoidal area input and interfacial tension (IFT) response for asphaltenes and diluted bitumen within the linear viscoelastic regime.

Acknowledgement

My stay at the University of Alberta would not have been possible if not because of the following people and entities: my supervisors Dr. Jacob Masliyah and Dr. Anthony Yeung, NSERC Research Chair in Oilsand Engineering, Alberta Ingenuity Fund, and colleagues in the oilsand group. I feel obliged to show my gratitude to my supervisors, colleagues and the financial support by NSERC Research Chair in Oilsand Engineering and Alberta Ingenuity Fund.

I am specifically indebted to Dr. Jacob Masliyah and Dr. Anthony Yeung for their guidance in my research and humane qualities showed me throughout my stay with them. It was, indeed, gratifying being your student. I also want to thank Dr. Lichun Zhang, post doctorial fellow of Dr. Yeung, for her insights and help

Finally, with reverence, I want to thank the Most High for the wisdom and assistance given me to stand the test of time. May his name be praised worldwide.

Table of Contents

CHAPTER ONE 1

1. INTRODUCTION 1

1.1 OIL SANDS OF ALBERTA 1

1.2 SIGNIFICANCE OF HEAVY OIL AND BITUMEN 1

1.3 COMPOSITION OF BITUMEN 2

1.3.1 Composition Based on Solubility 2

1.3.2 Composition Based on Elemental Analysis and Chemical Structures 3

1.4 INTERFACIAL RHEOLOGY: ITS RELEVANCE TO FROTH TREATMENT 4

1.5 RESEARCH OBJECTIVES 7

1.6 EXPERIMENTAL PLAN 7

1.7 OUTLINE OF THESIS 8

CHAPTER TWO 9

2. LITERATURE REVIEW 9

2.1 INTRODUCTION 9

2.1.1 Different Techniques for Measuring Interfacial Tension 11

2.1.2 Derivation of Young – Laplace Equation from Energy Balance 13

2.2 INTERFACIAL DILATATIONAL RHEOLOGY 17

2.3 THE LUCASSEN -VAN DEN TEMPEL MODEL (LVDT) MODEL 19

2.4 PREVIOUS STUDIES ON INTERFACIAL RHEOLOGY OF ADSORBED MOLECULES AT OIL- WATER INTERFACES 27

CHAPTER THREE 35

3. METHODOLOGY 35

3.1 MATERIALS 35

3.2 ASPHALTENE AND DE-ASPHALTED BITUMEN (DAB) EXTRACTION 36

3.3 EXPERIMENTAL PROCEDURE 37

3.3.1 Calibration *37*

3.3.2 Interfacial Tension Measurement *39*

3.3.3 Order-of-Magnitude Estimates of Dimensionless Groups *42*

3.3.4 Linearity Test *43*

3.3.5 Interfacial Rheology Measurement *43*

4. RESULTS AND DISCUSSION 45

4.1 IDEAL SYSTEMS 45

4.2 DE-ASPHALTED BITUMEN (DAB) 49

4.3 ASPHALTENES 58

4.4 BITUMEN 70

5. CONCLUSIONS AND RECOMMENDATIONS 83

6. REFERENCES 85

7. APPENDIX A 98

7.1 DERIVATION OF YOUNG - LAPLACE EQUATION FROM FORCE BALANCE 98

8. APPENDIX B 102

8.1 DE-ASPHALTED BITUMEN (DAB) 102

8.1.1 Graphs of IFT Response to Sinusoidal Area Input for 1wt% DAB Solution 102

8.1.2 Graphs of IFT Response to Sinusoidal Area Input for 10wt% DAB Solution 107

8.1.3 Graphs of IFT Response to Sinusoidal Area Input for 30wt% DAB Solution 111

9. APPENDIX C 115

9.1 ASPHALTENES 115

9.1.1 Graphs of IFT Response to Sinusoidal Area Input for 1wt% Asphaltenes Solution 115

9.1.2 Graphs of IFT Response to Sinusoidal Area Input for 10wt% Asphaltenes Solution 119

9.1.3 Graphs of IFT Response to Sinusoidal Area Input for 20wt% Asphaltenes Solution 123

10. APPENDIX D 127

10.1 BITUMEN 127

10.1.1 Graphs of IFT Response to Sinusoidal Area Input for 5wt% Bitumen Solution 127

10.1.2 Graphs of IFT Response to Sinusoidal Area Input for 15wt% Bitumen Solution 131

10.1.3 Graphs of IFT Response to Sinusoidal Area Input for 30wt% Bitumen Solution 135

List of Tables

Table 1-1 Elemental Composition of Alberta Bitumens (weight percent of element; data from Speight, 1991) 3

Table 3-1 Measured IFT and their Literature Values 39

Table 4-1 Equilibrium IFT versus Concentration for DAB 52

Table 4-2 Equilibrium IFT versus Concentration for Asphaltene Solutions 61

Table 4-3 Equilibrium IFT versus Concentration for Bitumen Solutions 73

List of Figures

Figure 1-1 Schematic diagram of bitumen extraction plant (Yan et al, 1999) 5

Figure 2-1 Geometry of Small Piece of Interface 14

Figure 2-2 IFT Response to step increase in area of static drop ($\theta = 0$) 25

Figure 2-3 IFT Response to step increase in area of static drop ($\theta = 45^0$) 26

Figure 2-4 IFT Response to step increase in area of static drop ($0 < \theta < 45^0$) 27

Figure 3-1 Optical Glass Cell Assembly 41

Figure 3-2 Pictorial view of Pendant Drop Apparatus 41

Figure 4-1 IFT (solid line) versus Static Area (dash line) for Toluene/Water Interface 46

Figure 4-2 IFT (solid line) versus Static Area (dash line) for Heptane – Water Interface 46

Figure 4-3 IFT (solid line) versus Sinusoidal Area (dash line) for Toluene, Period 20s 47

Figure 4-4 IFT (solid line) versus Sinusoidal Area (dash line) for Toluene, Period 40s 47

Figure 4-5 IFT (solid line) versus Sinusoidal Area (dash line) for Toluene, Period 80s 48

Figure 4-6 IFT (solid line) versus Sinusoidal Area (dash line) for Toluene, Period 160s 48

Figure 4-7 IFT (continuous line) versus Static Area (dash line), 1wt% DAB Solution 50

Figure 4-8 IFT (continuous line) versus Static Area (dash line), 10wt% DAB Solution 51

Figure 4-9 IFT (continuous line) versus Static Area (dash line), 30wt% DAB Solution 51

Figure 4-10 IFT Response (continuous line) to Area Change (dash line), 10wt% DAB Solution, Period 80s (Age 1day) 53

Figure 4-11 Dilatational Elastic Modulus versus Frequency, 1wt% DAB Solution (Ages 1hr & 1Day); ◊ Elastic Modulus for 1hr; ■ Elastic Modulus for 1day ... 54

Figure 4-12 Dilatational Elastic Modulus versus Frequency, 10wt% DAB Solution (Ages 1hr & 1Day); ◊ Elastic Modulus for 1hr; ■ Elastic Modulus for 1day ... 55

Figure 4-13 Dilatational Elastic Modulus versus Frequency, 30wt% DAB Solution (Ages 1hr & 1Day); ◊ Elastic Modulus for 1hr; ■ Elastic Modulus for 1day ... 56

Figure 4-14 Dilatational Elastic Modulus for 1, 10, and 30wt% DAB Solution versus Frequency (Age 1hr); ◊ Elastic Modulus for 1wt%; □ Elastic Modulus for 10wt%; ▲ Elastic Modulus for 30wt% ... 57

Figure 4-15 Dilatational Elastic Modulus for 1, 10, and 30wt% DAB Solution versus Frequency (Age 1Day); ◊ Elastic Modulus for 1wt%; □ Elastic Modulus for 10wt%; ▲ Elastic Modulus for 30wt% ... 58

Figure 4-16 IFT (continuous line) versus Static Area (dash line) for 1wt% Asphaltene Solution ... 59

Figure 4-17 IFT (continuous line) versus Static Area (dash line) for 10wt% Asphaltene Solution ... 60

Figure 4-18 IFT (continuous line) versus Static Area (dash line) for 20wt% Asphaltene Solution ... 60

Figure 4-19 Skin Formation for 10wt% Asphaltene Solution (4hrs after drop formation) ... 61

Figure 4-20 Phase Angle between IFT (continuous line) Response to Sinusoidal Area Input (dash line), 20wt%Asphaltene Solution ... 62

Figure 4-21 Dilatational Modulus versus Frequency, 1wt% Asphaltene Solution (Ages 1hr & 1Day); ▲ Elastic Modulus for 1day; ◊ Elastic Modulus for 1hr; x Viscous Modulus for 1day; □ Viscous Modulus for 1hr ... 63

Figure 4-22 Dilatational Modulus versus Frequency, 10wt% Asphaltene Solution (Ages 1hr & 1Day); ▲ Elastic Modulus for 1day; ◊ Elastic Modulus for 1hr; x Viscous Modulus for 1day; □ Viscous Modulus for 1hr ... 64

Figure 4-23 Dilatational Modulus versus Frequency, 20wt% Asphaltene Solution (Ages 1hr & 1Day); ▲ Elastic Modulus for 1day; ◊ Elastic Modulus for 1hr; x Viscous Modulus for 1day; □ Viscous Modulus for 1hr ... 65

Figure 4-24 Dilatational Elastic Modulus for 1, 10, and 20wt% Asphaltene Solutions (Age 1hr); ◊ Elastic Modulus for 1wt%; □ Elastic Modulus for 10wt%; ▲ Elastic Modulus for 20wt% 67

Figure 4-25 Dilatational Viscous Modulus for 1, 10, and 20wt% Asphaltene Solutions (Age 1hr); ◊ Viscous Modulus for 1wt%; □ Viscous Modulus for 10wt%; ▲ Viscous Modulus for 20wt% 68

Figure 4-26 Dilatational Elastic Modulus for 1, 10, and 20wt% Asphaltene Solutions (Age 1Day); ◊ Elastic Modulus for 1wt%; □ Elastic Modulus for 10wt%; ▲ Elastic Modulus for 20wt% 69

Figure 4-27 Dilatational Viscous Modulus, for 1, 10, and 20wt% Asphaltene Solutions (Age 1Day); ◊ Viscous Modulus for 1wt%; □ Viscous Modulus for 10wt%; ▲ Viscous Modulus for 20wt% 70

Figure 4-28 Static IFT Response for 5wt% Bitumen Solution 71

Figure 4-29 Static IFT (continuous line) Response for 15wt% Bitumen Solution 72

Figure 4-30 Static IFT Response for 30wt% Bitumen Solution 72

Figure 4-31 IFT (continuous line) Response to Area Change (dash line), 30wt% Bitumen Solution, Period 40s 73

Figure 4-32 Dilatational Modulus versus Frequency, 5wt% Bitumen Solution (Ages 1hr & 1Day); ▲ Elastic Modulus for 1day; ◊ Elastic Modulus for 1hr; x Viscous Modulus for 1day; □ Viscous Modulus for 1hr 74

Figure 4-33 Dilatational Modulus versus Frequency, 15wt% Bitumen Solution (Ages 1hr & 1Day); ▲ Elastic Modulus for 1day; ◊ Elastic Modulus for 1hr; x Viscous Modulus for 1day; □ Viscous Modulus for 1hr 75

Figure 4-34 Dilatational Modulus versus Frequency, 30wt% Bitumen Solution (Ages 1hr & 1Day); ▲ Elastic Modulus for 1day; ◊ Elastic Modulus for 1hr; x Viscous Modulus for 1day; □ Viscous Modulus for 1hr 76

Figure 4-35 Dilatational Elastic Modulus for 1, 15, and 30wt% Bitumen Solutions versus Frequency (Age 1hr); ◊ Elastic Modulus for 5wt%; □ Elastic Modulus for 15wt%; ▲ Elastic Modulus for 30wt% 77

Figure 4-36 Dilatational Viscous Modulus for 1, 15, and 30wt% Bitumen Solutions versus Frequency (Age 1hr); ◊ Viscous Modulus for 5wt%; □ Viscous Modulus for 15wt%; ▲ Viscous Modulus for 30wt% 78

Figure 4-37 Dilatational Elastic Modulus for 1, 15, and 30wt% Bitumen Solutions versus Frequency (Age 1Day); ◊ Elastic Modulus for 5wt%; □ Elastic Modulus for 15wt%; ▲ Elastic Modulus for 30wt% 79

Figure 4-38 Dilatational Viscous Modulus for 1, 15, and 30wt% Bitumen Solutions versus Frequency (Age 1Day); ◊ Viscous Modulus for 5wt%; □ Viscous Modulus for 15wt%; ▲ Viscous Modulus for 30wt% 80

Figure 8-1 IFT (solid line) Response to Area Change (dash line), 1wt% DAB Solution, Period 20s (Age 1hr) 102

Figure 8-2 IFT Response to Area Change, 1wt% DAB Solution, Period 20s (Age 1Day) 103

Figure 8-3 IFT (solid line) Response to Area Change (dash line), 1wt% DAB Solution, Period 40s (Age 1hr) 103

Figure 8-4 IFT (solid line) Response to Area Change (dash line), 1wt% DAB Solution, Period 40s (Age 1Day) 104

Figure 8-5 IFT (solid line) Response to Area Change (dash line), 1wt% DAB Solution, Period 80s (Age 1hr) 104

Figure 8-6 IFT (solid line) Response to Area Change (dash line), 1wt% DAB Solution, Period 80s (Age 1Day) 105

Figure 8-7 IFT (solid line) Response to Area Change (dash line), 1wt% DAB Solution, Period 160s (Age 1hr) 105

Figure 8-8 IFT (solid line) Response to Area Change (dash line), 1wt% DAB Solution, Period 160s (Age 1Day) 106

Figure 8-9 IFT (solid line) Response to Area Change (dash line), 10wt% DAB Solution, Period 20s (Age 1Day) 107

Figure 8-10 IFT (solid line) Response to Area Change (dash line), 10wt% DAB Solution, Period 40s (Age 1hr) 108

Figure 8-11 IFT (solid line) Response to Area Change (dash line), 10wt% DAB Solution, Period 40s (Age 1Day) 108

Figure 8-12 IFT (solid line) Response to Area Change (dash line), 10wt% DAB Solution, Period 80s (Age 1hr) 109

Figure 8-13 IFT (solid line) Response to Area Change (dash line), 10wt% DAB Solution, Period 80s (Age 1Day) 109

Figure 8-14 IFT (solid line) Response to Area Change (dash line), 10wt% DAB Solution, Period 160s (Age 1hr) 110

Figure 8-15 IFT (solid line) Response to Area Change (dash line), 10wt% DAB Solution, Period 160s (Age 1Day) 110

Figure 8-16 IFT (solid line) Response to Area Change (dash line), 30wt% DAB Solution, Period 20s (Age 1hr) 111

Figure 8-17 IFT (solid line) Response to Area Change (dash line), 30wt% DAB Solution, Period 20s (Age 1Day) 111

Figure 8-18 IFT (solid line) Response to Area Change (dash line), 30wt% DAB Solution, Period 40s (Age 1hr) 112

Figure 8-19 IFT (solid line) Response to Area Change (dash line), 30wt% DAB Solution, Period 40s (Age 1Day) 112

Figure 8-20 IFT (solid line) Response to Area Change (dash line), 30wt% DAB Solution, Period 80s (Age 1hr) 113

Figure 8-21 IFT (solid line) Response to Area Change (dash line), 30wt% DAB Solution, Period 80s (Age 1Day) 113

Figure 8-22 IFT (solid line) Response to Area Change (dash line), 30wt% DAB Solution, Period 160s (Age 1hr) 114

Figure 8-23 IFT (solid line) Response to Area Change (dash line), 30wt% DAB Solution, Period 160s (Age 1Day) 114

Figure 9-1 IFT (solid line) Response to Area Change (dash line), 1wt% Asphaltene Solution, Period 20s (Age 1hr) 115

Figure 9-2 IFT (solid line) Response to Area Change (dash line), 1wt% Asphaltene Solution, Period 20s (Age 1Day) 115

Figure 9-3 IFT (solid line) Response to Area Change (dash line), 1wt% Asphaltene Solution, Period 40s (Age 1hr) 116

Figure 9-4 IFT (solid line) Response to Area Change (dash line), 1wt% Asphaltene Solution, Period 40s (Age 1Day) 116

Figure 9-5 IFT (solid line) Response to Area Change (dash line), 1wt% Asphaltene Solution, Period 80s (Age 1hr) 117

Figure 9-6 IFT (solid line) Response to Area Change (dash line), 1wt% Asphaltene Solution, Period 80s (Age 1Day) 117

Figure 9-7 IFT (solid line) Response to Area Change (dash line), 1wt% Asphaltene Solution, Period 160s (Age 1hr) 118

Figure 9-8 IFT (solid line) Response to Area Change (dash line), 1wt% Asphaltene Solution, Period 160s (Age 1Day) 118

Figure 9-9 IFT (solid line) Response to Area Change (dash line), 10wt% Asphaltene Solution, Period 20s (Age 1hr) 119

Figure 9-10 IFT (solid line) Response to Area Change (dash line), 10wt% Asphaltene Solution, Period 20s (Age 1Day) 119

Figure 9-11 IFT (solid line) Response to Area Change (dash line), 10wt% Asphaltene Solution, Period 40s (Age 1hr) 120

Figure 9-12 IFT (solid line) Response to Area Change (dash line), 10wt% Asphaltene Solution, Period 40s (Age 1Day) 120

Figure 9-13 IFT (solid line) Response to Area Change (dash line), 10wt% Asphaltene Solution, Period 80s (Age 1hr) 121

Figure 9-14 IFT (solid line) Response to Area Change (dash line), 10wt% Asphaltene Solution, Period 80s (Age 1Day) 121

Figure 9-15 IFT (solid line) Response to Area Change (dash line), 10wt% Asphaltene Solution, Period 160s (Age 1hr) 122

Figure 9-16 IFT (solid line) Response to Area Change (dash line), 10wt% Asphaltene Solution, Period 160s (Age 1Day) 122

Figure 9-17 IFT (solid line) Response to Area Change (dash line), 20wt% Asphaltene Solution, Period 20s (Age 1hr) 123

Figure 9-18 IFT (solid line) Response to Area Change (dash line), 20wt% Asphaltene Solution, Period 20s (Age 1Day) 123

Figure 9-19 IFT (solid line) Response to Area Change (dash line), 20wt% Asphaltene Solution, Period 40s (Age 1hr) 124

Figure 9-20 IFT (solid line) Response to Area Change (dash line), 20wt% Asphaltene Solution, Period 40s (Age 1Day) 124

Figure 9-21 IFT (solid line) Response to Area Change (dash line), 20wt% Asphaltene Solution, Period 80s (Age 1hr) 125

Figure 9-22 IFT (solid line) Response to Area Change (dash line), 20wt% Asphaltene Solution, Period 80s (Age 1Day) 125

Figure 9-23 IFT (solid line) Response to Area Change (dash line), 20wt% Asphaltene Solution, Period 160s (Age 1hr) 126

Figure 9-24 IFT (solid line) Response to Area Change (dash line), 20wt% Asphaltene Solution, Period 160s (Age 1Day) 126

Figure 10-1 IFT (solid line) Response to Area Change (dash line), 5wt% Bitumen Solution, Period 20s (Age 1hr) 127

Figure 10-2 IFT (solid line) Response to Area Change (dash line), 5wt% Bitumen Solution, Period 20s (Age 1Day) 127

Figure 10-3 IFT (solid line) Response to Area Change (dash line), 5wt% Bitumen Solution, Period 40s (Age 1hr) 128

Figure 10-4 IFT (solid line) Response to Area Change (dash line), 5wt% Bitumen Solution, Period 40s (Age 1Day) 128

Figure 10-5 IFT (solid line) Response to Area Change (dash line), 5wt% Bitumen Solution, Period 80s (Age 1hr) 129

Figure 10-6 IFT (solid line) Response to Area Change (dash line), 5wt% Bitumen Solution, Period 80s (Age 1Day) 129

Figure 10-7 IFT (solid line) Response to Area Change (dash line), 5wt% Bitumen Solution, Period 160s (Age 1hr) 130

Figure 10-8 IFT (solid line) Response to Area Change (dash line), 5wt% Bitumen Solution, Period 160s (Age 1Day) 130

Figure 10-9 IFT (solid line) Response to Area Change (dash line), 15wt% Bitumen Solution, Period 20s (Age 1hr) 131

Figure 10-10 IFT (solid line) Response to Area Change (dash line), 15wt% Bitumen Solution, Period 20s (Age 1Day) 131

Figure 10-11 IFT (solid line) Response to Area Change (dash line), 15wt% Bitumen Solution, Period 40s (Age 1hr) 132
Figure 10-12 IFT (solid line) Response to Area Change (dash line), 15wt% Bitumen Solution, Period 40s (Age 1Day) 132

Figure 10-13 IFT (solid line) Response to Area Change (dash line), 15wt% Bitumen Solution, Period 80s (Age 1hr) 133

Figure 10-14 IFT (solid line) Response to Area Change (dash line), 15wt% Bitumen Solution, Period 80s (Age 1Day) 133

Figure 10-15 IFT (solid line) Response to Area Change (dash line), 15wt% Bitumen Solution, Period 160s (Age 1hr) 134

Figure 10-16 IFT (solid line) Response to Area Change (dash line), 15wt% Bitumen Solution, Period 160s (Age 1Day) 134

Figure 10-17 IFT (solid line) Response to Area Change (dash line), 30wt% Bitumen Solution, Period 20s (Age 1hr) 135

Figure 10-18 IFT (solid line) Response to Area Change (dash line), 30wt% Bitumen Solution, Period 20s (Age 1Day) 135

Figure 10-19 IFT (solid line) Response to Area Change (dash line), 30wt% Bitumen Solution, Period 40s (Age 1hr) 136

Figure 10-20 IFT (solid line) Response to Area Change (dash line), 30wt% Bitumen Solution, Period 40s (Age 1Day) 136

Figure 10-21 IFT (solid line) Response to Area Change (dash line), 30wt% Bitumen Solution, Period 80s (Age 1hr) 137

Figure 10-22 IFT (solid line) Response to Area Change (dash line), 30wt% Bitumen Solution, Period 80s (Age 1Day) 137

Figure 10-23 IFT (solid line) Response to Area Change (dash line), 30wt% Bitumen Solution, Period 160s (Age 1hr) 138

Figure 10-24 IFT (solid line) Response to Area Change (dash line), 30wt% Bitumen Solution, Period 160s (Age 1Day) 138

Nomenclature

ΔP	Pressure across a curved interface	(N/m^2)
γ	Interfacial tension	(N/m)
R_1, R_2	Radii of curvature	(m)
π	Surface pressure	(N/m)
Ca	Capillary number	(-)
V_o	Superficial displacement velocity	(m/s)
μ	Dynamic viscosity	(Pa s)
L_1, L_2	Sides of curved interface	(m)
X_1, X_2, X_3	Normal to curved interfaces	(-)
$\delta\zeta$	Small displacement of curved interface	(-)
δA	Small area displacement	(m^2)
δV	Small volume displacement	(m^3)

J	Mean curvature	(m^{-1})
i	$\sqrt{-1}$	(-)
ε	Complex dilatational modulus	(N/m)
ω	Angular frequency	(rad/s)
ϕ	Phase angle	(-)
ΔA	Change in surface area	(m^2)
Ao	Unperturbed surface area	(m^2)
$\bar{\gamma}$	Isotropic interfacial tension	(N/m)
t	time	(s)
ε'	Elastic modulus	(N/m)
ε''	Viscous modulus	(N/m)
G(t)	Dilational relaxation function	(N/m)
G_∞	Static modulus	(N/m)

ξ	Coordinate	(-)
η_d	Surface dilatational viscosity	(-)
D	Diffusivity	(m^2/s)
C	Concentration	($kmol/m^3$)
Γ	Surface excess of surfactant molecules	(-)
BPD	Barrels per day	(-)
l_o	Characteristic length of oil drop	(m)
ρ	Density of oil	(kg/m^3)
Re	Reynolds number	(-)
We	Weber number	(-)

CHAPTER ONE

1. INTRODUCTION

1.1 Oil Sands of Alberta

The Alberta oil sands resource plays a vital role in the Canadian economy. The production potential of Alberta's three oil sands deposits (Athabasca, Cold Lake and Peace River) could be as high as 1.7 trillion barrels of bitumen, of which about 300 billion barrels are recoverable by current technology (Precht and Rokosh, 1998).

About 15% of Canadian oil consumption comes from the Athabasca oil sands (Czarnecki, 2001). Only 15% of Alberta's bitumen is known to be surface-mineable. Oil sands are unconsolidated sand deposits consisting of high molar mass, density and viscosity relative to conventional crude oil. It contains roughly 82 wt% of minerals, with bitumen and water forming the remaining 18 wt%. The ore is characterized as "rich," "moderate" or "lean," depending on the bitumen content. If the bitumen content is more than 10 wt%, the ore is characterized as rich; the ore is moderate if the bitumen content is between 6 to 10wt%, and lean when the bitumen content is less than 6 wt% (Takamura, 1985).

1.2 Significance of Heavy Oil and Bitumen

Industrial development in the 20th Century depended greatly on oil and gas. Nonetheless, reserves of conventional crude in the World are dwindling. Indeed, energy experts predict that crude oil supplies may eventually become exhausted

(Campbell and Laherrere, 1998; Brown, 2000). Large reserves of heavy oil and bitumen are expected to be the major energy source of the 21st Century. Large deposits of heavy oil and bitumen are found in Canada, USA, Russia and Venezuela. Its is believed that in the not-too-distant future, Canada's heavy oil sands production alone will exceed 1.2million BPD (Lanier, 1998); that would help alleviate, at least in part, the World's imminent energy crisis.

1.3 Composition of Bitumen

Bitumen composition varies from one location (i.e., ore body) to another. Nonetheless, some of the salient features common to all known bitumen types are discussed below.

1.3.1 Composition Based on Solubility

There are a number of ways to achieve bitumen separation (from the sand ore) based on their molecular weight and type. Based on their solubility in low molecular weight n-alkenes, bitumen is divided into two fractions: asphaltenes and de-asphalted bitumen (abbreviated as DAB from here on). Asphaltenes are defined as the toluene-soluble fraction that precipitates from solution when an excess of n-heptane (or n-pentane) is mixed with bitumen (25 to 40 times). The fraction of bitumen that is soluble in n-heptane is called de-asphalted bitumen (DAB). The DAB fraction consists of saturates, aromatics, and resins; they can be separated, for example, by column chromatography.

"Saturates, aromatics, resins and asphaltenes" (SARA) is another method of bitumen separation. Asphaltenes are first precipitated using n-pentane, followed by resin separation that is done with a single column containing ion-exchange resins and a clay – $FeCl_3$ packing. This is followed by a silica-gel column for separation of saturates and aromatics (Jewell et al., 1974). Saturates consists of saturated straight or branched chains without ring structure (paraffins), or with one or more rings attached (cycloparafins). Aromatics contain one or more aromatic hydrocarbon rings. Resins, also polar, is the second heaviest fraction in crude oils. Resins are most commonly defined as the fraction of bitumen that is soluble in light alkanes — such as pentane and heptane — but insoluble in liquid propane (Speight, 1991).

1.3.2 Composition Based on Elemental Analysis and Chemical Structures

Surprisingly, as shown in Table 1-1, the elemental composition of Alberta Bitumens varies only in a very narrow range:

Table 1-1 Elemental Composition of Alberta Bitumens (weight percent of element; data from Speight, 1991)

Bitumen	C	H	N	O	S
Syncrude	83.1	10.6	0.4	1.1	4.8
Suncor	83.9	10.5	0.4	1.0	4.2
Cold Lake	83.7	10.5	0.4	1.1	4.4

The complexity of bitumen makes it difficult, and sometimes impossible, to identify every compound. Heavy oil contains somw 100,000 different types of molecules (Wiehe and Liang, 1996). Structurally, the hydrocarbon fraction is made up of a few

well-defined homologous series. These series are identified as paraffins, naphthenes, aromatics and olefins (alkenes). Depending on the origin, varying proportions of these various homologous series are present in the bitumen. Hetero-aromatic groups are also present. These include sulphur compounds (H_2S, mercaptans, sulphides, disulphides, thiophenes, etc.), nitrogen compounds (basic and non-basic), oxygen compounds (phenols, ketones, carboxylic acids), and trace metals (most abundant metals include nickel, iron, and vanadium). These metals may be present as porphyrin metal complexes or may be associated with the polar groups in asphaltene (Gray, 1994).

1.4 Interfacial Rheology: Its Relevance to Froth Treatment

The following is a brief description of the *froth treatment* process: During the extraction of bitumen, as shown in Figure 1-1, the mined oilsand is sent to a digester where bitumen is separated from the sand grains and becomes aerated (i.e., the attachment of bitumen droplets to air bubbles in an aqueous environment). The produced slurry, containing water, aerated bitumen, and solids, is fed to settling vessels where the aerated bitumen rises to the top of the vessel to form a froth. The froth from the settling vessels, stream A, is far from ideal: it contains approximately 60% bitumen, 30% water, and 10% solids. To remove the remaining unwanted water and solids, the froth is first diluted with naphtha, heated and deaerated, and is sent (stream B) to inclined plate settlers and centrifuges to separate the water and nearly all solids from the diluted bitumen. Nevertheless, it has been reported that the bitumen leaving the last centrifuge bank at position C in Figure 1-1 still contains

about 2% water and about 0.4% solid particles. This water is in the form of emulsified water droplets that do not coalesce easily with each other. The water droplets forming the dispersed phase carry with them significant amounts of salts (in particular, chlorides) and fine solids. The chloride ions have been identified as the leading cause of equipment corrosion (which is, in turn, a serious safety issue), while the fine solids may lead to the fouling of catalysts used in upgrading and refining. It is therefore of paramount importance to control the amount of emulsified water allowed to be present in an oil stream that is to be fed into refining and upgrading units; the dewatering of such oil streams is known generally as "froth treatment."

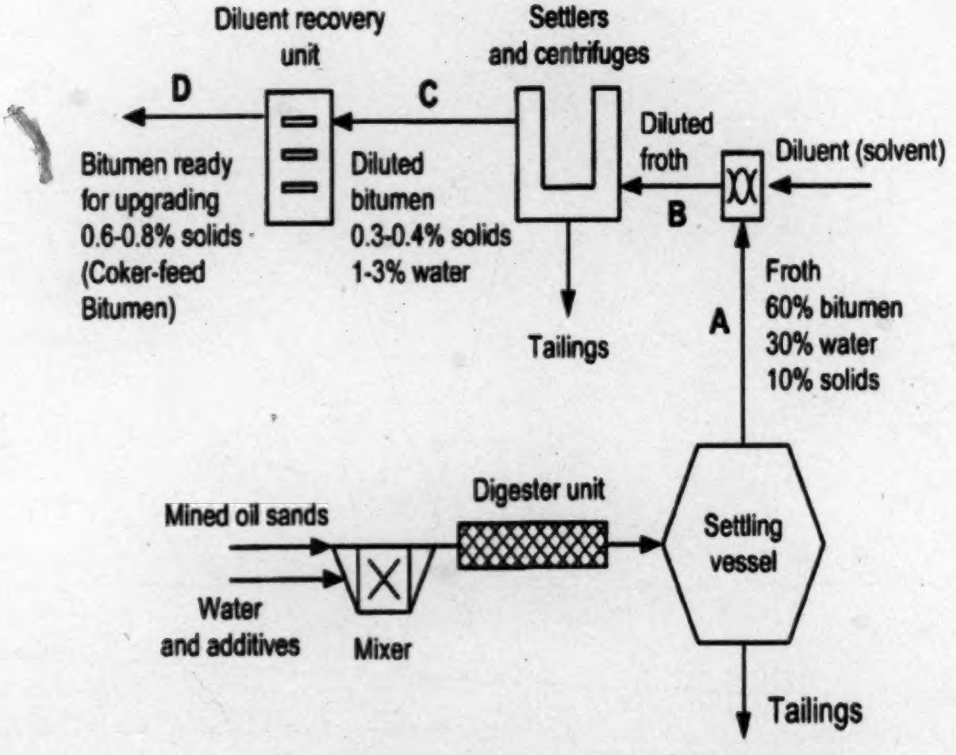

Figure 1-1 Schematic diagram of bitumen extraction plant (Yan et al, 1999)

It is imperative that water-in-oil emulsions be broken down so as to coalesce the dispersed water droplets and to remove the aqueous phase prior to any refining or upgrading. The question then arises as to how the various surface active components in bitumen create adsorbed layers at the oil-water interface, and how resistant are such surface layers to deformation. It is clear that, for coalescence to occur, the adsorbed layers at the water droplet surfaces — often only nanometres in thickness — must undergo considerable in-plane deformations. It follows that the *rheological properties* of the adsorbed layers (i.e., their deformation and flow behaviours in response to applied forces) must directly influence the stability of the water droplets. In order to better understand the rheological properties of the diluted bitumen-water interface, measurements of interfacial stresses in response to surface deformations must be performed. These measurements, as discussed above, are of particular relevance to froth treatment operations. There are, in general, two general classes of rheological properties:

- Dilational rheology: the area of the interface is distorted under applied tensions from all sides, but the shape remains constant. This is the property that is quantified in this study.
- Shear rheology: the interfacial material is distorted in shape, but the area remains constant.

1.5 Research Objectives

Interfacial rheological studies have been done on several diluted bitumen systems using different techniques. In this thesis, the following would be accomplished using the pendant drop technique:

1. Understand the rheological properties of oil-water interfaces. The oil phase consists of toluene as the solvent, with one the following bitumen components as the solute: (a) de-asphalted bitumen (DAB), (b) asphaltenes, and (c) "whole bitumen" (i.e., before separation of asphaltenes).
2. Investigate the effect of concentration and aging on the interfacial properties of de-asphalted bitumen, asphaltenes and bitumen.

In the subsequent sections, "DAB" is used to denote de-asphalted bitumen, and the "surfactants" are understood to be the indigenous surface-active components found in bitumen.

1.6 Experimental Plan

The primary aim is to subject each oil drop to sinusoidal oscillations in water and to ensure that each drop is sufficiently deformed by gravity (that is, not spherical) so that the Young-Laplace equation could be applied. Images of the oil drop during oscillation would be captured during each experimental run. At the end of each

experiment, the images would be analyzed by fitting each drop to the Young-Laplace equation to determine the interfacial tension as a function of time.

1.7 Outline of Thesis

Chapter One briefly summarizes the objectives of this thesis. The extensive research carried out on interfacial studies of crude oil and bitumen systems are reviewed in Chapter Two. Chapter Two also discusses the various techniques which are available for interfacial studies and gives insight into some of the theories used in surface rheology. In Chapter Three, the methodology and experimental set-up, DAB and asphaltenes extraction techniques are described. Chapter Four presents the results obtained from the experiments, their discussion and their implications. Conclusions and recommendations for further studies are presented in Chapter Five.

CHAPTER TWO

2. LITERATURE REVIEW

2.1 Introduction

The most fundamental physical property at any liquid-liquid interface is the interfacial tension (IFT). Interfacial tension is the reversible work needed to create a unit of interfacial area between two immiscible liquids. When surfactants are present at the interface, they build up a surface pressure π which lowers the interfacial tension. The surface pressure is directly related to the concentration of surfactants at the interface (much like pressure-volume relations for bulk fluids). There are two ways of varying the surface concentration of surfactants:

1. for the same surface area, the amount of surfactants is changed;
2. for the same amount of surfactants, the surface area is changed.

This thesis employs the second approach in changing the surface concentration of surfactants.

The pressure across a curved interface is related to the interfacial tension of that interface by the Young-Laplace equation (1805) according to:

$$\Delta P = \gamma\left(\frac{1}{R_1}+\frac{1}{R_2}\right) \qquad (2.1)$$

where ΔP is the pressure difference across a curved interface and γ is the interfacial tension. The parenthesis term refers to the mean curvature, with R_1 and R_2 being the radii of curvature in orthogonal directions (Adamson, 1976).

Researchers in the petroleum industry have long realized the importance of interfacial tension. The IFT between an oil and an aqueous phase plays a vital role in oil recovery where it is correlated to oil recovery efficiency by the capillary number, Ca, which is defined as

$$Ca = \frac{V_o \mu}{\gamma} \qquad (2.2)$$

Here, V_o is the superficial displacement velocity, μ is the viscosity of the aqueous phase, and γ is the interfacial tension between the oil and the aqueous phase (Taber, 1981). In fact, the capillary number is the critical displacement ratio and is a measure of the ratio of viscous forces to capillary forces.

Interfacial tension is also important in the separation of bitumen from oil sands. Currently, the most viable method of bitumen extraction from oil sands is the Clark hot water process. In this process, bitumen separation from oil sands is also affected by interfacial tension between all the major interfaces involved (solid/solution, bitumen/solution and air-gas/solution).

2.1.1 Different Techniques for Measuring Interfacial Tension

There are many methods of measuring interfacial tensions; these include, but not limited to: capillary rise, maximum bubble pressure, drop weight, Du Noüy ring, Wilhelmy plate, sessile drop, pendant drop and micropipette methods.

Depending on which method of measurement one chooses, the interfacial tension of a surfactant-laden fluid-fluid interface can be very different (Adamson, 1967; Yeung, 1998). Many of the aforementioned techniques have limitations which make them unsuitable for the current research work: certain methods capture only a "snapshot" of tension taken at one instant during a transient process (dynamic drop volume, maximum bubble pressure (Kloubek, 1972; Bendure, 1971; Mysels, 1986); some of the transient measurements, although capable of tracking the IFT over time, cannot subject the interface to oscillatory excitations (Du Noüy ring, Wilhelmy plate, and micropipette) which is a requirement in this study. For our purpose, the oscillating pendant drop technique for determining dynamic interfacial tension is most suitable. This technique spans a large range of time scales — from short times, pertinent for short-chain surfactants (e.g. sodium dodecyl sulfate above the critical micelle concentration; Iliev et al., 1992), to hours, as for surfactant mixtures containing dilute impurities (Mysels, 1986) or slowly unfolding proteins (Ward et al., 1980). Further, this technique is desirable as it requires only a few drops (several microlitres) of surfactant-laden samples and is capable of monitoring the transient tension in real-time. Most importantly, the surfactant-laden interface can be subjected to oscillations; this is a limitation to many other techniques. In the

oscillating pendant drop method, a small liquid drop is grown from a capillary tip into a second immiscible fluid. The drop is made large enough that it is well distorted to obtain the Laplacian shape for the Young-Laplace equation to apply. It is the allure of surfactant-laden interfacial excitation, applicability to a wide range of time scales, along with small sample volumes that gives the pendant drop technique powerful appeal for this study.

2.1.2 Derivation of Young – Laplace Equation from Energy Balance

Consider a small piece of interface, curved and with sides L_1 and L_2 as shown in figure 2-1. X_3 is normal to the surface. In general, a curved surface requires two radii to specify its curvature: R_1 and R_2

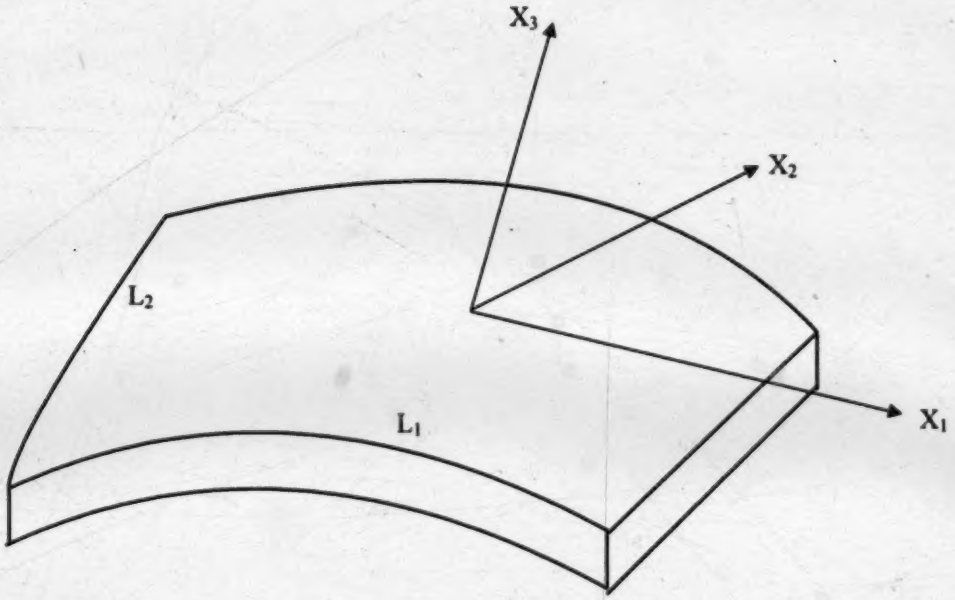

Side views

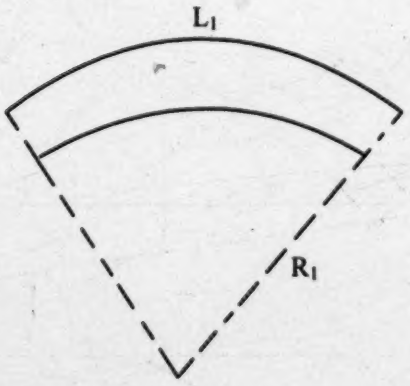

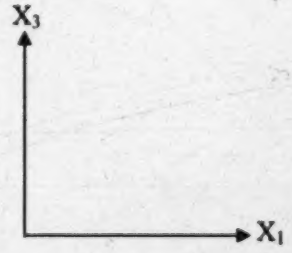

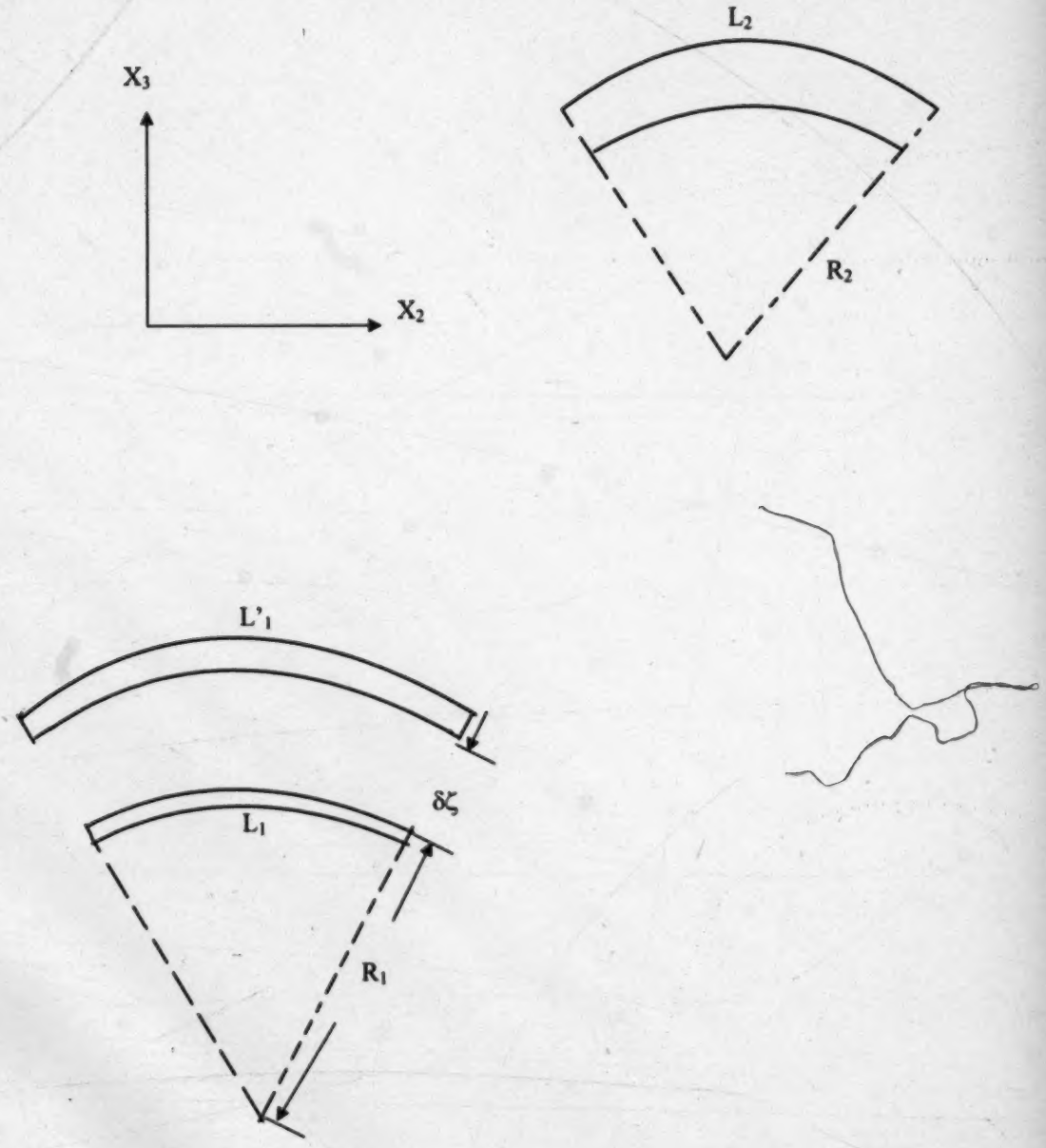

Figure 2-1 Geometry of Small Piece of Interface

Now let surface extend outward in X_3 direction by a small amount $\delta\zeta$, then

$$L_1 \rightarrow L_1'; \quad L_2 \rightarrow L_2' \tag{2.3}$$

Increase in area: $\delta A = L_1' L_2' - L_1 L_2$ (2.4)

Increase in volume: $\delta V = L_1 L_2 \times \delta\zeta$ (2.5)

Now, $$\frac{L_1}{R_1} = \frac{L_1'}{R_1 + \delta\zeta} \tag{2.6}$$

$$\Rightarrow \qquad L_1' = \left(1 + \frac{\delta\zeta}{R_1}\right) L_1 \tag{2.7}$$

Similarly, $$L_2' = \left(1 + \frac{\delta\zeta}{R_2}\right) L_2 \tag{2.8}$$

From equations 2.7 and 2.8,

$$L_1' L_2' = \left[1 + \left(\frac{1}{R_1} + \frac{1}{R_2}\right)\delta\zeta + \frac{\delta\zeta^2}{R_1 R_2}\right] L_1 L_2 \tag{2.9}$$

Assuming $\delta\zeta$ is small, $\Rightarrow \quad \delta\zeta^2 \approx 0$

Equation 2.9 becomes

$$L_1'L' - L_1L_2 = \left(\frac{1}{R_1} + \frac{1}{R_2}\right) L_1L_2 \times \delta\zeta \qquad (2.10)$$

Inserting equations 2.4 and 2.5 into 2.10 gives

$$\delta A = J \times \delta V \qquad (2.11)$$

Where $J = \frac{1}{R_1} + \frac{1}{R_2}$ is the "mean curvature" (2.12)

Now, work to change volume = work to create new surface

$$\Rightarrow \quad \Delta P \times \delta V = \gamma \times \delta A \qquad (2.13)$$

Where, ΔP is the change in pressure across the interface and γ is the interfacial tension.

From equation 2.11,

$$\Delta P \times \delta V = \gamma \times J \times \delta V \qquad (2.14)$$

$$\Rightarrow \quad \Delta P = \gamma \times J \qquad (2.15)$$

Equation 2.15 is called the Young-Laplace equation.

2.2 Interfacial Dilatational Rheology

Apart from interfacial tension (IFT), which is the most important property in the study of fluid-fluid interfaces, other higher order surface properties include interfacial viscosities (Plateau, 1869; Boussinesq, 1913) and interfacial elasticities (Evans and Skalak, 1980; Edwards et al., 1991). One dilatational rheological property of importance to this study is the complex interfacial dilatational modulus, $\varepsilon(\omega)$, which is defined as the proportionality factor between a periodically applied strain and the resulting dynamic tension:

$$\bar{\gamma} e^{i(\omega t+\phi(\omega))} = \varepsilon(\omega)\frac{\Delta A}{A_0} e^{i\omega t} \qquad (2.16)$$

Here, ΔA is the amplitude of interfacial area change, A_0 is the unperturbed oil-drop interfacial area, ω is the angular frequency, and ϕ is the phase angle difference between the applied strain and the resulting tension. The isotropic interfacial tension, $\bar{\gamma}$, is distinguished from the thermodynamic interfacial tension, γ, in that it may generally include non-equilibrium contributions [i.e. diffusion and viscous dissipation, (Edwards et al., 1991)]. The dilational modulus, as can be seen, is in general a complex quantity. As the drop area oscillates periodically, the interfacial dilatational modulus exhibits its two components: an elastic part that accounts for the recoverable energy stored in the interface (storage modulus ε'), and a viscous part that accounts for energy loss through relaxation process (loss modulus ε''). The

interfacial storage and loss moduli are respectively the real and imaginary parts of the interfacial dilatational modulus:

$$\varepsilon = \varepsilon' + i\varepsilon'' \tag{2.17}$$

As a drop oscillates sinusoidally at a given frequency ω, ε' and ε'' can independently be determined by equations (2.18) and (2.19) according to Tschoegl (1989):

$$\varepsilon' = \frac{\Delta\bar{\gamma}}{\Delta A / A_o}\cos\phi \tag{2.18}$$

$$\varepsilon'' = \frac{\Delta\bar{\gamma}}{\Delta A / A_o}\sin\phi \tag{2.19}$$

where $\Delta\bar{\gamma}$ is the amplitude of periodic interfacial-stress variation, ΔA is the amplitude of periodic interfacial area variation, A_0 is the unperturbed interfacial area of the oil drop, and ϕ is the phase angle between the stress and strain curves.

The other rheological property is the dilatational relaxation function, $G(t)$, which is the time dependent IFT in response to a sudden strain, of unit magnitude, that is applied to a static drop (i.e., a step excitation). The dilatational relaxation function $G(t)$ is related to the complex dilatational modulus, $\varepsilon(\omega)$ through Fourier sine and cosine transforms. The relaxation function is given by equation (2.20):

$$G(t) = \frac{\Delta\bar{\gamma}(t)}{\Delta A / A_0} \tag{2.20}$$

where $\Delta\bar{\gamma}$ is the difference between the static tension prior to interfacial deformation and the measured isotropic interfacial stress. The relations between $G(t)$ and $\varepsilon(\omega)$ are

$$\varepsilon'(\omega) = G_\infty + \omega \int_0^\infty [G(t) - G_\infty] \sin \omega t \, dt \tag{2.21}$$

$$\varepsilon''(\omega) = \omega \int_0^\infty [G(t) - G_\infty] \cos \omega t \, dt \tag{2.22}$$

where G_∞ is the static modulus (zero frequency response) or the Gibbs elasticity of irreversibly adsorbed species (Morrison, 2001; Tschoegl, 1989).

2.3 The Lucassen -van den Tempel Model (LVDT) Model

If values of the surface dilatational modulus were known as a function of frequency, predictions can be made about the importance of the Marangoni effect for a given system.[1] The modulus (combined with liquid densities, viscosities, and characteristic rate of deformation) determines the propensity of the interface to create surface tension gradients, as well as the rate at which such gradients disappear once the system is left to itself (Lucassen et al. 1972).

[1] Marangoni effect is the retardation of thin film drainage by induced tension gradients; this, in turn, creates resistance to droplet coalescence.

The response of a surface to sinusoidal area variations, for solutions containing surface-active materials, is described by a surface dilatational modulus:

$$\varepsilon = \frac{d\gamma}{d\ln A} \tag{2.23}$$

where γ is the surface tension and A is the surface area of the liquid drop. The modulus ε in (2.23) is in general a complex number. In the trivial case of a clean interface that is devoid of surfactants, the IFT must remain invariant to area perturbations; the resulting modulus ε is therefore zero. With surfactants at the interface, the dynamics of adsorption/desorption can give rise to a modulus that can be frequency-dependent. In this section, we describe the Lucassen-van den Tempel — or "LVDT" — model (1972) which considers reversible adsorption/desorption of surfactants at a liquid-liquid interface. The energy barrier of adsorption/desorption is assumed negligible, and the dynamics of the process is consequently governed by the mass transport (i.e., diffusion) of surfactants in the bulk liquids. With the assumption of homogeneous deformation (i.e., uniform area dilation), it is the total surface area of the interface — and not its shape — that is important. The analysis of interfacial dynamics is therefore more conveniently carried out in the simple case of a flat liquid surface confined between movable barriers (as in a Langmuir trough situation); the results from this analysis can be carried over directly to pendant drop experiments. For the case of uniform area deformation, a coordinate ξ is introduced to describe the displacement of a material point in the plane of the surface from its

position at rest. The x-direction is in the surface, perpendicular to the barrier — where $x = 0$ — and the opposite wall is located at $x = L$. If the barrier oscillates back and forth at an angular frequency ω and amplitude ξ_B, we have:

$$\xi = \xi_B \frac{L - x}{L} e^{i\omega t} \tag{2.24}$$

The corresponding relative change in area of a surface element is:

$$\frac{\Delta A}{A} = \frac{\partial \xi}{\partial x} = \frac{-\xi_B}{L} e^{i\omega t} \tag{2.25}$$

If the applied area and surface tension are of sufficiently small amplitudes, then combining equations (2.23) and (2.25) would yield

$$\varepsilon = \frac{\Delta \gamma}{\Delta A / A} = \frac{L \cdot \Delta \gamma}{\xi_B} \tag{2.26}$$

If the surface behaviour were perfectly elastic, no relaxation process (tending to reduce deviations of the surface tension from its equilibrium value) will occur at a characteristic time comparable to the time scale of the experiment, and the excitation and response signals are in phase. However, when such relaxation process plays a role, the surface is said to show viscoelastic behaviour. In this case, phase

differences occur between the surface tension variation and the area variation, which can formally be accounted for by introducing a complex modulus:

$$\varepsilon = |\varepsilon| e^{i\theta} = |\varepsilon| \cos\theta + i|\varepsilon| \sin\theta \tag{2.27}$$

The imaginary part of this quantity accounts for energy-dissipation processes. Its contribution can be expressed in terms of a surface dilational viscosity η_d given by

$$\eta_d = \frac{|\varepsilon|}{\omega} \sin\theta \tag{2.28}$$

Assuming the IFT and the surface concentration of adsorbed molecules follow equilibrium thermodynamic relations, the surface tension dynamics is solely due to variations of surfactant concentration C in the sub-layer. Such variations must satisfy the one-dimensional diffusion equation

$$\frac{\partial C}{\partial t} = D \frac{\partial^2 C}{\partial y^2} \tag{2.29}$$

where the coordinate y is normal to the interface, and $y = 0$ is the location of the interface. The parameter D is the diffusion coefficient of the surfactant molecules in the bulk liquid. The solution to equation (2.29) is:

$$C = C_\infty + E e^{\omega t} e^{i\omega t} \tag{2.30}$$

Provided that:

$$n=(1+i)\sqrt{\frac{\omega}{2D}} \tag{2.31}$$

In order to find the influence of this relaxation process on the modulus ε, the modulus is express as a function of the surface excess Γ of the surfactant molecules at the interface:

$$\varepsilon \equiv \frac{d\gamma}{d\ln A} = \frac{d\gamma}{d\ln \Gamma}\cdot\frac{d\ln\Gamma}{d\ln A} \tag{2.32}$$

The first term on the right-hand side is an equilibrium surface property; the second term measures adsorption changes during area changes and can be obtained from the conservation of surface active material at the interface:

$$\frac{1}{A}\frac{d(\Gamma A)}{dt} + D\left(\frac{\partial C}{\partial y}\right)_{y=0} = 0 \tag{2.33}$$

This gives, upon rearrangement:

$$\frac{d\ln\Gamma}{d\ln A} = -\left\{1 + D\frac{dC}{d\Gamma}\frac{\left(\partial C/\partial y\right)_{y=0}}{\left(\partial C/\partial t\right)_{y=0}}\right\}^{-1} \tag{2.34}$$

Combining equations (2.30) to (2.32) and (2.34) finally gives:

$$\varepsilon = \varepsilon_0 \frac{1+\zeta+i\zeta}{1+2\zeta+2\zeta^2} \qquad (2.35)$$

Where

$$\zeta \equiv \frac{dC}{d\Gamma}\sqrt{\frac{D}{2\omega}} \quad and \quad \varepsilon_0 \equiv -\frac{d\gamma}{d\ln\Gamma}$$

The dimensionless parameter ζ is determined by the ratio of the time scales of the experiment and of the diffusion process. Its magnitude depends mainly on the slope of the equilibrium adsorption isotherm of the surface-active solute. The depth of penetration of the diffusion process into the solution is also determined by the characteristic length $d\Gamma/dC$.

Combining equations (2.27) and (2.35) gives:

$$|\varepsilon| = \frac{\varepsilon_0}{\sqrt{1+2\zeta+2\zeta^2}} \qquad (2.36)$$

with

$$\tan\theta = \zeta/(1+\zeta) \qquad (2.37)$$

Equations (2.35) and (2.36) are various forms of the Lucassen and Van den Temple (LVDT) model for relaxation process of reversible adsorption of surface-active material, coupled with diffusion of the material in the bulk solution to and from the surface. As a limitation to this model and other rheological models (e.g. Maxwell model), it cannot predict the dilatational modulus as a function of bulk concentration of a given system.

ζ can vary between zero and infinity; however the values for the phase angle θ are in the range between 0 and 45^{O} for a diffusion-controlled relaxation process. In the limit of 0 and 45^{0} phase angles, the following relaxation processes are expected to happen. For very slow diffusion processes (i.e., characteristic time much longer than experimental time scales), the following relaxation process is expected:

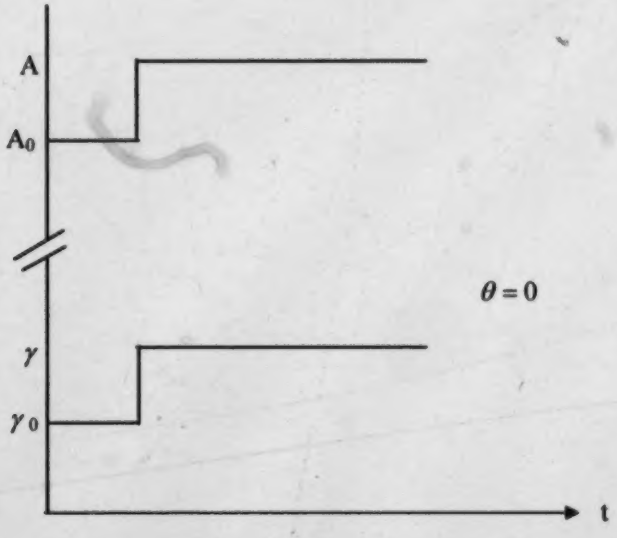

Figure 2-2 IFT Response to step increase in area of static drop ($\theta = 0$)

Conversely, for very fast diffusion processes (i.e., characteristic time much shorter than experimental time scales), we have instead

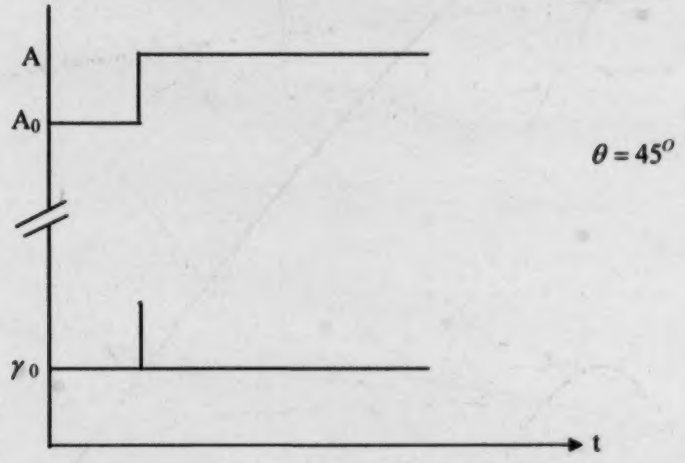

Figure 2-3 IFT Response to step increase in area of static drop ($\theta = 45^O$)

For all other cases, the relaxation process is expected to follow this trend. The magnitude of the phase angle, however, will determine the slope of the relaxation curve:

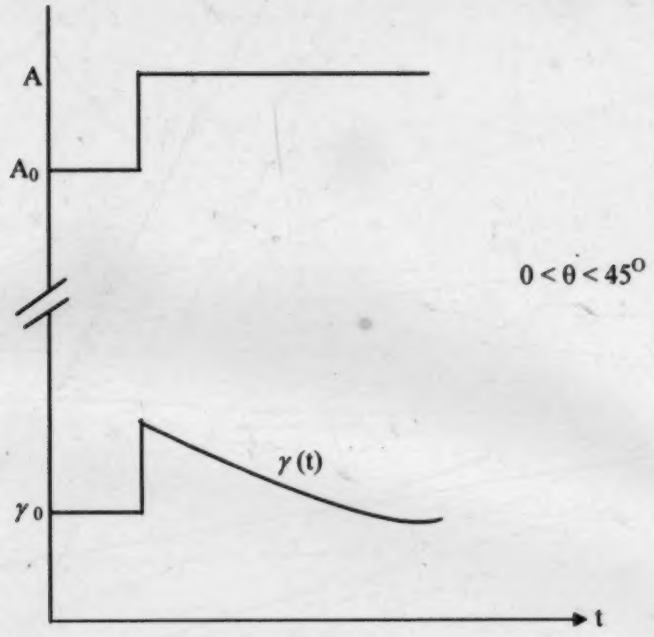

Figure 2-4 IFT Response to step increase in area of static drop ($0 < \theta < 45^O$)

2.4 Previous Studies on Interfacial Rheology of Adsorbed Molecules at Oil- Water Interfaces

Rheological studies of liquid-liquid and liquid-air interfaces had been reported in many instances in the literature. This may be due to the important relevance of this subject in both technological processes such as enhanced oil recovery, foaming, emulsification, and detergency, and physiological processes such as alveolar stability and the mechanics of biomembranes.

Bartell and Neiderhauser (1949) used the pendant drop technique to observe the so-called "rigid skin" at crude oil-water interface upon retraction of the oil droplet in water. They also observed that the rigid skin (interfacial film) formation was accompanied by lowering of interfacial tension, and thus concluded that the film was formed by an adsorption process. Reisberg and Doscher (1956) used rigorously controlled anaerobic conditions during crude oil sampling and laboratory measurements to study interfacial film formation of crude oil-water systems. Above pH of 8 (aqueous solution), they noted that rigid film formation was negligible. Many believed, before the experiment of Reisberg and Doscher, that since the film-forming material was strongly adsorbed by solid surfaces, it would not be present in crude oils as the oil exists in their natural subsurface reservoirs. In order to gain more insights into the reason(s) for "skin" formation, Dodd (1960) developed an interfacial film viscometer and measured rheological properties at oil-water interfaces.

Kimbler et al. (1966) and Strassner (1968), in their bid to expound emulsion stability, studied the compressibility and collapse pressure of interfacial films (crude oil-water interface) using Langmuir balance and pendant drop technique, respectively. In particular, Strassner (1968) found that depending on the quantity of asphaltenes and resins in a crude oil, the pH and chemical composition of the brine strongly affected emulsion stability. Indeed, Neustadter et al. (1979) and Mohammed et al. (1993) demonstrated that crude oil/water interfaces, especially those from asphaltenic oils, exhibited substantial elastic mechanical strength.

Among others, this is one reason why crude oil/water emulsions are very difficult to break (McLean and Kilpatrick, 1997a, b). Lucassen and Van den Temple (1972) illustrated a method for the measurement of dilational surface properties of solutions containing surface-active materials using the Wilhelmy plate technique. For the system of decanoic acid, they found that the surface dilational modulus decreased with increasing concentration of decanoic acid solutions.

Pendant drop technique was also used by Ward et al. (1980) and Beverung et al. (1999) to study protein adsorption at oil/water interfaces. Ward et al. (1999) demonstrated that, for the adsorption of bovine serum albumin (BSA), constant values of interfacial tension were reached after short time scales and are independent of bulk protein concentration above 0.01-0.04%. Beverung et al. (1999) showed that the kinetics of adsorption of proteins (used in their study) display three distinct regimes (1. induction regime, 2. monolayer saturation regime, and 3. interfacial gelation regime).

The role of the dispersion effect of resins in the adsorption of asphaltenes at the interface of water-in-crude oil emulsions was studied by Acevedo et al. (1993). Axisymmetric drop shape analysis was used to probe pressure dependence of interfacial tension of hydrocarbon-water systems and surface tension response to area changes of surfactant (SDS) laden interface (Susnar et al., 1993; Susnar et al., 1996). Susnar et al., in 1996 showed that for the concentrations studied and the range of area change values used, there is no phase shift for a sawtooth interfacial

response to sawtooth area change. Effects of different demulsifiers on the interfacial rheology and emulsion stability of water-in-crude oil emulsions have been studied by Mohammed et al. (1994). Acevedo et al. (1998) established that counterions in the aqueous phase play a significant role in dynamic interfacial tension of heavy crude oil-alkaline systems.

Yeung et al. (1998) used a novel micropipette technique, originally developed for the biophysical sciences (Evans et al., 1980), s to establish that equilibrium interfacial tension (in the presence of surfactants) can depend strongly on the experimental design. This, they showed, was due to the partitioning (or distribution) of surfactants between the two bulk phases and the interface. Yeung et al. (1999) studied the adsorbed layer formed at the surfaces of micrometre-sized emulsion droplets in diluted bitumen using "heptol" (1:1 mixture of n-heptane and toluene) as the diluent. Using the micropipette technique, the interfacial properties examined included adsorption, surface mechanical properties, and emulsion stability. At low bitumen concentrations (< 1%) where, according to their obtained interfacial tension vs. concentration isotherm, there should be little or no adsorbed substances on the droplet surfaces, the authors found as an "anomaly" that the interface exhibits surface rigidity, dissipative properties, and is resistant to both coalescence and coagulation. On the contrary, at higher bitumen concentrations (> 1 wt%) where, according to the obtained interfacial tension vs. concentration isotherm, there are more adsorbed substances at the interface, another "anomaly" was that the adsorbed layer transforms into a flexible interface capable of creating new emulsion droplets

through a budding process[2]. Yeung et al. (1999) noted in their communication that the transition, however, did not appear abrupt. They also concluded that dynamic behaviours of the adsorbed interface were well described by the Boussinesq-Scriven (two-dimensional Newtonian) model. Wu (2003), following the work of Yeung et al. (1999), investigated the stability mechanism of water-in-diluted bitumen emulsions through isolation and characterisation of the stabilizing materials at the interface. He found that, in heptol-diluted bitumen emulsions, the flexible interfacial film was composed of a mixture of asphaltenes and carboxylic salts with a combined H/C ratio of 1.32, while the rigid interfacial film was composed of asphaltenes alone with a H/C ratio of 1.13. He concluded that the presence of the carboxylic salts (which are water insoluble and are likely sodium naphthenates containing > 20 carbons) might hinder the conformational change of asphaltenes at the interface, necessary for rigid film formation.

To better understand the time dependence of the interfacial behaviour of asphaltenes, Jeribi et al. (2002) used the floating drop technique to probe the adsorption kinetics of asphaltenes at oil-water and air-oil interfaces. They showed that, when asphaltenes adsorbed at liquid interfaces, after the rapid initial diffusion step toward the interface, a long reorganisation and a progressive building of multilayers occurred. The reorganisation was faster at oil-water interfaces than at air-oil interfaces, but the multilayer formation took similar times. Freer et al. (2002),

[2] A process whereby upon shrinking a water drop immersed in a continuous oil phase small protrusions begin to appear, become more prominent as the interfacial area continues to decrease and eventually detach as micrometre-size droplets.

following the work of Kovscek et al. (1993), used the oscillating drop technique and contact angle measurements to emphasize the role oil/water interfacial microstructures play in establishing the mixed-wet state of reservoirs. They found the interfacial loss modulus E'' was considerably smaller than the interfacial storage modulus E' for each crude oil that was studied. Thus, the asphaltene films which grew at the oil/water interface were primarily elastic in nature. Moreover, they found that interfacial elasticity was increased slowly in time (over days) and was clearly manifested even when "rigid skins" were not visible to the eye. In addition to their contact angle measurements, one of their conclusions was the aging of the asphaltene deposits on the solid surface expelled trapped water, giving a more coherent and finer textured coating depending on the asphaltene content of the crude oil. Thus, aging of the oil/water interface and the asphaltene-coated surface were both important in the evolution of mixed wettability. Using oscillating pendant drop technique, Aske et al. (2002) measured the dilatational elasticity modulus and dynamic interfacial tension of 21 crude oils and condensates originating from different production fields. The samples were diluted in different heptane/toluene solvent at different concentrations. They found that both the solvent composition and oil concentration had great influence on the measurements. Work by Zhang et al. (2003), using Langmuir trough, showed that asphaltene formed nanoaggregates at both the air-water and heptol-water interfaces. They showed that the presence of demulsifier in the mixed monolayer rendered the monolayer more compressible at both the air-water and heptol-water interfaces.

Most recently, Freer and Radke (2004) adopted interfacial rheology using the oscillating pendant drop with axisymmetric drop shape analysis (ADSA) to investigate the relaxation mechanisms of asphaltenes adsorbed at toluene/water interface. They compared classical viscoelastic models with measured rheological data and found that the frequency response of the dilatational moduli fitted a combination of diffusion-exchange and surface-rearrangement mechanisms consistent with the results by Jeribi et al. (2002). Spiecker and Kilpatrick (2004) used a biconical bob interfacial shear rheometer to study the mechanical properties of asphaltenic films adsorbed at the oil-water interface. Solutions of asphaltenes isolated from four crude oils were dissolved in a model oil of heptane and toluene and allowed to adsorb and aged in contact with water. Film elasticity values were measured over a period of several days, and yield stresses and film masses were determined at the end of testing. They found that asphaltenes were well solvated in high aromatic solvents, formed films of lower elasticity and yield stress, and formed weaker emulsions. They also found that asphaltene chemistry dictated the properties of adsorbed films and concluded that high aromaticity solvents would render a higher amount of the crude oil surfactants non interfacial-active. Ongoing research in Masliyah and Xu's laboratory (University of Alberta) is to study Langmuir and Langmuir-Blodgett films formed with bitumen, de-asphalted bitumen, ultra-fine solids and mixtures of each. This study, they believe, will provide information about the role of ultra-fine solids in emulsion stability. Researchers in Yarranton's group (Univeristy of Calgary) are also using oscillating pendant drop technique to investigate the role of asphaltenes in emulsion stability.

With this background knowledge, and following the early work of Yeung et al. (1999), this study endeavour to use interfacial dilatational rheology (using the oscillating pendant drop with axisymmetric drop shape analysis) to discern the ageing effect on the behaviour of toluene dilutions of de-asphalted bitumen (DAB), asphaltenes and bitumen in water pre-equilibrated with the oil under study. The effect of concentration on toluene dilutions of DAB, asphaltenes and bitumen on interfacial rheological properties on such systems was also investigated.

CHAPTER THREE

3. METHODOLOGY

3.1 Materials

Vacuum feed bitumen was supplied by Suncor Canada Limited and was used as received. Distilled water, further purified using a Millipore filtration unit (greater than 18.2 MΩ cm resistivity), was used. HPLC grade toluene, n-heptane and technical grade n-heptane (96%) were all purchase from Fisher scientific; they were used as received. All water solutions were pre-contacted with the oil system in a 6:1 volume ratio for at least 12h to permit equilibration of the water with the diluted bitumen solutions. The pH of the oil-equilibrated water is about 7.2 and its interfacial tension is about 71.95mN/m.

In all the experiments described herein, the water was always pre-equilibrated with the oil system under study. De-asphalted bitumen (maltene) will be called DAB. Oil-water interface is always the interface between toluene-diluted sample (e.g. DAB, asphaltene, or whole bitumen) immersed in pre-equilibrated water. So, for example, 1wt% DAB solution is understood to mean a 1wt% toluene-diluted DAB liquid drop formed in pre-equilibrated water; 1wt% asphaltene solution is understood to mean a 1wt% toluene-diluted asphaltene liquid drop formed in pre-equilibrated water; etc. All experiments were performed at ambient temperature. The pendant drop apparatus and the image analysis software are manufactured by First Ten Angstroms Instruments, USA (http://www.firsttenangstroms.com).

3.2 Asphaltene and De-asphalted Bitumen (DAB) Extraction

The procedure used for asphaltene and DAB extraction was according to Zhang et al. (2003). Vacuum feed bitumen was dissolved in toluene at a toluene/bitumen volume ratio of 5:1. The dissolved bitumen was shaken on a laboratory shaker for 2h. The solids were removed by centrifugation of the toluene-diluted bitumen at 15000 rpm (20000g) for 30min. The mass of the recovered solids was 0.7% of that of the original bitumen. Toluene in the diluted bitumen was removed by natural evaporation in a fume hood until there was no further change in mass under ambient conditions. HPLC grade n-heptane was then added to the toluene-free bitumen at a heptane/bitumen volume ratio of 40:1. The heptane-diluted bitumen was shaken on a laboratory shaker for 2h and left overnight for asphaltene precipitation. The supernatant (DAB) was carefully decanted and then left in a fume hood to remove n-heptane by natural evaporation until there was no further change in mass under ambient conditions. Precipitated asphaltenes must be repeatedly dissolved into toluene and subsequently precipitated with n-heptane to remove co-precipitated resin molecules bound to asphaltene aggregates (Strausz et al., 2002). Here, a single precipitation step was used and the precipitated asphaltenes was washed with an excess amount of (10 L) of technical grade n-heptane until the effluent was colourless. As such, only minute amounts of surface-active resins and/or smaller molecular weight asphaltenes are likely present in the extracted asphaltenes sample. The mass of precipitated asphaltene was 10.5% of that of the original bitumen.

3.3 Experimental Procedure

All experiments were conducted using the pendant drop apparatus. Accuracy and reproducibility are important when conducting this type of experiments. To accomplish good accuracy, it was always ensured that the glass tube (used as needle, 0.96mm outside diameter, from Kimble Glass), PFTE tubing (from Action Electronics, 0.869mm inside diameter), and glass cell (from Fisher Scientific) were all clean and that the only impurities introduced into the system were the "natural surfactants" already present in the oil system. Data was recorded only when it was reproducible. Three different DAB concentrations (1 wt%, 10 wt%, and 30 wt%), three asphaltenes concentrations (1 wt%, 10 wt%, and 20wt%) and three diluted bitumen concentration (5wt%, 15 wt% and 30wt%) in toluene were studied for different periods of oscillation (20s, 40s, 80s, 160s). Two different ageing times (1hour and 24hours) were studied for each experiment. The densities of these solutions were determined by weighing known volumes of samples (accuracy estmated to be ±0.2% or better).

3.3.1 Calibration

Before actual measurement of interfacial tensions, the pendant drop apparatus must first be calibrated. This amounts, in effect, to determining accurately the magnification of the CCD camera (i.e., the actual size of a captured image must be known). The magnification can be adjusted by:

1. providing the image of an object of know dimensions (e.g., the needle tip);

2. providing a system of known interfacial tension (e.g., between clean fluids);

3. by directly specifying the number of nanometres per pixel.

In this study, calibration was done using the first option — with a needle of known outside diameter. The diameter was entered in the computer program and the measured tip width in each image was presumed to reflect this size. The magnification was recomputed to make the tip width equal the known diameter in just this image and just for the interfacial tension quantities. The measured tip width was reported as it was originally measured, not with the adjusted magnification.

After calibration, and before the start of actual experiments, the interfacial tensions of standard fluids (i.e. fluids with known IFT) were determined to verify that the calibration was done correctly. Below are comparison of measured IFT and their literature values.

Table 3-1 Measured IFT and their Literature Values

Fluid	Measured Value (mN/m)	Literature Value (mN/m)
Water	73.2	72.8
Heptane	51.0	50.5
Toluene	36.4	36.0

3.3.2 Interfacial Tension Measurement

To determine the dynamic interfacial tension of each oil/water interface using the pendant drop apparatus, the less dense oil drop is formed upwards at the tip of a glass needle immersed in the aqueous solution. The First Ten Angstroms apparatus combines both the interfacial tension and interfacial rheology measurements. However, to be certain of our results, the interfacial rheology measurements in this study were done manually. This is because the computer base calculation was almost always 10% off the manually obtained results. The system consists of a measurement platform and a frame grabber (video capture) card running on a personal computer, high resolution CCD camera and zoom microscope, computer controlled syringe pump, and computer controlled lighting.

The action appears live on the computer screen and the salient images are captured and digitised for subsequent analyses. From the drop profile and the known densities of the oil and aqueous phases, the interfacial tension can be determined to a high accuracy (based on the Young-Laplace equation). The time scale can vary from 1/60 second (60 images/second) to hours and can be varied nonlinearly. The system can

capture both static and dynamic behaviour of liquid interactions. Analysis is based on the drop shape's size and shape. The system functions as a transient analyzer, which means it can continually capture images and can recall any number of past images after a triggered event. A variety of dynamic events can furnish the trigger. One such trigger is real-time software detection of the drop detaching from the dispensing tip. The automatic syringe pump, a timer, and user input, can also furnish triggers.

The optical glass cell (Figure 3.1) contains the aqueous solution. The cell is sealed with a teflon lid to prevent water evaporation and is kept in a closed chamber with a narrow opening for illumination. The entire apparatus is mounted on a TMC vibration isolation table (www.techmfg.com). After forming a fresh oil drop at the needle tip, the dynamic tension is followed in time using axisymmetric drop-shape analysis. The computer-controlled syringe pump is capable of maintaining constant drop volume for long time periods (few days) over which dynamic tensions are measured. Typical precision in tension measurements is ±1%. Figure 3-2 is a photograph of the pendant drop apparatus.

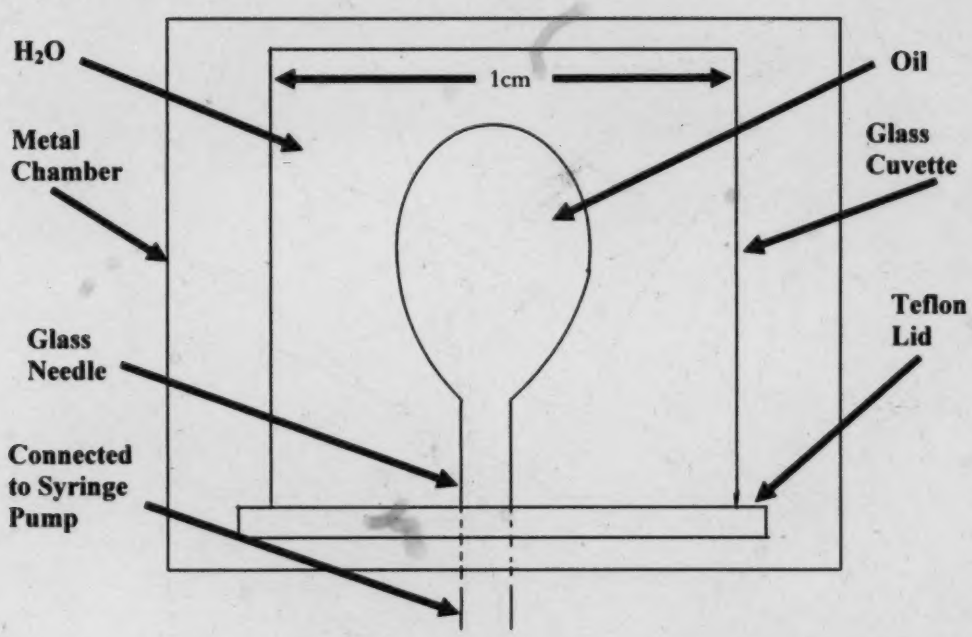

Figure 3-1 Optical Glass Cell Assembly

Figure 3-2 Pictorial view of Pendant Drop Apparatus

3.3.3 Order-of-Magnitude Estimates of Dimensionless Groups

The Young-Laplace equation is predicated on negligible inertial and viscous forces compared to capillary forces and is shown in this thesis as follows:

Reynolds number, the ratio of inertial forces to viscous forces, is given by equation (3.1):

$$\mathrm{Re} = \left[\frac{l_o V_o \rho}{\mu}\right] \tag{3.1}$$

Here, l_o is the characteristic length of the oil drop, V_o is the superficial displacement velocity, ρ is the oil drop density and μ is the oil viscosity (Bird et. al, 2002). Capillary number, the ratio of viscous forces to capillary forces, is given by equation (2.2). Weber number, the ratio of capillary forces to inertial forces, is given by equation (3.2)

$$We = \left[\frac{\gamma}{l_0 V_o^2 \rho}\right] \tag{3.2}$$

Typical values in this study are $l_o \sim 10^{-3}$ m, $V_o \sim 10^{-5}$ ms^{-1}, $\rho \sim 10^{3}$ kgm^{-3}, $\gamma \sim 10^{-2}$ Nm^{-1}, and $\mu \sim 10^{-3}$ Pa s. This leads to a Capillary number of Ca $\sim 10^{-6}$, a Reynolds number of Re $\sim 10^{-2}$ and a Weber number of We $\sim 10^{8}$.

Ca << 1 means viscous forces are much smaller than capillary forces and We >> 1 means inertial forces are much smaller than capillary forces.

Even though Re $\sim 10^{-2}$ suggesting that the inertial and viscous forces are about the same magnitude they are both much smaller than the capillary forces as shown by Capillary number and Weber number in this study.

3.3.4 Linearity Test

A sinusoidal input will result in a sinusoidal output if and only if the imposed strains lie within the linear regime. To determine the linear regime of the systems studied, the following simple tests were conducted: Step-strain deformations (step increase and step decrease) were applied to each equilibrium system and the interfacial tension (IFT) was allowed to recover back to its equilibrium value. The condition of linearity was satisfied if the IFT response was proportional to the applied step strain. In this study, all the systems that were studied exhibited linearity if the maximum strain amplitudes $\Delta A/A_0$ were kept below 10%.

3.3.5 Interfacial Rheology Measurement

By subjecting the oil/water interface to periodic expansion and contraction of small amplitudes (i.e., for $\Delta A/A_0$ below 10%), the surface dilatational storage modulus, ε', and the surface dilatational loss modulus, ε'', are computed using the measured area and interfacial tension variations. Similar to the dynamic-tension measurements, surface rheological behaviour was followed over long time scales (up

to 24 hrs). Rather than continually oscillating the system for such long times, oil drops were formed for each experiment and aged for the desired amount of time before the syringe pump is turned on. Immediately after the syinge pump was activated, the will be several cycles of transient effects before steady state set in. To avoid recording transient effects, the first few oscillations were allowed to elapse before each experiment was triggered. Also, the oscillation frequency was restricted to below 1.75 rad/s to avoid hydrodynamic effects (i.e., the hydrodynamic stresses must remain negligible relative to the Laplace pressure; Wong et al. 1998).

CHAPTER FOUR

4. RESULTS AND DISCUSSION

4.1 Ideal Systems

An "ideal system" refers to an interface between pure immiscible liquids, in the absence of adsorbed components. In such situation, the interfacial tension (IFT) must depend only on the nature of the two liquids; it is expected to be insensitive to dynamic changes in the interfacial area. As control tests, we will first verify that the IFT is indeed invariant to area changes for ideal systems. The systems will be comprised of water and one of two non-polar liquids: toluene and n-heptane (both HPLC grade). In Figures 4-1 to 4-6, IFTs in response to static and dynamic area input are shown. The IFT vs time relations are shown as solid lines, while the area vs time relations are plotted as dashed lines. The sinusoidal area excitations have periods 20s, 40s, 80s, and 160s.

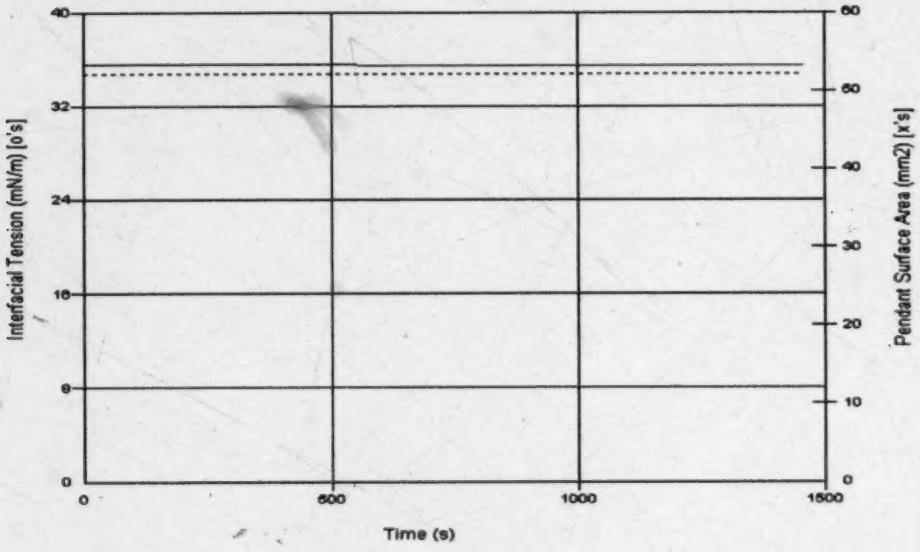

Figure 4-1 IFT (solid line) versus Static Area (dash line) for Toluene/Water Interface

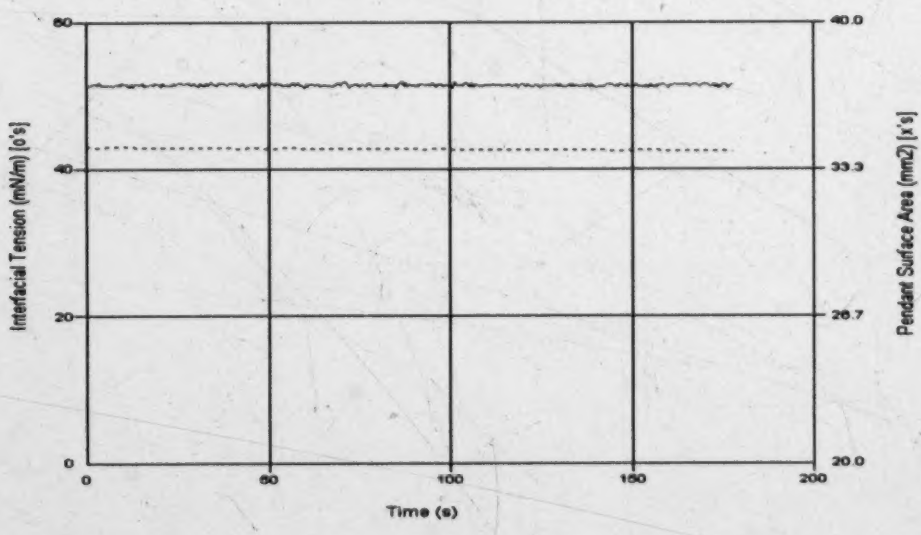

Figure 4-2 IFT (solid line) versus Static Area (dash line) for Heptane – Water Interface

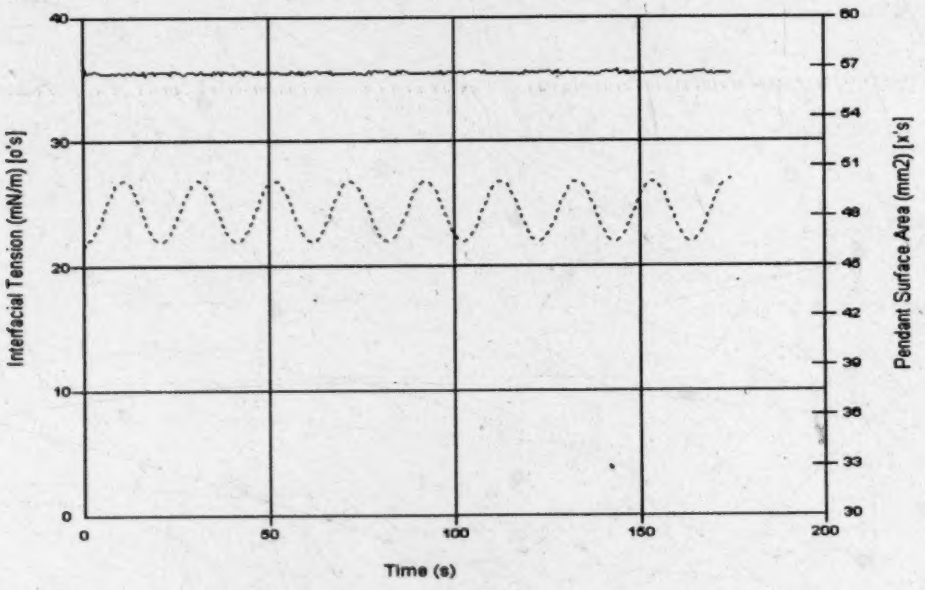

Figure 4-3 IFT (solid line) versus Sinusoidal Area (dash line) for Toluene, Period 20s

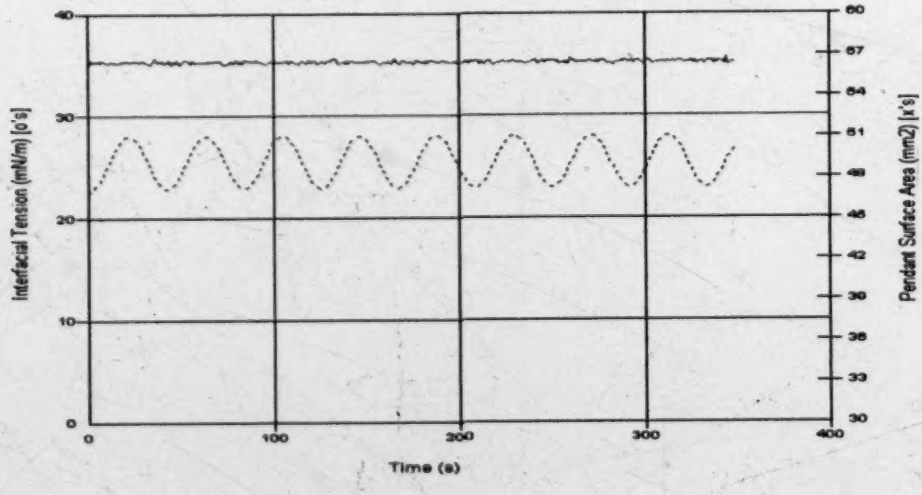

Figure 4-4 IFT (solid line) versus Sinusoidal Area (dash line) for Toluene, Period 40s

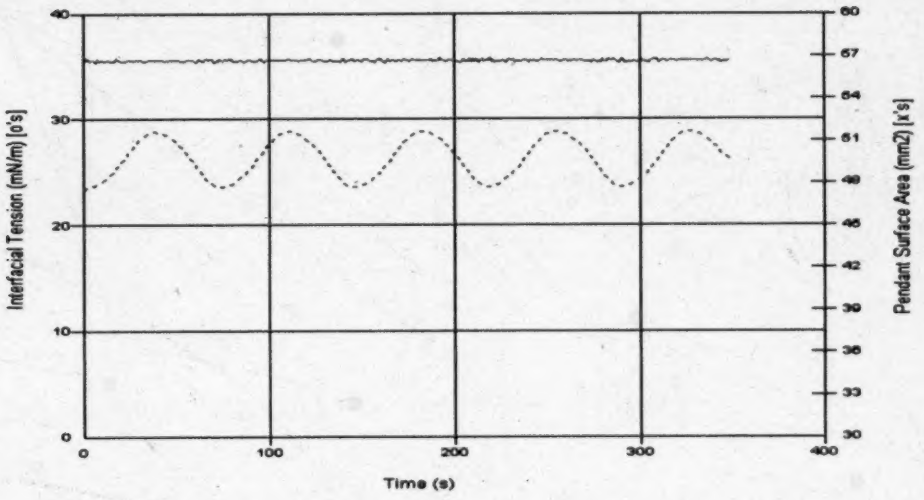

Figure 4-5 IFT (solid line) versus Sinusoidal Area (dash line) for Toluene, Period 80s

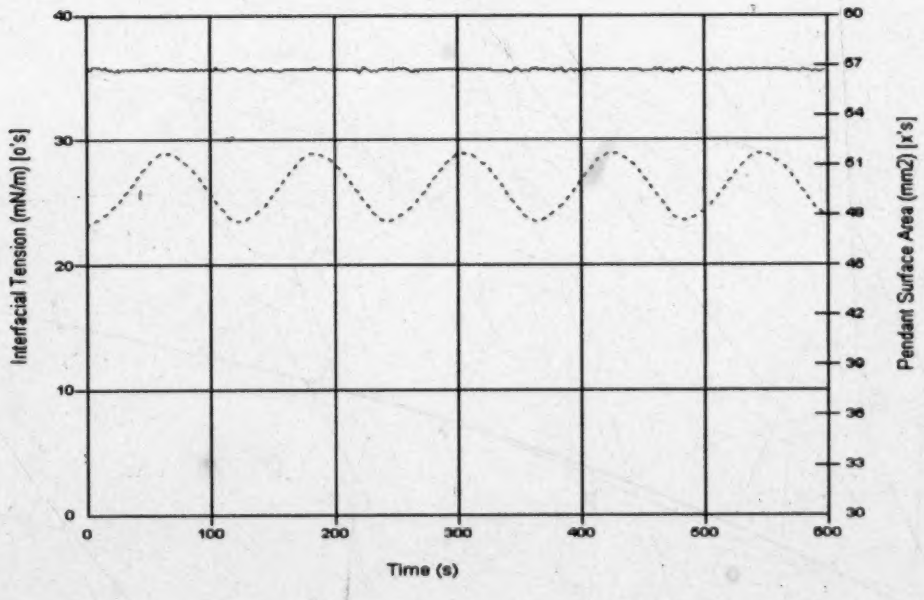

Figure 4-6 IFT (solid line) versus Sinusoidal Area (dash line) for Toluene, Period 160s

An examination of the above graphs reveals that there are typically small fluctuations of the data. The fluctuations are most likely the result of vibrations which distort the shape of the drop and noise resulting from mechanical vibration. Vibrations are most likely to occur during the first few drop images, as a result of drop formation, and tend to be damped out after a short while. An air table was used to limit mechanical vibration. The IFTs of the ideal systems show very slight (almost negligible) decreases over time. This may be due to the slow build-up of impurities at the interface. This trend has also been reported by Neuman and coworkers (1993) and Radke and coworkers (1999).

4.2 De-asphalted Bitumen (DAB)

Here, the interface in question is between water and toluene-diluted de-asphalted bitumen. In Figures 4-7 to 4-10, the interfacial tension responses (solid line) to static area (dash line) and sinusoidal area changes (dash line) are shown. From this data, the effects of frequency, aging of surfactant-laden interface, and bitumen concentration on the dilatational elastic modulus for DAB will be examined.

In the case of static response (Figures 4-7 to 4-9), initially, the tension decays sharply after several seconds or minutes (depending on the concentration), at which point there is a subtle change in slope, suggesting a transition to interfacial-network formation (Beverung et al., 1999). The time dependence of IFT may be due to the migration of surface-active agents from the bulk to the oil-water interface; as a result, a surface pressure at the interface is built up, thereby decreasing the interfacial

tension. The driving force for surfactant migration would depend on the concentration of surface-active agents below the CMC (critical micelle concentration), by analogy with simple surfactant systems. Thus, the lower concentration system should take longer to reach equilibrium and have a higher steady state value. In the case of dynamic excitations (Figure 4-10), the phase angle between the IFT response and the sinusoidal area input for DAB was always approximately zero, suggesting that the interfacial area is essentially elastic. This is true for the range of frequencies probed in this study (periods of 20s, 40s, 80s, and 160s); the phase angle might probably not be zero for frequencies outside of this range. Elastic behavior, however, has been reported for some polymer and copolymer systems (Rolf et al. 1998).

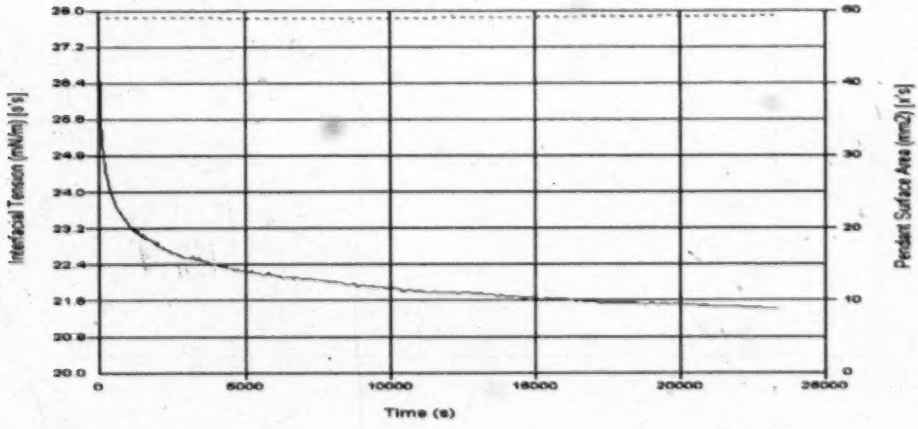

Figure 4-7 IFT (continuous line) versus Static Area (dash line), 1wt% DAB Solution

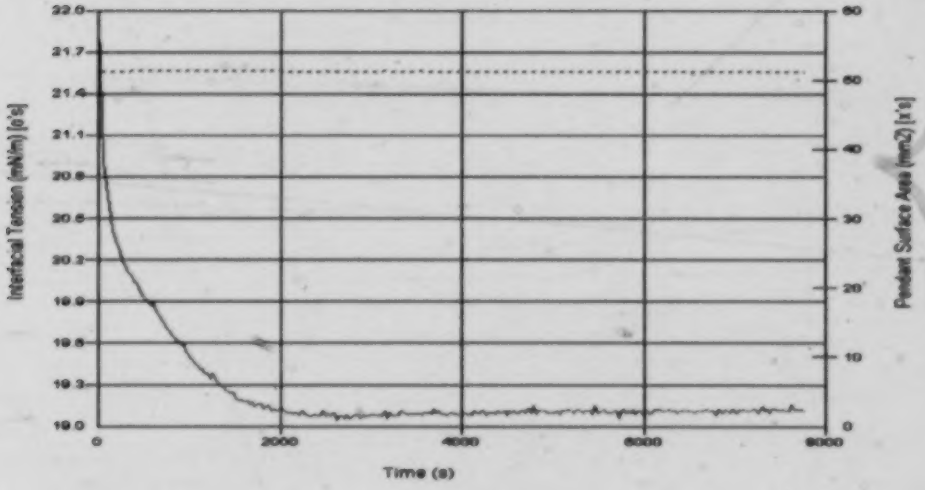

Figure 4-8 IFT (continuous line) versus Static Area (dash line), 10wt% DAB Solution

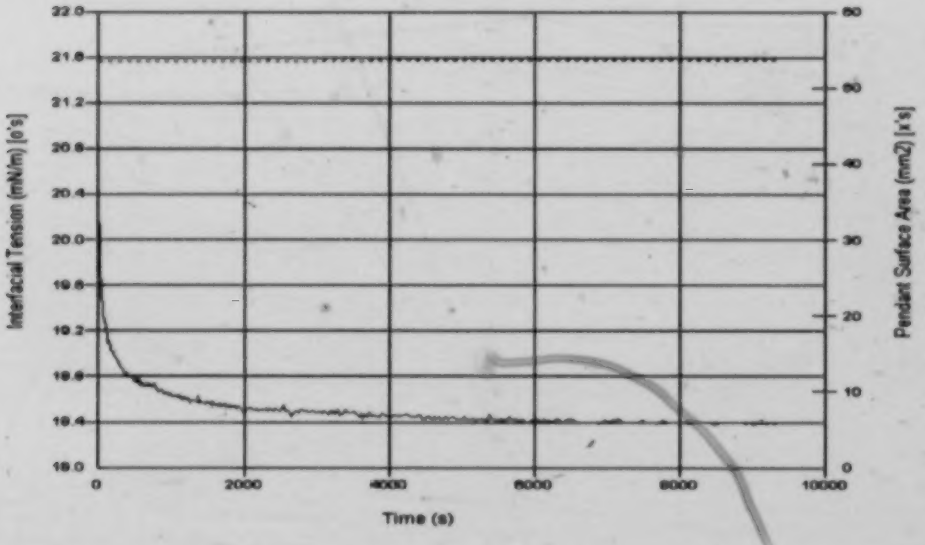

Figure 4-9 IFT (continuous line) versus Static Area (dash line), 30wt% DAB Solution

Table 4-1 Equilibrium IFT versus Concentration for DAB

Concentration	Equilibrium IFT
1wt%	20.8
10wt%	19.1
30wt%	18.4

As the sinusoidal area (input) and interfacial tension (output) can, in general, be out of phase, the interfacial dilatational modulus will be comprised of two parts: an elastic part (storage modulus ε') that accounts for the recoverable energy stored in the interface, and a viscous part (loss modulus ε'') that is responsible for the energy loss through internal relaxation processes (see eqns 2.18 and 2.19). Here, for deasphalted bitumen, the phase difference between the IFT and area waveforms is virtually zero. One may conclude from this that the loss modulus is negligible for DAB systems (i.e., the interface is elastic). Zero phase angles also suggest that, on the molecular level, there are no relaxation processes which occur with characteristic times comparable to the time scale of the experiment (Lucassen et al., 1972). For our present study, the experimental time scales are given by the peroids of area oscillations, which are of order 10 – 200 s. It is entirely possible that relaxation mechanisms within DAB systems do exist, but their characteristic times are not within the range of 10–160 s. In order to detect these out-of-reach mechanisms, a wider range of oscillating frequencies will be required.

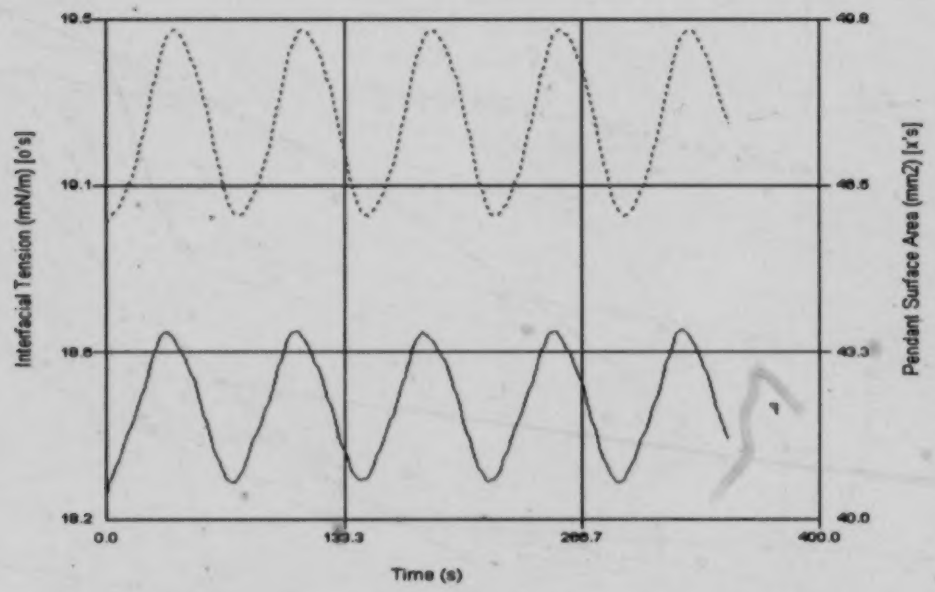

Figure 4-10 IFT Response (continuous line) to Area Change (dash line), 10wt% DAB Solution, Period 80s (Age 1day)

From Figures 4-11 to 4-13, it is seen that the elastic modulus (ε') increases with the age of the interface and the frequency of oscillation. The increase of elastic modulus with interfacial aging suggests that interfacial-network formation strengthens with time. The frequency response of the elastic modulus (ε') is characteristic of systems that obey diffusion exchange mechanism of reversibly adsorbed molecules (Lucassen et al., 1972). Detailed study is required to discern whether the frequency response includes Maxwell response (i.e. surface relaxation (Monray et al., 1999;

Monray et al., 2001)) and multilayer exchange kinetics (Van den Tempel et al., 1983). This will be the object of future work.

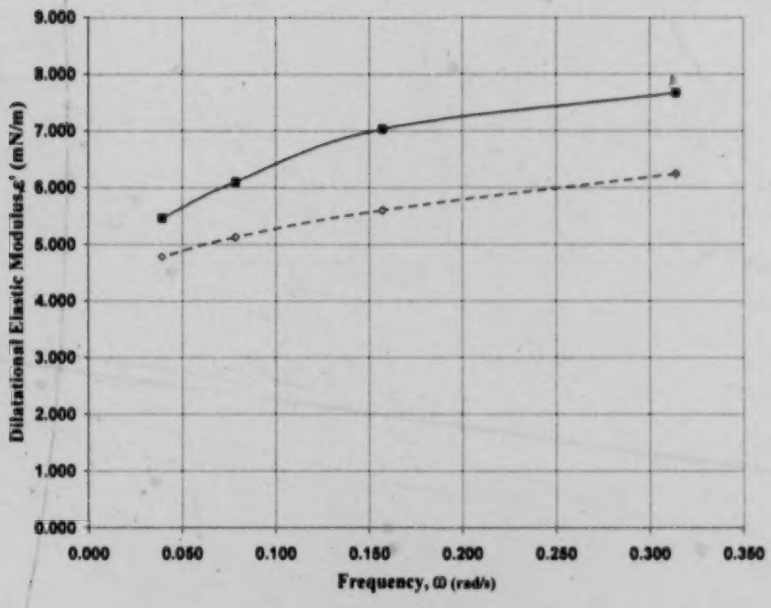

Figure 4-11 Dilatational Elastic Modulus versus Frequency, 1wt% DAB Solution (Ages 1hr & 1Day); ◊ Elastic Modulus for 1hr; ■ Elastic Modulus for 1day

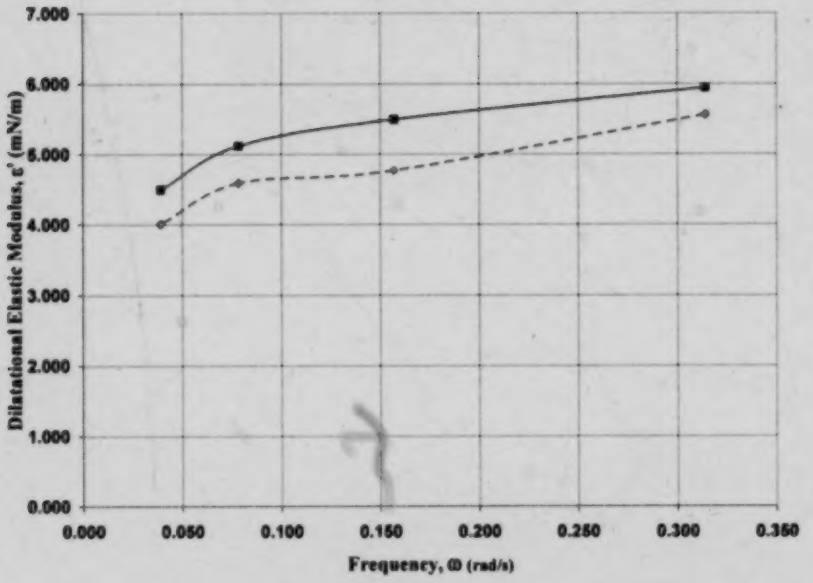

Figure 4-12 Dilatational Elastic Modulus versus Frequency, 10wt% DAB Solution (Ages 1hr & 1Day); ◊ Elastic Modulus for 1hr; ■ Elastic Modulus for 1day

Figures 4-14 and 4-15 show that, surprisingly, the elastic modulus appears to decrease with increasing concentration. This trend has in fact been reported for some polymers and copolymers (Myrvold and Hansen 1998). Lucassen and Van den Tempel (1972), using decanoic acid solutions, also observed elasticity moduli decrease with increasing bulk concentration. The trend is also consistent with what is seen in asphaltene and diluted bitumen systems studied in this work; this will be discussed in the subsequent sections. The reason for the reduction of elastic modulus with increasing bulk DAB concentration is not clear. It is probable that

configurational change in the surface layer is causing the elastic modulus to decrease with increasing bulk concentration.

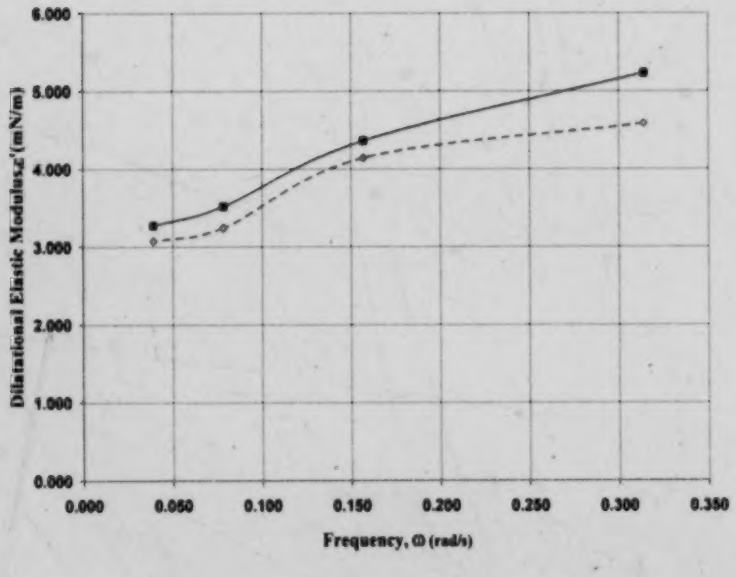

Figure 4-13 Dilatational Elastic Modulus versus Frequency, 30wt% DAB Solution (Ages 1hr & 1Day); ◊ Elastic Modulus for 1hr; ■ Elastic Modulus for 1day

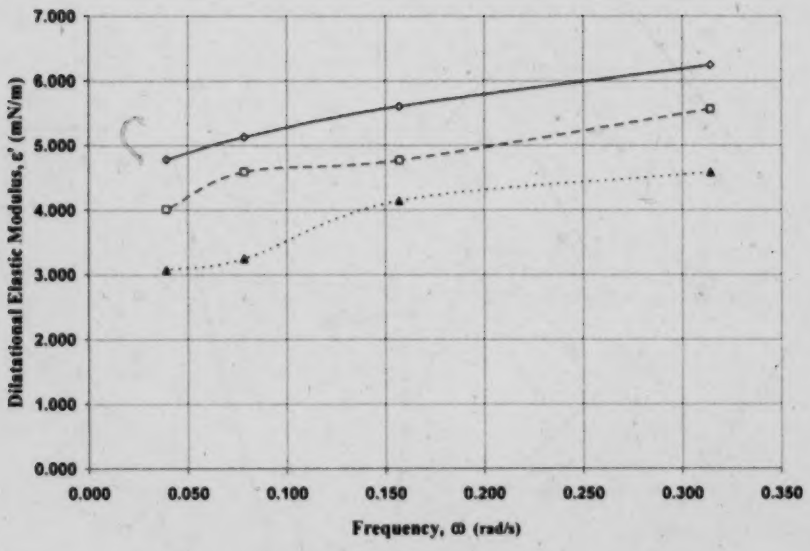

Figure 4-14 Dilatational Elastic Modulus for 1, 10, and 30wt% DAB Solution versus Frequency (Age 1hr); ◊ Elastic Modulus for 1wt%; □ Elastic Modulus for 10wt%; ▲ Elastic Modulus for 30wt%

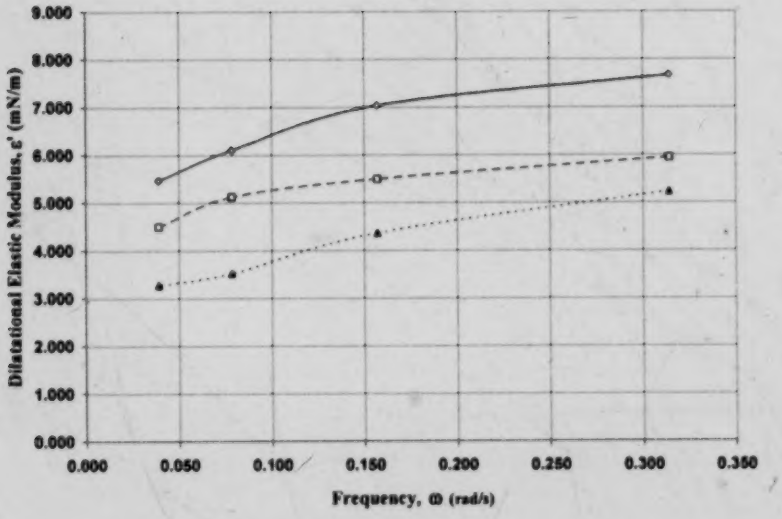

Figure 4-15 Dilatational Elastic Modulus for 1, 10, and 30wt% DAB Solution versus Frequency (Age 1Day); ◊ Elastic Modulus for 1wt%; □ Elastic Modulus for 10wt%; ▲ Elastic Modulus for 30wt%

4.3 Asphaltenes

Here, the interface in question is between water and toluene-diluted asphaltenes. The static IFT response, dynamic IFT response to sinusoidal area change, as well as the effects of frequency, aging, and asphaltene concentration on the interfacial dilational modulus will be discussed (see Figures 4-16 to 4-27). The time dependence of IFT during equilibrium measurement shown in Figure 4-16 was similar to that of DAB. However, the steady state value was reached sooner. This is

consistent with much faster "skin" formation rate (Figure 4-19) than DAB and indicates that asphaltenes are much more surface active than DAB. From Table 4-2 and Figures 4-16 to 4-18, the interfacial tension (IFT) depends weakly on concentration. This suggests that these concentrations are around or above critical aggregation concentration (CAC) (Rogel et al., 1999; Anderson et al., 1991).

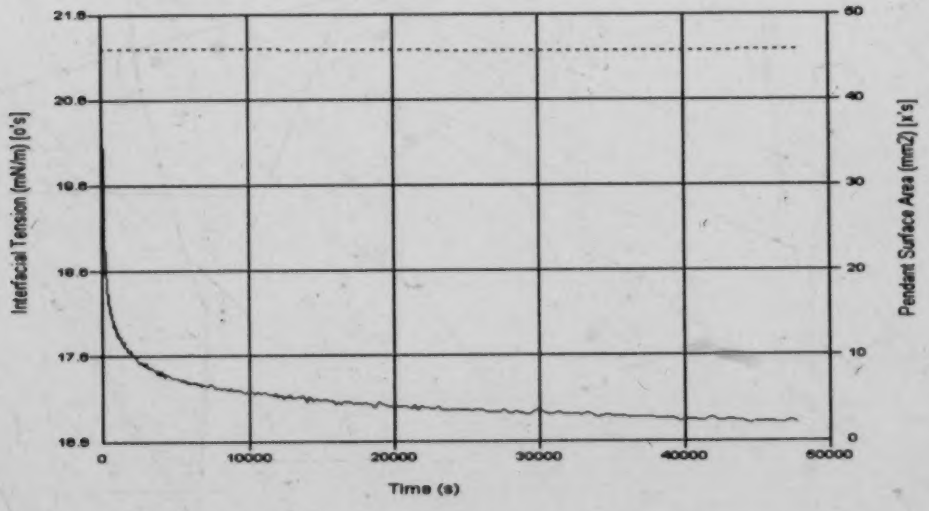

Figure 4-16 IFT (continuous line) versus Static Area (dash line) for 1wt% Asphaltene Solution

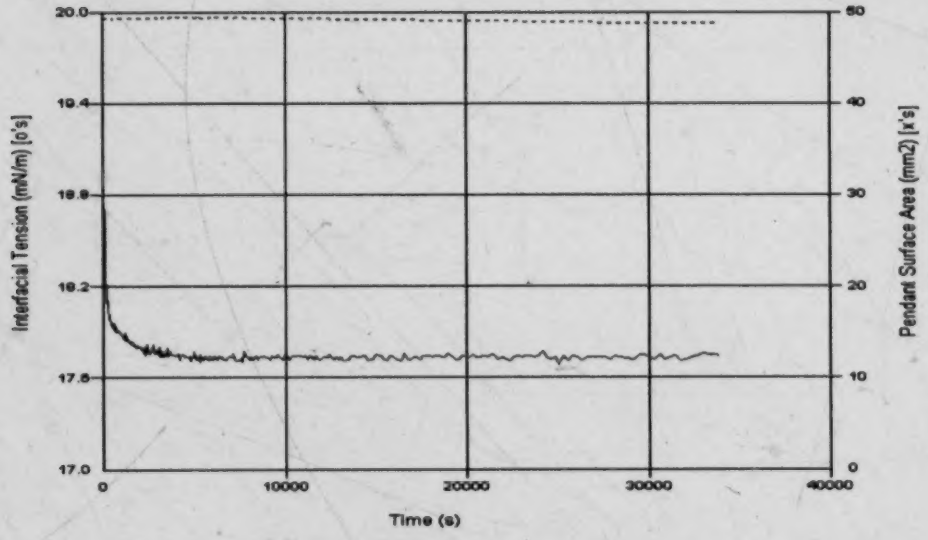

Figure 4-17 IFT (continuous line) versus Static Area (dash line) for 10wt% Asphaltene Solution

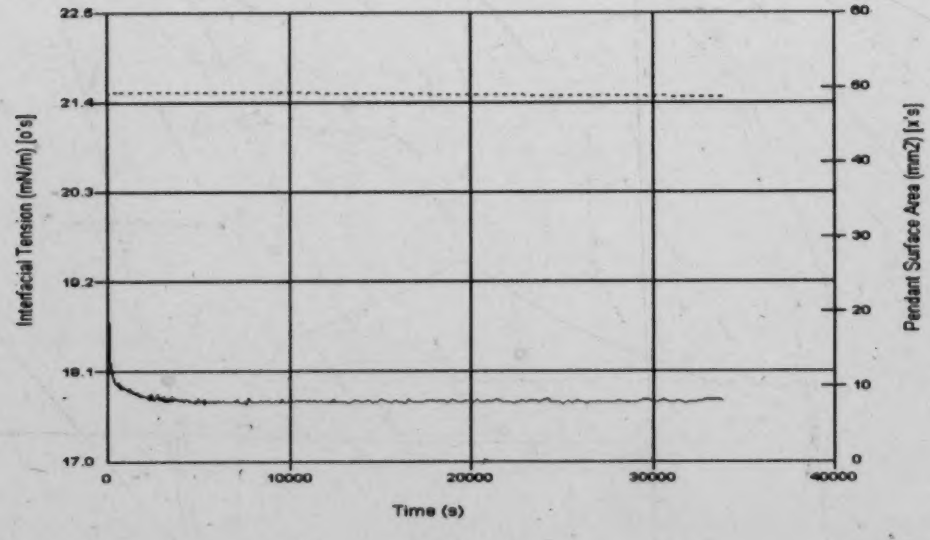

Figure 4-18 IFT (continuous line) versus Static Area (dash line) for 20wt% Asphaltene Solution

Table 4-2 Equilibrium IFT versus Concentration for Asphaltene Solutions

Concentration	Equilibrium IFT
1wt%	16.8
10wt%	17.8
20wt%	17.7

"Skin" formation was observed (upon retraction) and the structure appeared to rigidify with time (Figure 4-19). This situation is very similar to that encountered with protein adsorption at air-water or oil-water interfaces (Li et al., 2001; Beverung et al., 1999). This rigid, wrinkled skin was relatively short lived, and after the initial retraction, the drop slowly relaxes back to a shape similar to that prior to retraction in about 15 minutes.

Figure 4-19 Skin Formation for 10wt% Asphaltene Solution (4hrs after drop formation)

This "skin" is postulated to result from irreversible adsorption and aggregation of asphaltene molecules through hydrogen and π-π aromatic ring bonding at the oil-water interface (Mclean et al., 1997).

The dilatational modulus changes more substantially upon interface aging than does the interfacial tension, which is similar to the findings of Mohammed et al., 1994.

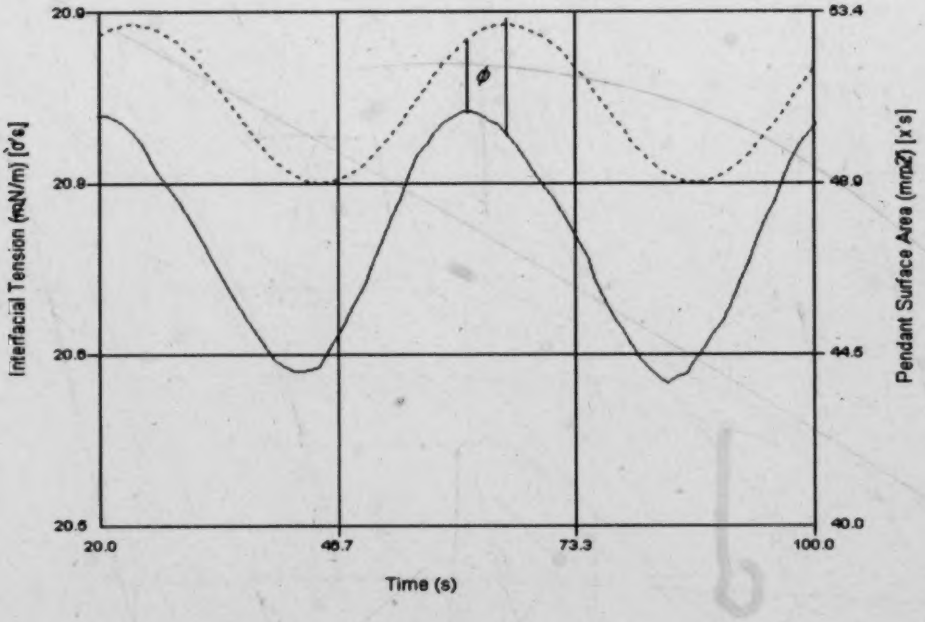

Figure 4-20 Phase Angle between IFT (continuous line) Response to Sinusoidal Area Input (dash line), 20wt%Asphaltene Solution

Unlike interfaces formed from de-asphalted bitumen, obvious phase angle between IFT response and the sinusoidal area input was observed, as shown in Figure 4-21.

The phase shift suggests that the interfacial area is not purely elastic and that dissipative effects are taking place at the interface. A similar trend as in the case of DAB was observed between the interfacial dilatational modulus with frequency and aging time.

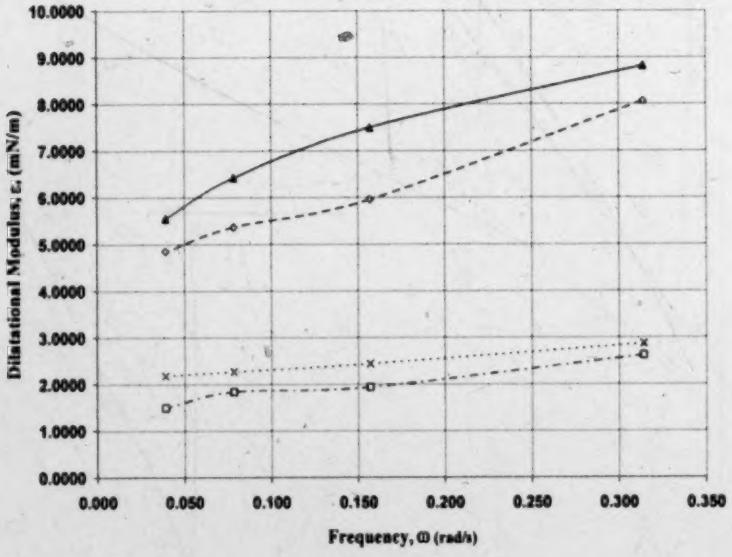

Figure 4-21 Dilatational Modulus versus Frequency, 1wt% Asphaltene Solution (Ages 1hr & 1Day); ▲ Elastic Modulus for 1day; ◊ Elastic Modulus for 1hr; x Viscous Modulus for 1day; □ Viscous Modulus for 1hr

Here, we speculate that the increase in dilatational modulus with aging is due to the formation of interfacial asphaltenic network structure. Mohammed et al. (1993), using heptane/xylene oil containing asphaltenes, measured the compressional

modulus of the oil-water interface using the Langmuir trough technique. They concluded that the rigidity of the oil-water interface arises from the formation of an asphaltenic network structure that strengthens with age. The findings of this study are consistent with their conclusion.

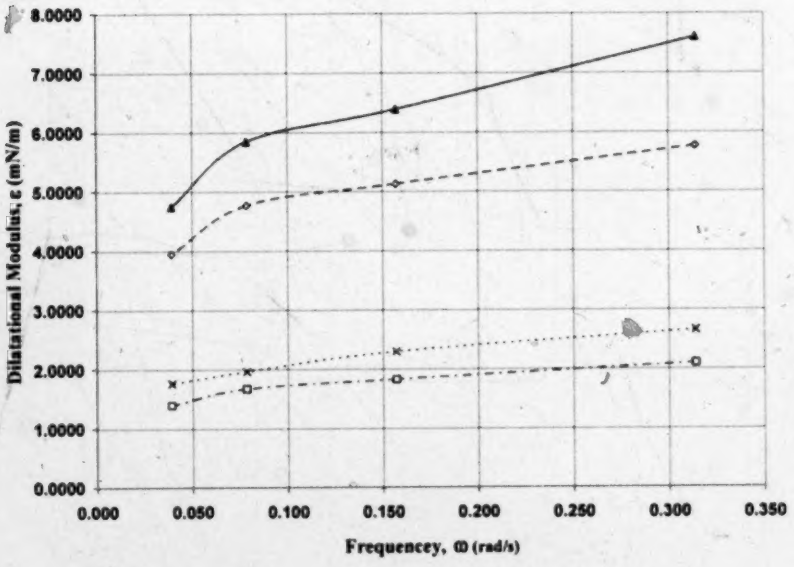

Figure 4-22 Dilatational Modulus versus Frequency, 10wt% Asphaltene Solution (Ages 1hr & 1Day); ▲ Elastic Modulus for 1day; ◊ Elastic Modulus for 1hr; x Viscous Modulus for 1day; □ Viscous Modulus for 1hr

The frequency response of the elastic modulus (ε') and the loss modulus (ε'') are characteristic of relaxation processes that include diffusion exchange (Lucassen et al., 1972), multilayer exchange kinetics (Van den Tempel et al., 1983), and surface

relaxations (i.e. Maxwell response (Monray et al., 1999; Monray et al., 2001)). Freer and Radke (2004) studied the relaxation of asphaltenes at toluene-water interface and concluded that the frequency response fitted a combination of diffusion-exchange and surface-rearrangement mechanisms (i.e. a combination of modified LVDT model and modified Maxwell model).

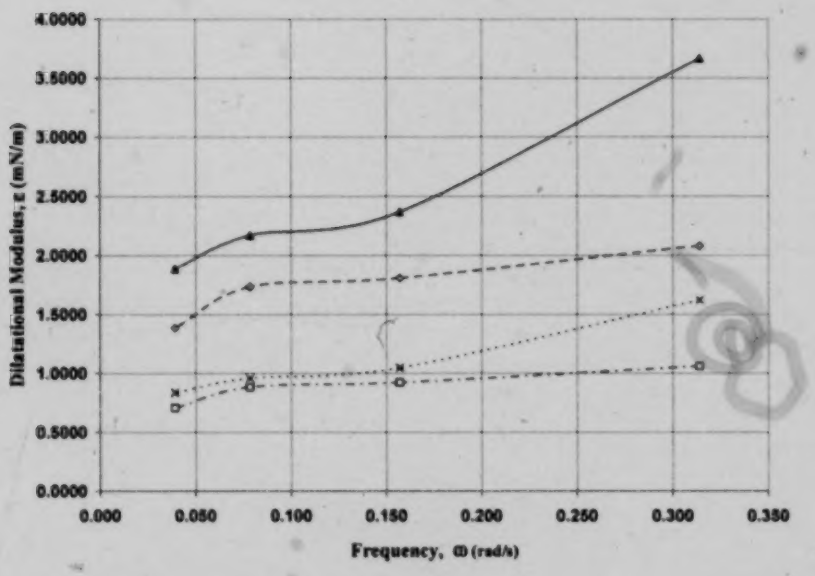

Figure 4-23 Dilatational Modulus versus Frequency, 20wt% Asphaltene Solution (Ages 1hr & 1Day); ▲ Elastic Modulus for 1day; ◊ Elastic Modulus for 1hr; x Viscous Modulus for 1day; □ Viscous Modulus for 1hr

The interfacial loss modulus (ε''), however, is considerably smaller than the interfacial storage modulus ε' for each concentration studied; this is similar to the

findings of Myrvold and Hansen (1998) in their study of proteins, and by Freer et al. (2003) in their study of model crude oil systems.

An important question yet to be answered is why there is an inverse relation (i.e., one decreasing as the other increases) between the measured dilatational moduli and bulk asphaltene concentration in this study (Figures 4-24 to 4-27). Certainly, asphaltene precipitation cannot be a plausible explanation for this trend, as asphaltene is highly solvated in aromatic hydrocarbons such as toluene (McLean and Kilpatrick, 1997). In the paper of Freer and Radke (2004), they demonstrated that smaller asphaltene or resins molecules that can be solvent washed from the interface acted as solubilizers to disrupt asphaltene aggregation at the oil-water interface, resulting in a more tenuous and weaker interfacial network structure. To test the theory of Freer and Radke in this present study, it will be necessary to solvent-wash the interfacial film, followed by dilatational rheological study over a broad experimental time scale (Van den Tempel and Lucassen-Reynders, 1983) and step-strain deformation experiment. Unfortunately, this is just above the limit of this study for the following reasons. First, in the study of Freer and Radke (2004), the continuous phase was toluene-diluted asphaltene solution contained in optical cuvette, while in this study the continuous phase is water contained in optical cuvette. Unlike the experimental setup of this study, the setup of Freer and Radke makes it relatively easy to flush volumes of asphaltene-free toluene (IFT 36mN/m) through the optical cuvette, thereby washing away smaller asphaltene or resins molecules that can be solvent washed from the interface. Second, the period probed in this study is over a narrow

range (20s, 40s, 80s, and 160s) and no step-strain deformation experiment is done. It is, therefore, difficult to demonstrate in this study that indeed smaller asphaltene molecules act as solubilizers to soften the irreversibly adsorbed viscoelastic interfacial network. Nevertheless, the theory of Freer and Radke (2004) can in fact be used to explain the inverse relation of dilatational moduli with bulk asphaltene concentration as it is in agreement with the findings of this study.

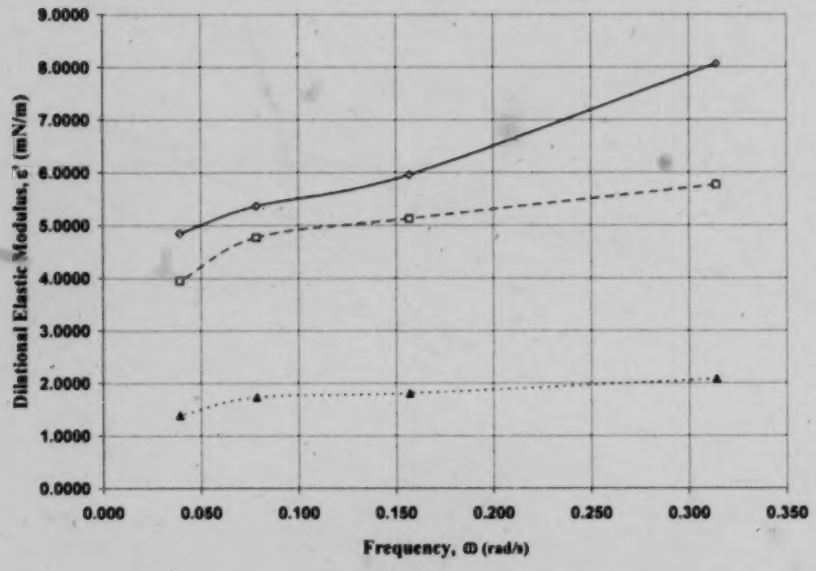

Figure 4-24 Dilatational Elastic Modulus for 1, 10, and 20wt% Asphaltene Solutions (Age 1hr); ◊ Elastic Modulus for 1wt%; □ Elastic Modulus for 10wt%; ▲ Elastic Modulus for 20wt%

In the Freer and Radke (2004) communication, only one single asphaltene concentration was studied. It is speculated here that the number of smaller asphaltene molecules in the bulk increases proportionately with the overall

asphaltene concentration, and hence their solubilizing effect also increases accordingly. This means an interfacial film formed from a more concentrated asphaltene solution will have relatively lower mechanical strength than a film which is formed from a less concentrated asphaltene solution.

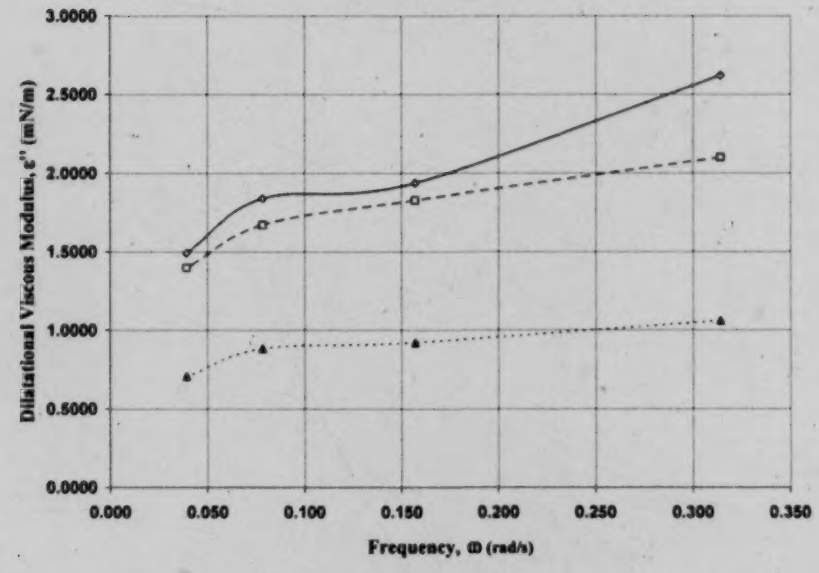

Figure 4-25 Dilatational Viscous Modulus for 1, 10, and 20wt% Asphaltene Solutions (Age 1hr); ◊ Viscous Modulus for 1wt%; □ Viscous Modulus for 10wt%; ▲ Viscous Modulus for 20wt%

It is striking to note the following from Table 4-2: even though the equilibrium IFTs suggest that the oil-water interfaces of the three concentrations have roughly the same amount of interfacial material, the interfaces are rheologically very different.

Therefore, when comparing oil-water interfaces, caution must be taken to not predict interfacial behaviours based on equilibrium IFTs alone.

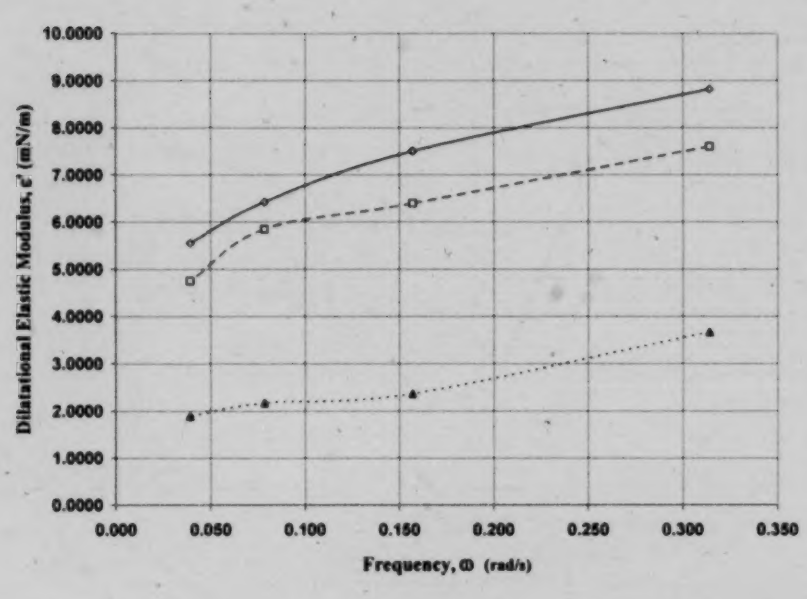

Figure 4-26 Dilatational Elastic Modulus for 1, 10, and 20wt% Asphaltene Solutions (Age 1Day); ◊ Elastic Modulus for 1wt%; □ Elastic Modulus for 10wt%; ▲ Elastic Modulus for 20wt%

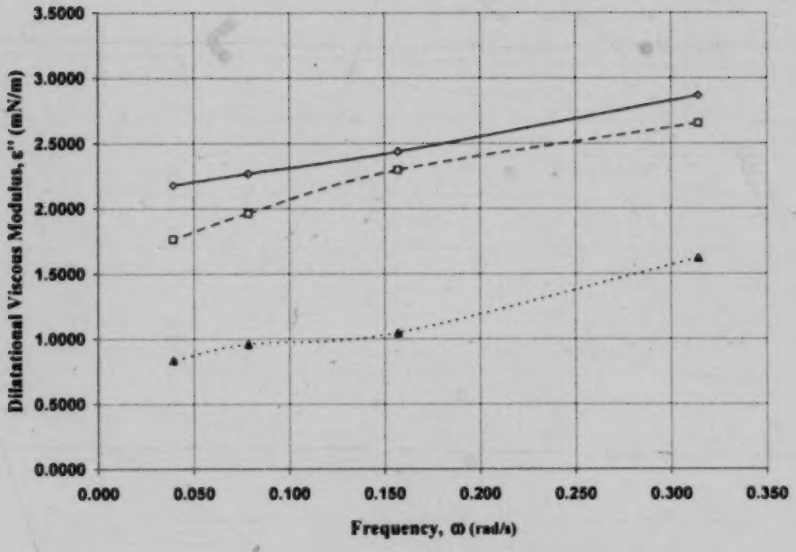

Figure 4-27 Dilatational Viscous Modulus, for 1, 10, and 20wt% Asphaltene Solutions (Age 1Day); ◊ Viscous Modulus for 1wt%; □ Viscous Modulus for 10wt%; ▲ Viscous Modulus for 20wt%

4.4 Bitumen

Here, the interface in question is between water and toluene-diluted bitumen. The static IFT response, dynamic IFT response to sinusoidal area change, as well as the effects of frequency, aging, and concentration on the dilatational moduli for the bitumen system are shown in Figures 4-28 to 4-38 below. The time dependence of IFT shown in Figure 4-28 is likely due to the migration of surface-active materials from the bulk to the oil-water interface.

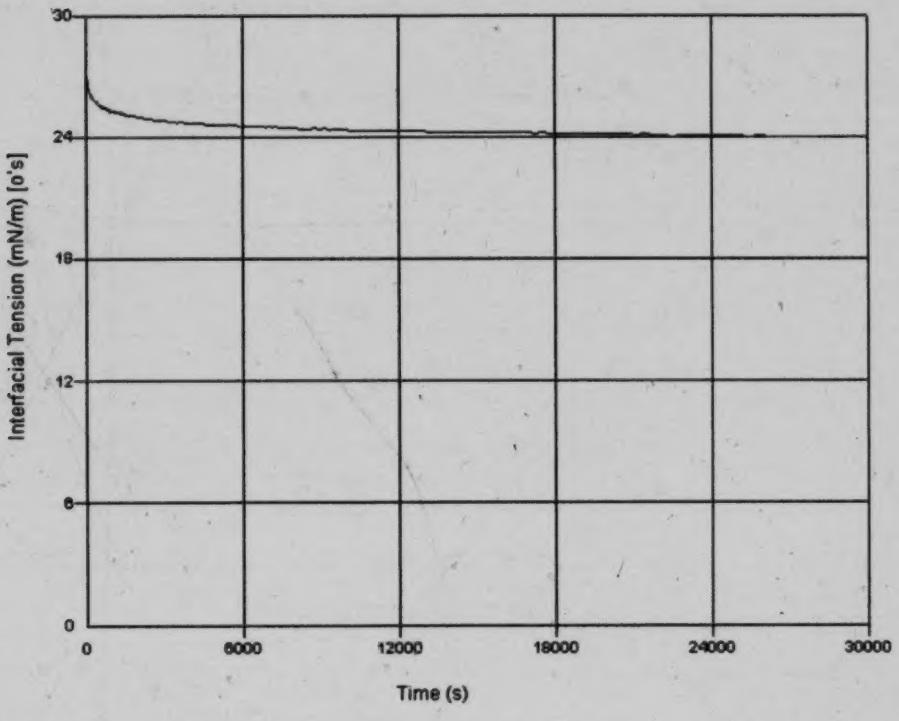

Figure 4-28 Static IFT Response for 5wt% Bitumen Solution

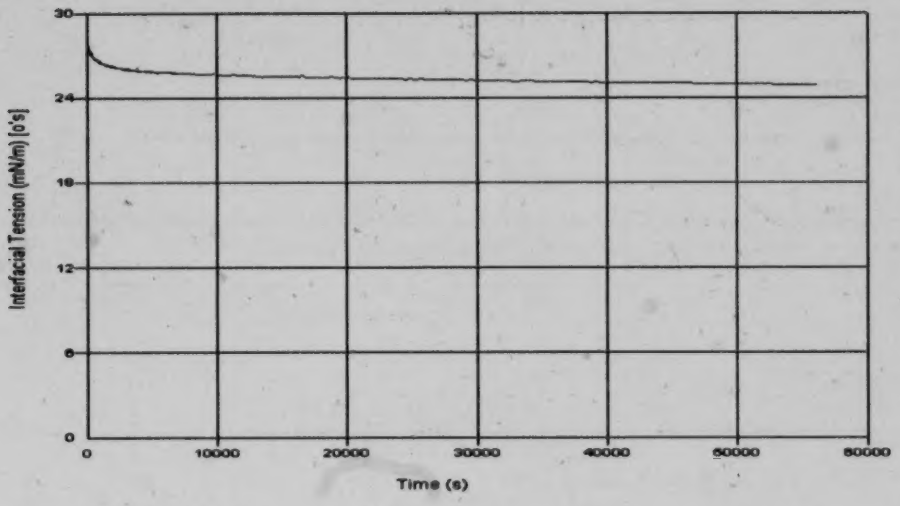

Figure 4-29 Static IFT (continuous line) Response for 15wt% Bitumen Solution

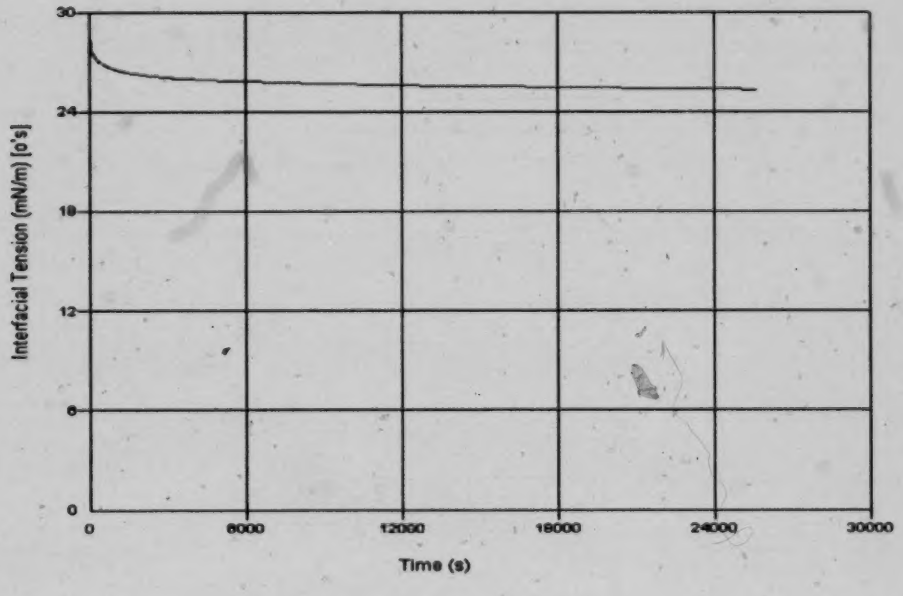

Figure 4-30 Static IFT Response for 30wt% Bitumen Solution

Table 4-3 Equilibrium IFT versus Concentration for Bitumen Solutions

Concentration	Equilibrium IFT
5wt%	24.0
15wt%	24.8
30wt%	25.5

From Table 4-3 and Figures 4-28 to 4-30, we see that the IFT weakly depends on concentration. This has been observed by Yeung et al. (1999) at higher bitumen concentration according to interfacial tension vs. concentration isotherm prepared using heptane/toluene (1:1)-diluted bitumen.

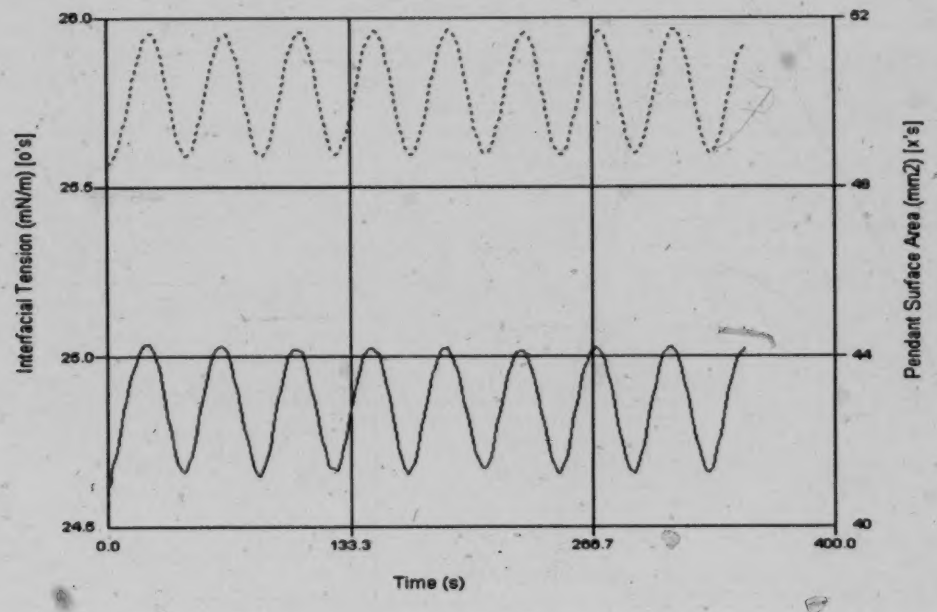

Figure 4-31 IFT (continuous line) Response to Area Change (dash line), 30wt% Bitumen Solution, Period 40s

The variation of dilatational modulus with frequency (Figures 4-32 to 4-34), interfacial aging (Figures 4-32 to 4-34), and concentration (Figures 4-35 to 4-38) follows similar trends as that for asphaltene systems. Since bitumen is a mixture of DAB and asphaltenes, it is perhaps not surprising too see also a phase shift between the IFT response and the sinusoidal area input for the present bitumen system. The phase shift indicates that the interfacial dilatational modulus has elastic and viscous contributions, suggesting internal relaxation processes occurring at the interface.

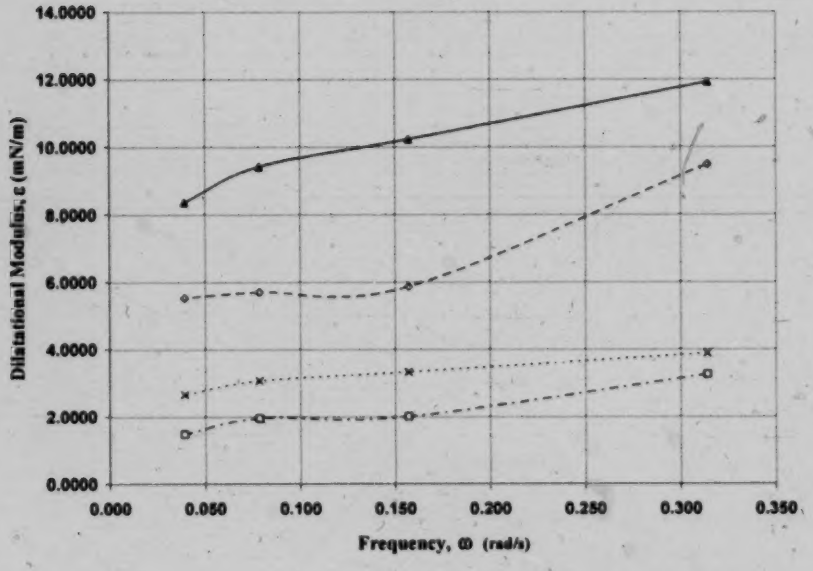

Figure 4-32 Dilatational Modulus versus Frequency, 5wt% Bitumen Solution (Ages 1hr & 1Day); ▲ Elastic Modulus for 1day; ◊ Elastic Modulus for 1hr; x Viscous Modulus for 1day; □ Viscous Modulus for 1hr

Due to the multitude of surface-active agents in bitumen (Wu, 2003), it is probable that there is mixed adsorption of molecules at the oil-water interface. The relaxation process undoubtedly will occur through multiple mechanisms with different characteristic times. Determination of the specific relaxation mechanisms requires the rheological response over a broad experimental time scale (Van den Tempel and Lucassen-Reynders, 1983).

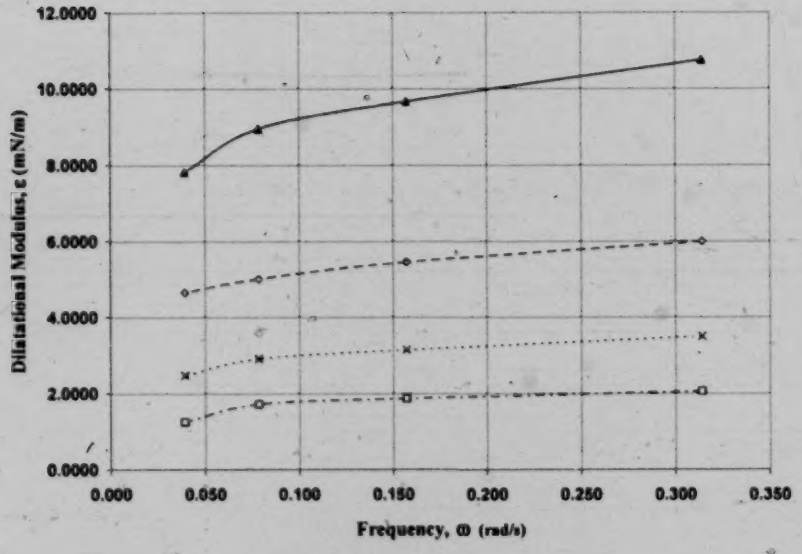

Figure 4-33 Dilatational Modulus versus Frequency, 15wt% Bitumen Solution (Ages 1hr & 1Day); ▲ Elastic Modulus for 1day; ◊ Elastic Modulus for 1hr; x Viscous Modulus for 1day; □ Viscous Modulus for 1hr

The narrow experimental time scale and the lack of step-strain deformation experiment in this work make it difficult, if not impossible, to determine the exact relaxation mechanisms which take place. However, for the de-asphalted component of bitumen, the frequency response is likely to be characteristic of diffusion exchange mechanism. For the other bitumen component (i.e., asphaltenes), Freer and Radke (2004) reported that the frequency response of the dilatational moduli fitted a combination of diffusion-exchange and surface rearrangement mechanisms. Since bitumen is a mixture of the two components, it is probable that the frequency response of the dilatational moduli will fit also a combination of diffusion-exchange and surface rearrangement mechanisms.

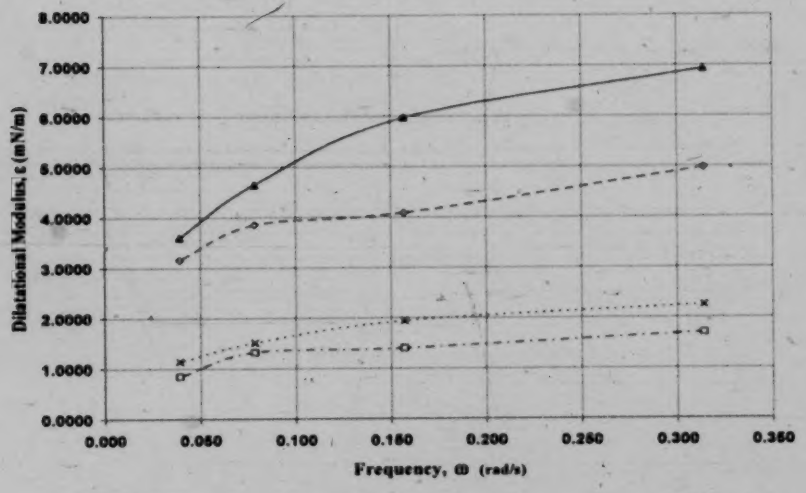

Figure 4-34 Dilatational Modulus versus Frequency, 30wt% Bitumen Solution (Ages 1hr & 1Day); ▲ Elastic Modulus for 1day; ◊ Elastic Modulus for 1hr; x Viscous Modulus for 1day; □ Viscous Modulus for 1hr

As expected, with aging of the drop, the interfacial film shows higher mechanical strength than a relatively fresh interface. This is manifested in higher dilatational moduli for an aged interface than a relatively fresh interface (Figures 4-32 to 4-34).

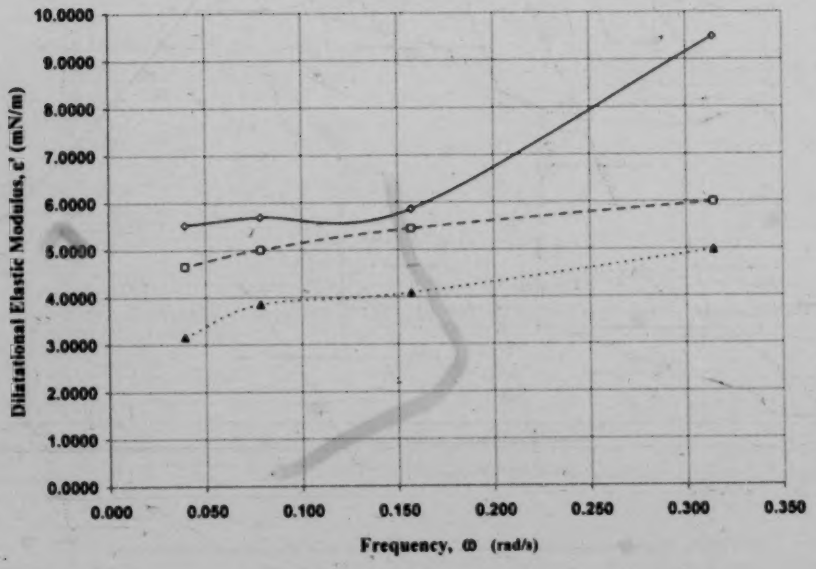

Figure 4-35 Dilatational Elastic Modulus for 1, 15, and 30wt% Bitumen Solutions versus Frequency (Age 1hr); ◊ Elastic Modulus for 5wt%; □ Elastic Modulus for 15wt%; ▲ Elastic Modulus for 30wt%

Similar to DAB and asphaltenes, the dilatational moduli decrease with increasing bitumen concentration (Figures 4-35 to 4-38). This suggests that interfacial films formed from low concentration diluted bitumen have higher mechanical strengths than those formed from high concentration diluted bitumen. This is, however, not

entirely surprising as Yeung et al. (1999) observed a similar trend in their micrometre-sized water droplets in diluted bitumen. Although, the chemistry of their system (using heptane/toluene mixture as solvent) is different from the chemistry of our present system (using toluene as solvent), the general trends are comparable.

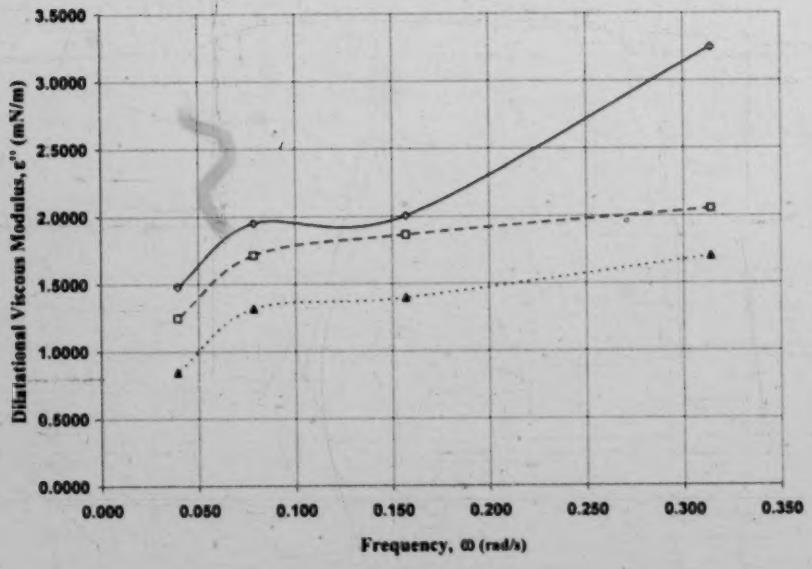

Figure 4-36 Dilatational Viscous Modulus for 1, 15, and 30wt% Bitumen Solutions versus Frequency (Age 1hr); ◊ Viscous Modulus for 5wt%; □ Viscous Modulus for 15wt%; ▲ Viscous Modulus for 30wt%

For instance, in their study, Yeung et al. (1999) observed critical bitumen concentration of approximately 1%, below which the oil-water interface is rigid and water-in-diluted bitumen emulsion is unstable; above this concentration, the interface

is flexible and the water-in-oil emulsion is stable. The critical bitumen concentration in toluene-diluted bitumen has also been determined to be around 1% using the same micropipette technique (Wu, 2003).

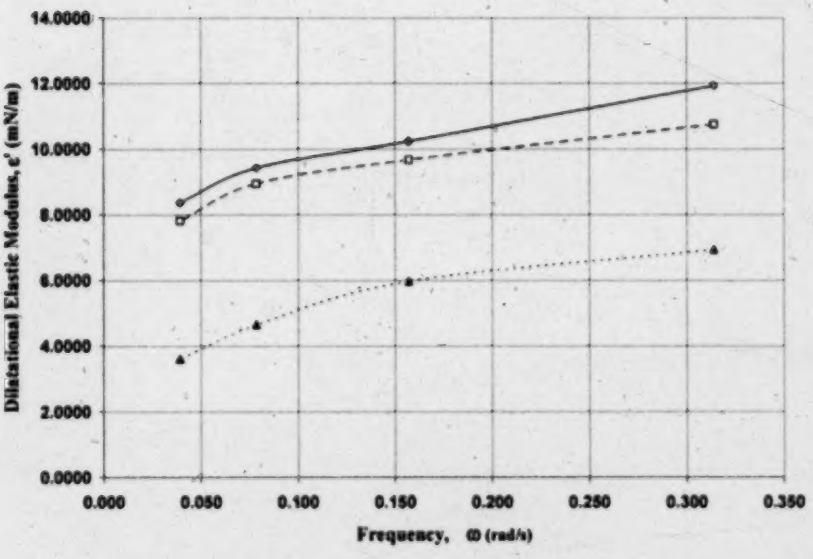

Figure 4-37 Dilatational Elastic Modulus for 1, 15, and 30wt% Bitumen Solutions versus Frequency (Age 1Day); ◊ Elastic Modulus for 5wt%; □ Elastic Modulus for 15wt%; ▲ Elastic Modulus for 30wt%

From the concentrations used, it appears that this study is in the flexible regime; however, the mechanical strength of interfacial films is seen to decrease with increasing bulk concentration of diluted bitumen. In the context of emulsion stability, Yeung et al. (1999) showed that stable emulsions are associated with

flexible rather than rigid interfacial films in diluted bitumen; this is contradictory to literature assertion, which regards rigid interfacial film as an emulsion stabilizer in conventional crude oil systems.

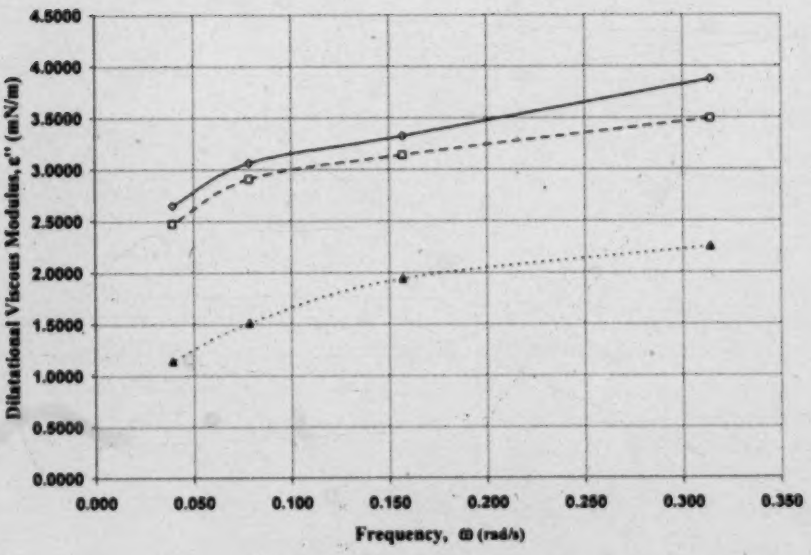

Figure 4-38 Dilatational Viscous Modulus for 1, 15, and 30wt% Bitumen Solutions versus Frequency (Age 1Day); ◊ Viscous Modulus for 5wt%; □ Viscous Modulus for 15wt%; ▲ Viscous Modulus for 30wt%

Drawing on the assertion by Yeung et al. (1999), it can be speculated here that the high concentration diluted bitumen in this study will form more stable emulsions than low concentration diluted bitumen. Two hypothetical mechanisms were proposed by Wu (2003) to explain the interfacial structure of water-diluted bitumen

interface and to explain the inverse relationship between interfacial film mechanical strength and bulk diluted bitumen concentration. One mechanism assumes that the compositional change in interfacial material causes the changes of interfacial properties. The other mechanism assumes that asphaltene precipitation causes the changes in interfacial properties.

According to literature (McLean and Kilpatrick, 1997), the solubility state of asphaltenes plays a pivotal role in the rheological properties of an oil-water interface, regardless of the interfacial composition; however, asphaltene is highly solvated in solvent of high aromaticity such as toluene. Therefore, in toluene-diluted bitumen, the compositional change of interfacial material more likely causes the changes of interfacial properties. Mclean et al. (1997) postulated that asphaltene molecules irreversibly adsorb and cross-link with each other through hydrogen and π-π aromatic ring bonding at the oil-water interface. Wu (2003) proposed that the compositional change and/or the cross-linking of asphaltenes might be hindered in the presence of sodium naphthenates — a resinous species. Indeed, according to many reports, asphaltenes are dispersed in the oil medium by resins; hence, resins hinder the adsorption of asphaltenes at the interface of water-in-crude oil emulsions (Swanson, 1942; Acevedo et al., 1993). Thus, the idea that asphaltenes exist in crude oils as "micelles" or "colloids" dispersed by resins is widely accepted (Pfeiffer and Saal, 1940; Swanson, 1942; Acevedo et al., 1993). Model for these micelles, in which the asphaltenes and resins are located at the centre and periphery, respectively, has been proposed (Pfeiffer and Saal, 1940).

It is, therefore, probable that as bulk bitumen concentration increases, the resin fraction in bitumen also increases, and hence its hindrance effect becomes more pronounced which results in decreasing interfacial mechanical strength.

CHAPTER FIVE

5. CONCLUSIONS AND RECOMMENDATIONS

Surface rheology, using the oscillating pendant drop technique, has been used to probe qualitatively and quantitatively the mechanical strength of interfacial films formed when a droplet of model oil (toluene-diluted de-asphalted bitumen, toluene-diluted asphaltene, and toluene-diluted bitumen) is in contact with pre-equilibrated water.

For three concentrations and four frequencies of the sinusoidal excitations on the interfacial area studied, it is concluded that: the complex dilatational modulus increases with frequency and ageing of interfacial film, but decreases with increasing bulk concentration. Also, the phase angle between the sinusoidal area input and the sinusoidal interfacial tension response for de-asphalted bitumen (DAB) is approximately zero. This suggests that, for the frequencies probed, no relaxation processes (tending to reduce deviations of the surface tension from its equilibrium value) occurred with a characteristic time comparable to the time scale of the experiment. There is, however, an obvious phase shift between the sinusoidal area input and the sinusoidal IFT response for asphaltenes and diluted bitumen within the linear viscoelastic regime.

For asphaltenes, it is conceivable that the smaller molecular weight asphaltenes might be responsible for the inverse relation of dilatational elastic moduli with concentration. For diluted bitumen, it is believed that resins are responsible for the

inverse relation of dilatational elastic moduli with concentration; little is known about the inverse relation of dilatational elastic moduli with concentration for DAB and will be the object of future work. Also wide frequency range is recommended for future work.

6. REFERENCES

Acevedo, S.; Escobar, G.; Gutierrez, L. B.; Rivas, H. and Gutierrez, X. (1993), "Interfacial Rheological Studies of Extra-Heavy Crude Oils and Asphaltenes: Role of the Dispersion Effect of Resins in the Adsorption of Asphaltenes at the Interface of Water-in-Crude Oil Emulsions", *Colloids and Surfaces A: Physicochemical and Engineering Aspects, Vol. 71,(1)*, pp. 65-71.

Acevedo, S.; Ranaudo, M. A.; Escobar, G. and Gutierrez, X. (1998), "Dynamic Interfacial Tension Measurement of Heavy Crude Oil-Alkaline Systems: The Role of the Counterion in the Aqueous Phase", *Fuel, Vol. 78*, pp. 309-317.

Adamson, A. W. (1967); *Physical Chemistry of Surfaces*, John Wiley & Sons, New York, NY, USA pp. 9-42.

Adamson, A. W. (1976); *Physical Chemistry of Surfaces*, John Wiley & Sons, New York, NY, USA pp. 1-6, 47-98.

Anderson, S. I., Birdi, K. S., (1991) " Aggregation of Asphaltenes as Determined by Calorimetry" *Journal of Colloid and Interface Science, Vol. 141*, pp. 497-502.

Aske, N.; Orr, R.; Sjoblom, J.; (2002), "Dilatational Elasticity Moduli of Water-Crude Oil Interfaces Using the Oscillating Pendant Drop" *Journal of Dispersion Science and Technology, Vol. 23, (6),* pp. 809-825.

Bartell, F. E.; Neiderhauser, D. O. (1949); "Film Forming Constituents of Crude Petroleum Oils", *Fundamental Research on Occurrence and Recovery of Petroleum, API, Vol. 57*, pp. 1946-1947.

Bendure R. L. (1971), "Dynamic Surface Tension Determination with the Maximum Bubble Pressure Method", *J. Colloid Interface Sci. Vol. 35(2)*, pp. 238-248.

Beverung, C. J., Radke, C. J. and Blanch, H. W. (1999), "Protein Adsorption at the Oil/Water Interface: Characterization of Adsorption Kinetics by Dynamic Interfacial Tension Measurements", *Biophysical Chemistry, Vol. 81*, pp. 59-80.

Bird, B. R., Stewart, W. E., Lightfoot, E. N., (2002), *Transport Phenomena, 2nd Ed.*, John Wiley & Sons, Inc., NY, NY, USA, pp. 98

Bland, D. R; (1960), *The Theory of Linear Viscoelasticity,* Pergamon Press Inc., New York, NY, USA, pp. 114

Boussinesq, J. (1913), Sur l'existence d'une viscosite superficielle, dans la mince couche de transition separant un liquide d'un autre fluide contgu. "Annales de

Chemie et de Physique, Huiteme Serie, 24, 349-357; Boussinesq, J. (1913), "Application des formulas de viscosite superficielle a la surface d'une goute liquide spherique, tombant lentement, d'un movement devenu uniforme, au sien d'une masse fluide indefinite en physique, Huiteme Series", 24, 357-371.

Boyce, J. F., Schurch, S., Rotenberg, Y., Neumann, A. W., (1984) "The Measurement of Surface and Interfacial-Tension by the Axisymmetric Drop Technique" *Colloids and Surfaces, Vol. 9(4)*, pp. 307-317.

Cambridge, V. J., Wolcott, J. M. and Constant, D. W. (1989), "An Investigation of the Factors Influencing Transient Interfacial Tension Behaviour in Crude Oil/Alkaline Water Systems", *Chem. Eng. Comm., Vol. 84*, pp. 97-111.

Cheng, P., Li., D., Boruvka, L., Rotenberg, Y., Neumann, A. W., (1990) "Automation of Axisymmetric Drop Shape-Analysis for Measurement of Interfacial-Tensions and Contact Angles" *Colloids and Surfaces, Vol. 43(2-4)*, pp. 151-167.

Cheng, P., Neumann, A. W., (1992) "Computational Evaluation of Axisymmetric Drop Shape Analysis-Profile (ADSA-P)" *Colloids and Surfaces, Vol. 62(4)*, pp. 297-305.

Czarnecki, J. (2001), "Water-in-oil Emulsions in Recovery of Hydrocarbons from Oil Sands", *Encyclopedic Handbook of Emulsion Technology (J. Sjoblom, Ed.)* Marcel Dekker, New York, NY, USA pp. 497-514.

De Laplace, P. S. (1806), *Mechanique Celeste*, Suppliement to Book 10.

Dodd, C. G. (1960), "The Rheological Properties of Films at Crude Petroleum-Water Interfaces", *Journal of Physical Chemistry, Vol. 64*, pp. 544-550.

Drelich, J., Hupka, J., Miller, J. D. and Hanson, F. V. (1992), "Water Recycle in Moderate-Temperature Bitumen Recovery from Whiterocks Oil Sands", *AOSTRA Journal of Research, Vol. 8*,139-147.

Edwards, D. A., Wasan, D. T. and Brenner, H. (1991), *Interfacial Transport Processes and Rheology*, Butterworth-Heinemann, Boston, MA, USA Chapter 4.

Evan E. and Skalak R. (1980), *Mechanics and Thermodynamics of Biomembranes*, CRC, Boca Raton, Fla., 254pp.

Evans, E. A. and Skalak, R. (1980), "Mechanics and Thermodynamics of Bio-Membranes", *Boca Raton, FL*, CRC.

Freer, E. M. and Radke, C. J. (2004), "Relaxation of Asphaltenes at the Toluene/Water Interface: Diffusion Exchange and Surface Rearrangement", *Journal of Adhession, Vol. 80(6)*, pp. 481-496.

Freer, E. M., Svitova, T. and Radke, C. J. (2002), "The Role of Interfacial Rheology in Reservoir Mixed Wettability", *Journal of Petroleum Science and Engineering, Vol. 39*, pp. 137-158.

Gray, M. R. (1994), *Upgrading Petroleum Residues and Heavy Oils*, Marcel Dekker, New York, NY, USA 348pp.

Iliev, T. H. and Dushkin, C. D. (1992), "Dynamic Surface-Tension of Micellar Solutions Studied by the Maximum Bubble Pressure Method 1. Experiment", *Colloid Polym. Sci. Vol. 270*, pp. 370-376.

Jeribi, M., Almir-Assad, B., Langevin, D., Henaut, I. and Argillier, J. F. (2002), "Adsorption Kinetics of Asphaltenes at Liquid Interfaces", *Journal of Colloid and Interface Science, Vol. 256*, pp. 268-272.

Jewell, D. M., Albaugh, E. W., Davis, B. E. and Ruberto, R. G. (1974), "Integration of Chromatographic and Spectroscopic Techniques for the Characterization of Residual Oils", *Ind. Eng. Chem. Fund, Vol. 13*, pp. 278-568.

Kimbler, O. K., Reed, R. L., and Silberberg, I. H. (1966), "Physical Characteristics of Natural Films Formed at Crude Oil-Water Interfaces", *Soc. Petr. Eng. J., Vol. 6*, pp. 153-165.

Kloubek J. (1972), "Measurement of the Dynamic Surface Tension by the Maximum Bubble Pressure Method II. Calculation of the Effective Age of the Solution-Air Interface", *J. Colloid Interface Sci. Vol. 41(1)*, pp. 1-6.

Kovscek, A. R., Wang, H. and Radke, C. J. (1993), "A Pore-Level Scenario for the Development of Mixed Wettability in Oil Reserviors", *AIChe J., Vol. 39(6)*, pp. 1072-1085.

Li, J. B., Zhang Y., Yan, L. L., (2001), "Multilayer formation on a curved drop surface", *Angewandte Chemie-International Edition, 40(5)*, pp. 891-894.

Lucassen, J., Van den Tempel, M., (1972) "Dynamic Measurements of Dilational Properties of a Liquid Interface", *Chemical Engineering Science, Vol. 27, (6)*, pp. 1283-1291.

Lucassen, J.; Hansen, R. S.; (1967) "Damping of Waves on Monolayer-Covered Surfaces II. Influence of Bulk-to-Surface Diffusional Interchange on Ripple Characteristics", *Journal of Colloid and Interface Science, Vol. 23*, pp. 319-328.

McLean, J. D. and Kilpatrick, P. K. (1997a), "Effects of Asphaltene Solvency on Stability of Water-in-Crude-Oil Emulsions", *Journal of Colloid Interface Science, Vol. 189*, pp. 242-253.

McLean, J. D. and Kilpatrick, P. K. (1997b), "Effects of Asphaltene Aggregation in Model Heptane-Toluene Mixtures on Stability of Water-in-Oil Emulsion", *Journal of Colloid Interface Science, Vol. 196*, pp. 23-34.

Mohammed, R. A., Bailey, A. I., Luckham, P. F. and Taylor, S. E. (1993), "Dewatering of Crude Oil Emulsions: 1. Rheological Behaviour of the Crude Oil-Water Interface", *Colloids and Surfaces A: Physicochemical and Engineering Aspects, Vol. 80*, pp. 223-235.

Mohammed, R. A., Bailey, A. I., Luckham, P. F. and Taylor, S. E. (1994), "The Effect of Demulsifiers on the Interfacial Rheology and Emulsion Stability of Water-in-Crude Oil Emulsions", *Colloids and Surfaces A: Physicochemical and Engineering Aspects, Vol. 91*, pp. 129-139.

Monroy, F., Ortega, F., Rubio, R. G., (1999) "Rheology of a Miscible Polymer Blend at the Air-Water Interface. Quasielastic Surface Light Scattering Study and Analysis in terms of Static and Dynamic Scaling Laws" *journal of Physical Chemistry B, Vol. 103, (12)*, pp. 2061-2071.

Monroy, F., Rivillon, S., Ortega, F., Rubio, R. G., (2001) "Dilational Rheology of Langmuir Polymer Monolayers: Poor-solvent conditions" *Journal of Chemical Physics" Vol. 115, (1),* pp. 530-539.

Morrison, F. A. (2001), *Understanding Rheology*, Oxford University Press, New York, USA, Chapter 8.

Mysels, K. J. (1986), "Improvements in Maximum-Bubble-Pressure Method of Measuring Surface Tension", *Langmuir, Vol. 2*, pp. 428-432.

Neustadter, E. L., Whittingham, K. P. and Graham, D. E. (1979), "Interfacial Rheological Properties of Crude Oil/Water Systems", *Shah, D. O. (Ed.), Surface Phenomenon in Enhanced Oil Recovery*, Plenum Press, New York, NY, USA, pp. 307-326.

Pfeiffer, J. P; Saal, R. N. J; (1940), "Asphaltic Bitumen as Colloid System", *Journal of Physical Chemistry, Vol. 44, (2),* pp. 139-149.

Plateau, J. (1869), Recherche's Experimental et Theoriques sur les fiqures d'equilibre d'une masse liquide sans pesanteur, 8^{e} Serie. "Annales de Chimie et de Physique, Quatrieme Serie", 17, 260-276; Plateau, J. (1869), "Experimental and Theoretical Researches into the Figures of Equilibrium of a Liquid Mass without Weight, Eight Series. Phil. Mag., Fourth Series, 38, 445-455.

Precht P. and Rokosh C. (1998), "Oil Sands Development in Alberta: The New Paradigm", 7th UNITAR International Conference on Heavy Crude and Tar Sands, October 27-30.

Reisberg, J. and Doscher, T. M. (1956), "Interfacial Phenomenon in Crude-Oil-Water Systems", *Producers Monthly, Vol. 21(1)*, pp. 43-50.

Rogel, E., Leon, O., Torres, G., Espidel, J., (2000) "Aggregation of Asphaltenes in Organic Solvents Using Surface Tension Measurements", *Fuel, Vol. 79*, pp. 1389-1394.

Rotenberg, Y., Boruvka, L., Neumann, A. W., (1983) "Determination of Surface-Tension and Contact-Angle from the Shapes of Axisymmetric Fluid Interfaces" *Journal of Colloid and Interface Science, Vol. 93*, pp. 169-183.

Speight, J. G. (1991), *The Chemistry and Technology of Petroleum, 2nd Ed.*, Marcel Dekker, New York, NY, USA 760pp.

Spiecker, M. P., Kilpatrick, P. K., (2004), "Interfacial Rheology of Petroleum Asphaltenes at the Oil-Water Interface", *Langmuir, Vol. 20*, pp. 4022-4032.

Strassner, J. E. (1968), "Effects of pH on Interfacial Films and Stability of Crude Oil-Water Emulsions", *Journal of Petroleum Technology, Vol. 20*, pp. 303-312.

Strausz, O. P; Peng, P; Murgich, J; (2002), "About the Colloidal Nature of Asphaltenes and the MW of Covalent Monomeric Units" *Energy & Fuels, Vol. 16 (4)*, pp. 809-822.

Susnar, S. S., Chen, P., del Rio, O. I. and Neumann, A. A. (1996), "Surface Tension Response to Area Changes Using Axisymmetric Drop Shape Analysis", *Colloids and Surfaces A: Physicochemical and Engineering Aspects, Vol. 116*, pp. 181-194.

Susnar, S. S., Hamza, H. A. and Neuman, A. W. (1993), "Pressure Dependence of Interfacial Tension of Hydrocarbon-Water Systems Using Axisymmetric Drop Shape Analysis", *Colloids and Surfaces A: Physicochemical and Engineering Aspects, Vol. 89*, pp. 169-180.

Swanson, J. M; (1942), "A contribution to the Physical Chemistry of the Asphalt", *Journal of Physical Chemistry, Vol. 46, (1)*, pp. 141-150.

Taber, J. J. (1981), *Surface Phenomena in Enhanced Oil Recovery*, Plenum Press, New York, NY, USA pp. 13-52.

Tschoegl, N. W. (1989), *The Phenomenological Theory of Linear and Viscoelastic Behaviour: An Introduction, Springer-Verlag, Berlin*, Chap. 8, pp. 413-415.

Tschoegl, N. W. (1989), *The Phenomenological Theory of Linear Behaviour: An Introduction, Springer-Verlag, Berlin*, pp. 413-415.

Van den Tempel, M., Lucassen-Reynders, E. H., (1983) "Relaxation processes at fluid interfaces", *Advances in Colloid and Interface Science, Vol. 18, (3-4)* pp. 281-301.

Van den Tempel, M.; Lucassen-Reynders, E. H; (1983) "Relaxation processes at fluid interfaces", *Advances in Colloid and Interface Science, Vol. 18,* pp. 281-301.

Wantke, K. D., Fruhner, H., Fang, J., Lunkenheimer, K., (1998) "Measurement of the Surface Elasticity in Medium Frequency Range Using the Oscillating Bubble Method" *Journal of Colloid and Interface Science, Vol. 208*, pp. 34-48.

Ward, A. J. I. and Regan, L. H. (1980), "Pendant Drop Studies of Adsorbed Films of Bovine Serum Albumin", *Journal of Colloid and Interface Science, Vol. 78*, pp. 389-394.

Wiehe, L. A. and Liang, K. S. (1996), "Asphaltenes, Resins and Other Petroleum Macromolecules", *Fluid Phase Equilibria, Vol. 117*, 201.

Wong, H.; Rumschitzki, D.; Maldarelli, C.; (1998), "Theory and experiment on the low-Reynolds-number expansion and contraction of a bubble pinned at a submerged tube tip", *Journal of Fluid Mechanics, Vol. 356,* pp. 93-124.

Wu, X.; (2003), "Investigating the Stability Mechanism of Water-in-Diluted Bitumen Emulsions through Isolation and Characterization of the Stabilizing Materials at the Interface" *Energy fuels, Vol. 17, (1),* pp. 179-190.

Xu, Y. (1994), "Dynamic Interfacial Tension Between Bitumen and Aqueous Sodium Hydroxide Solutions", *Energy and Fuels, Vol. 9,* pp. 148-154.

Yan, Z; Elliott, J. A. W; Masliyah, J. H; (1999), "Roles of Various Bitumen Components in the Stability of Water-in-Diluted-Bitumen Emulsions", *Journal of Colloids and Interface Science, Vol. 220,* pp. 329-337.

Yeung, A., Dabros, T. and Masliyah, J. (1998), "Does Equilibrium Interfacial Tension Depend on Method of Measurement?" *Journal of Colloid and Interface Science, Vol. 208,* pp. 241-247.

Yeung, A; Dabros, T; Czarnecki, J; Masliyah, J; (1999), "On the interfacial properties of micrometer-sized water droplets in crude oil", *Proceedings of the Royal Society of London, Vol. 455,* pp. 3709-3723.

Young, T. (1855), *Miscellaneous Works*, (G. Peacock Ed.), J. Murray, London, Vol. 1, pp. 418.

Zhang, L. Y., Xu, Z., Masliyah, J. H (2003), "Langmuir and Langmuir-Blodgett Films of Mixed Asphaltene and a Demulsifier", *Langmuir, Vol. 19*, pp. 9730-9741.

7. APPENDIX A

7.1 Derivation of Young - Laplace Equation from Force Balance

Consider small piece of curved interface with dimensions L_1 and L_2

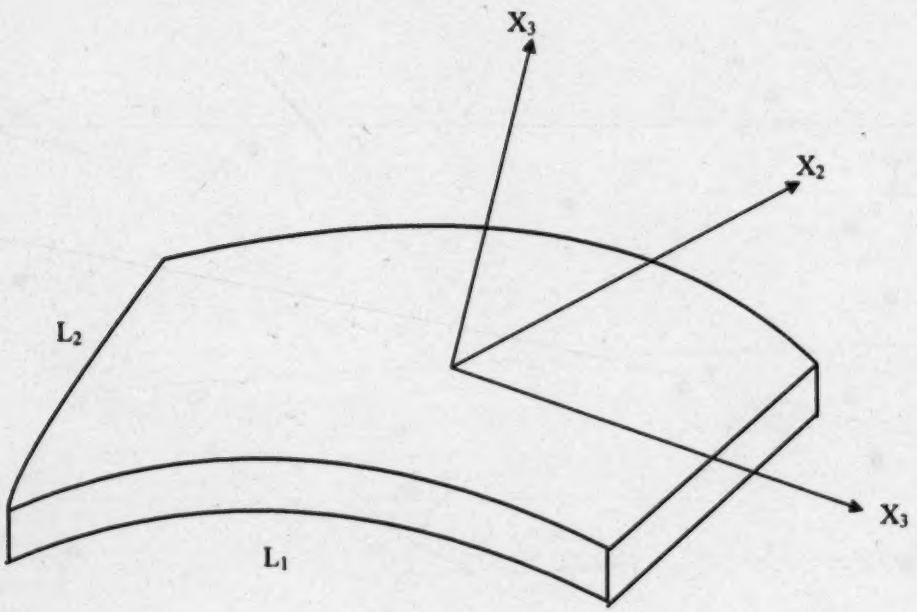

External stresses (N/m^2) on the interface are

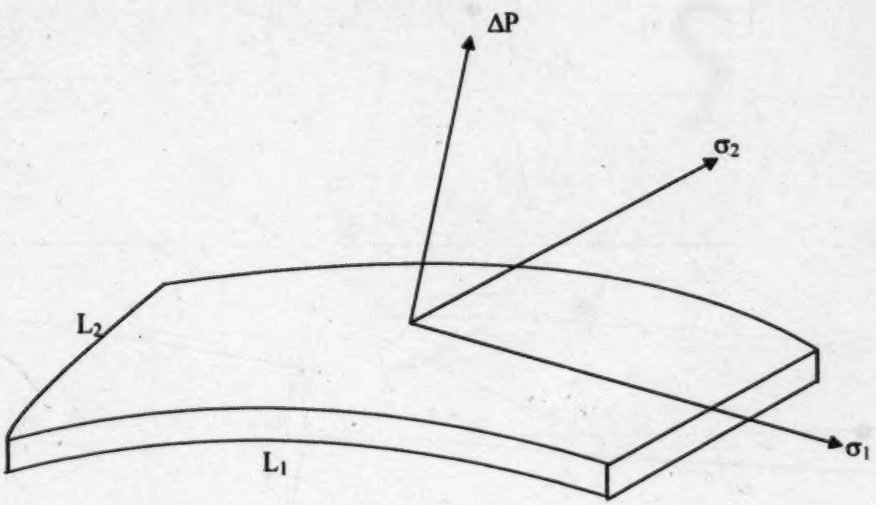

Where, σ_1 and σ_2 are the shear stresses. The actual forces are $\Delta P * L_1L_2$, $\sigma_1 * L_1L_2$, $\sigma_2 * L_1L_2$

No flow at the interface means $\sigma_1 = \sigma_2 = 0$

⇒ Balance forces only in the normal (X_3) direction. Consider X_1-X_3 projections:

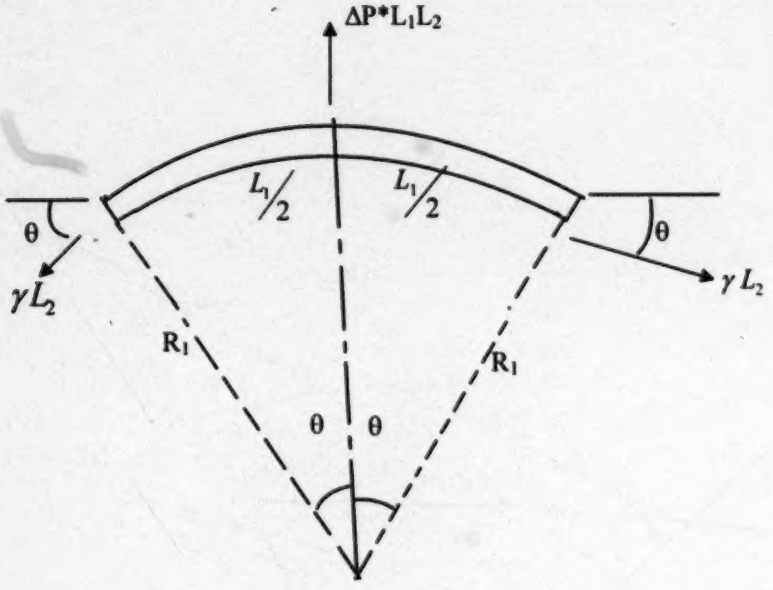

When $L_1/R_1 <<< 1$, $\theta \approx \frac{L_1/2}{R_1} = \frac{L_1}{2R_1}$

Note that interfacial tension (IFT) force is always tangent to the surface. Partial force balance gives:

$$\Delta P\, L_1 L_2 = 2(\gamma\, L_2 Sin\theta) \approx 2\gamma\, L_2 \sin\theta = 2\gamma\, L_2 \left(L_1/2R_1\right) = \gamma\, L_1 L_2/R_1$$

$$\Rightarrow \quad \Delta P\, L_1 L_2 = \frac{\gamma L_1 L_2}{R_1} + \text{ term from } X_2 - X_3 \text{ projections}$$

From similar analysis the extra term from X2 –X3 projection is $\gamma L_1 L_2 / R_2$.

Therefore, total force balance force balance is given by:

$$\Rightarrow \quad \Delta P\, L_1 L_2 = \frac{\gamma L_1 L_2}{R_1} \cdot \frac{\gamma L_1 L_2}{R_2}$$

$$\Rightarrow \quad \Delta P = \gamma\left(\frac{1}{R_1} + \frac{1}{R_2}\right)$$ This is the Young-Laplace equation.

8. APPENDIX B

8.1 De-asphalted Bitumen (DAB)

8.1.1 Graphs of IFT Response to Sinusoidal Area Input for 1wt% DAB Solution

The solid line is the sinusoidal interfacial tension response and the dash line is the sinusoidal area input.

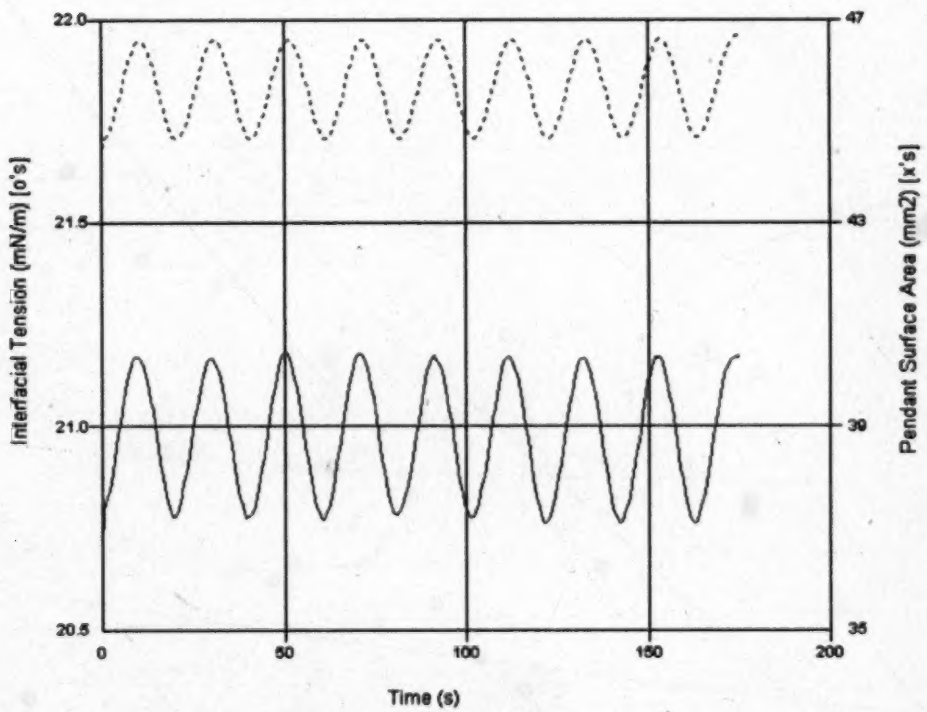

Figure 8-1 IFT (solid line) Response to Area Change (dash line), 1wt% DAB Solution, Period 20s (Age 1hr)

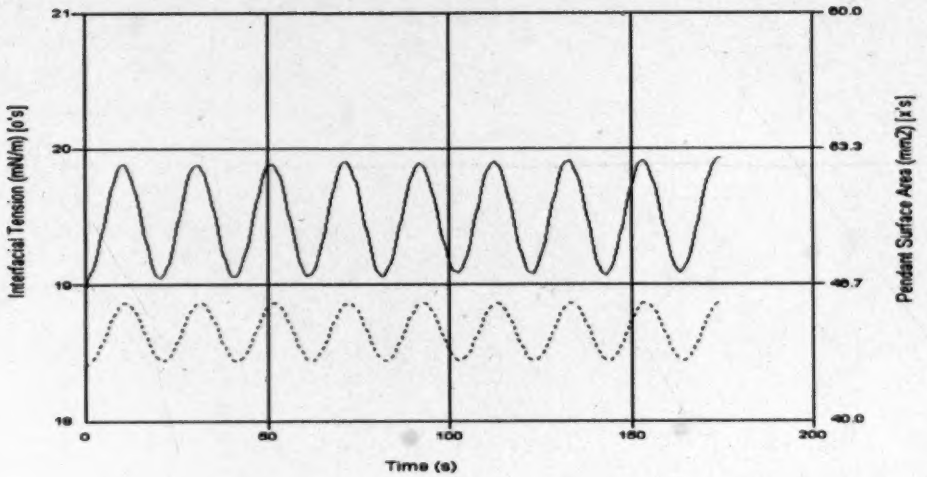

Figure 8-2 IFT Response to Area Change, 1wt% DAB Solution, Period 20s (Age 1Day)

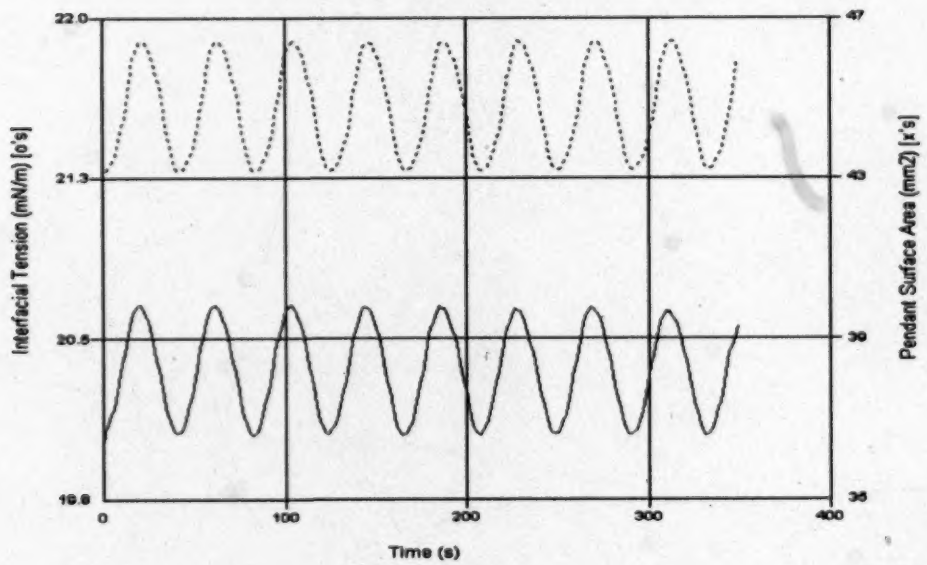

Figure 8-3 IFT (solid line) Response to Area Change (dash line), 1wt% DAB Solution, Period 40s (Age 1hr)

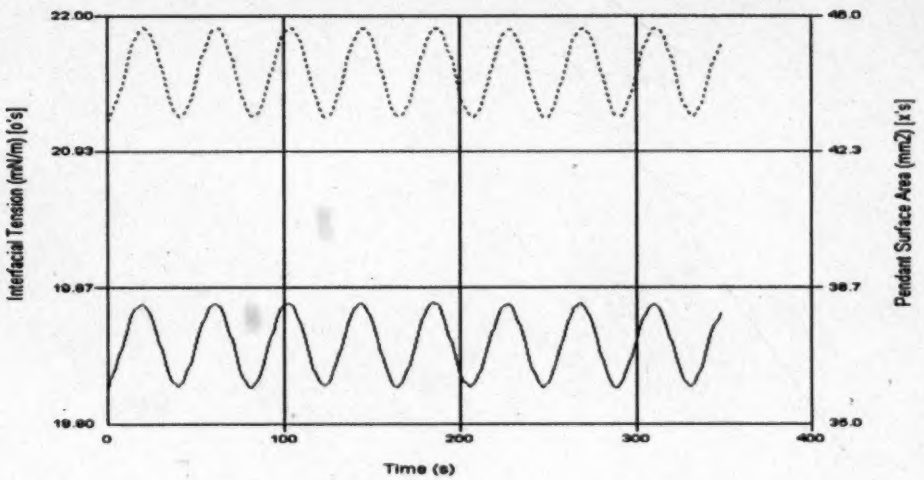

Figure 8-4 IFT (solid line) Response to Area Change (dash line), 1wt% DAB Solution, Period 40s (Age 1Day)

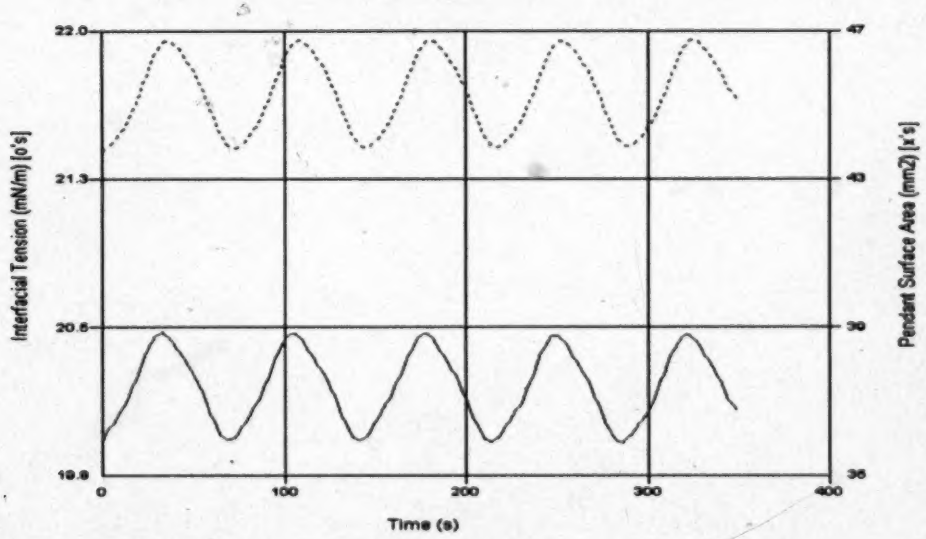

Figure 8-5 IFT (solid line) Response to Area Change (dash line), 1wt% DAB Solution, Period 80s (Age 1hr)

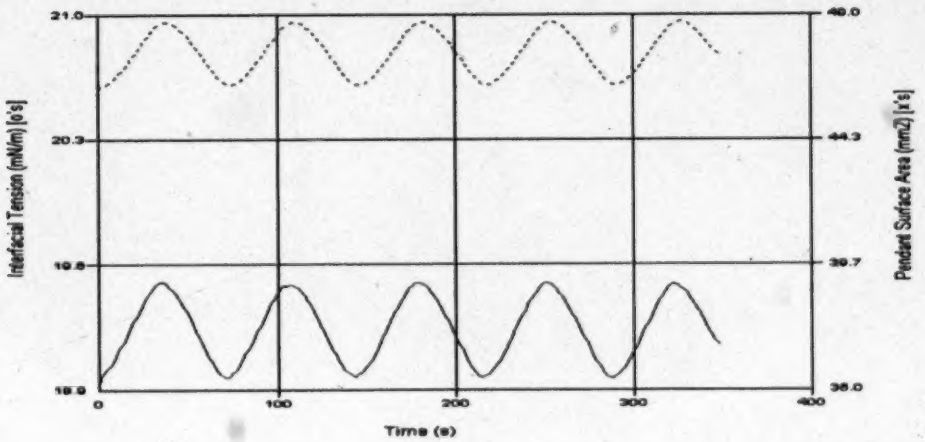

Figure 8-6 IFT (solid line) Response to Area Change (dash line), 1wt% DAB Solution, Period 80s (Age 1Day)

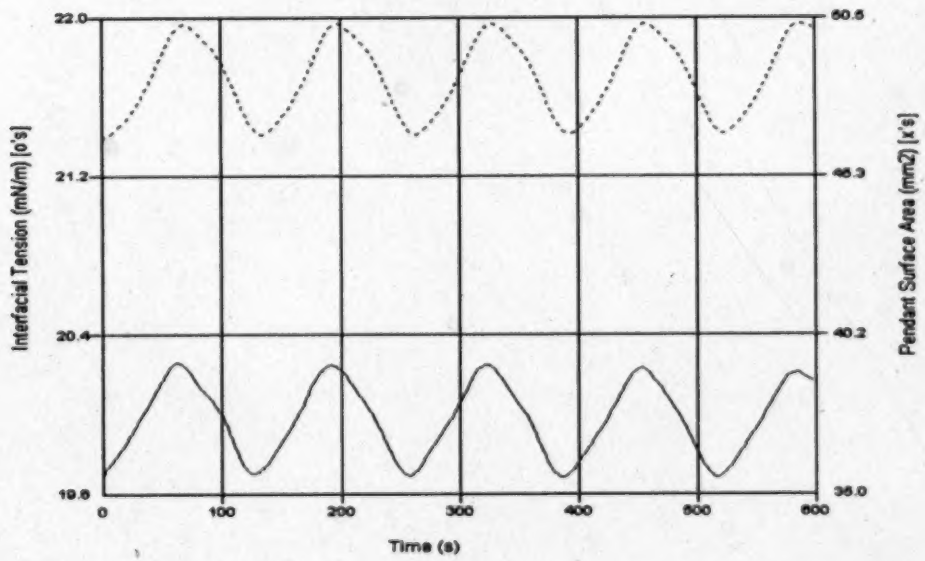

Figure 8-7 IFT (solid line) Response to Area Change (dash line), 1wt% DAB Solution, Period 160s (Age 1hr)

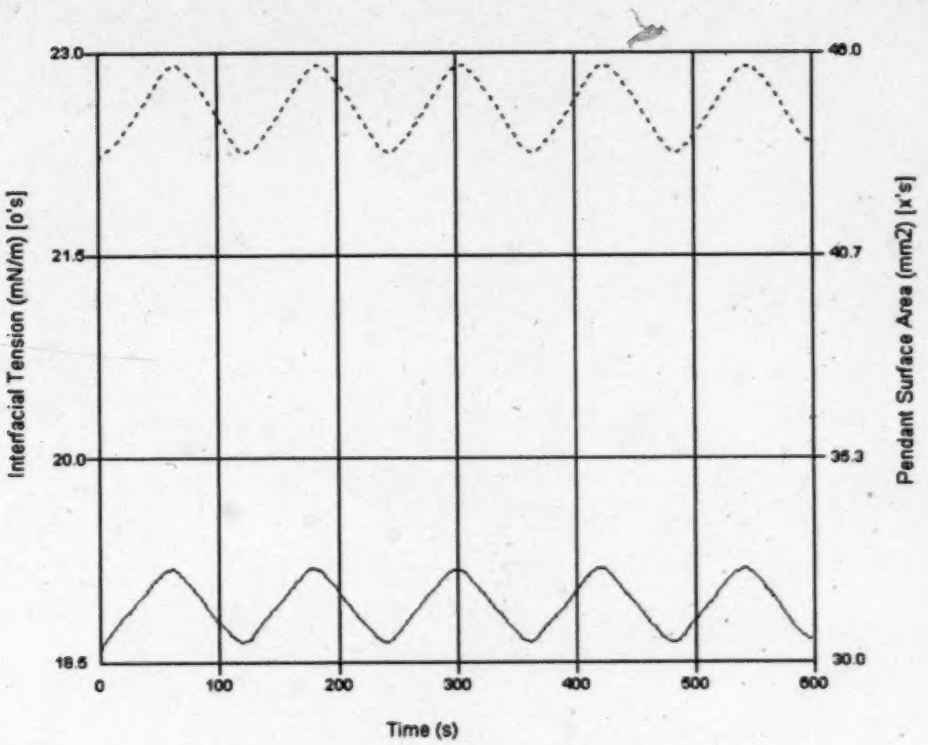

Figure 8-8 IFT (solid line) Response to Area Change (dash line), 1wt% DAB Solution, Period 160s (Age 1Day)

8.1.2 Graphs of IFT Response to Sinusoidal Area Input for 10wt% DAB Solution

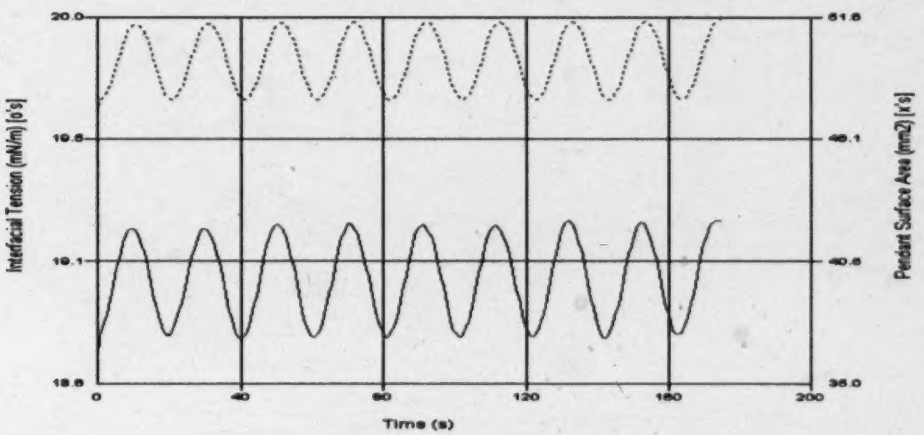

Figure 8- IFT (solid line) Response to Area Change (dash line), 10wt% DAB Solution, Period 20s (Age 1hr)

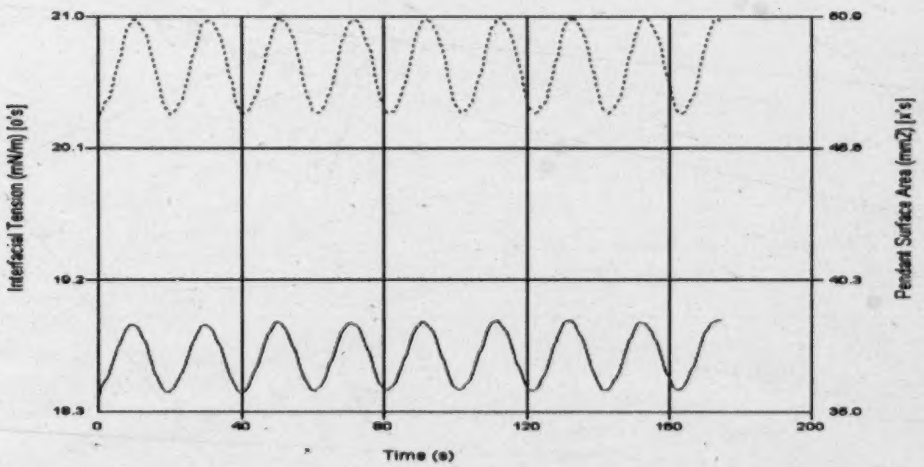

Figure 8-9 IFT (solid line) Response to Area Change (dash line), 10wt% DAB Solution, Period 20s (Age 1Day)

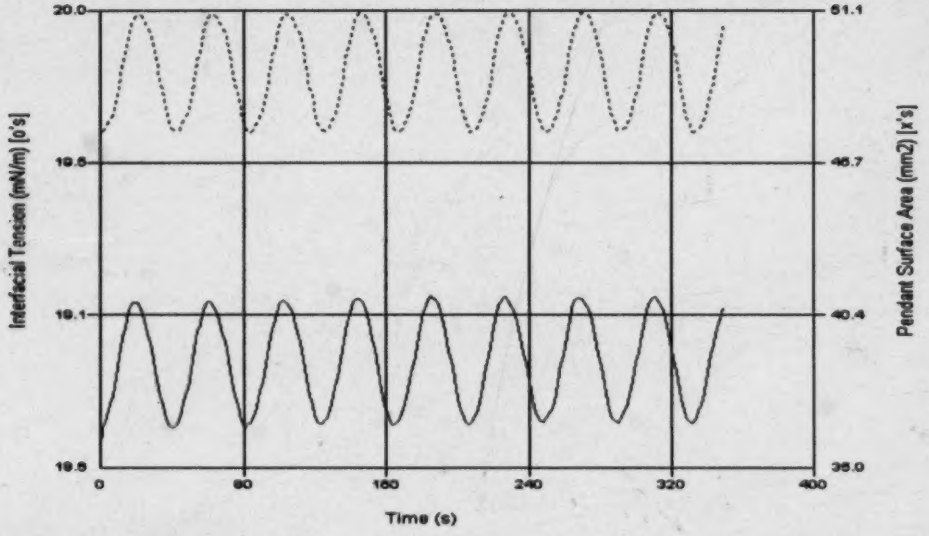

Figure 8-10 IFT (solid line) Response to Area Change (dash line), 10wt% DAB Solution, Period 40s (Age 1hr)

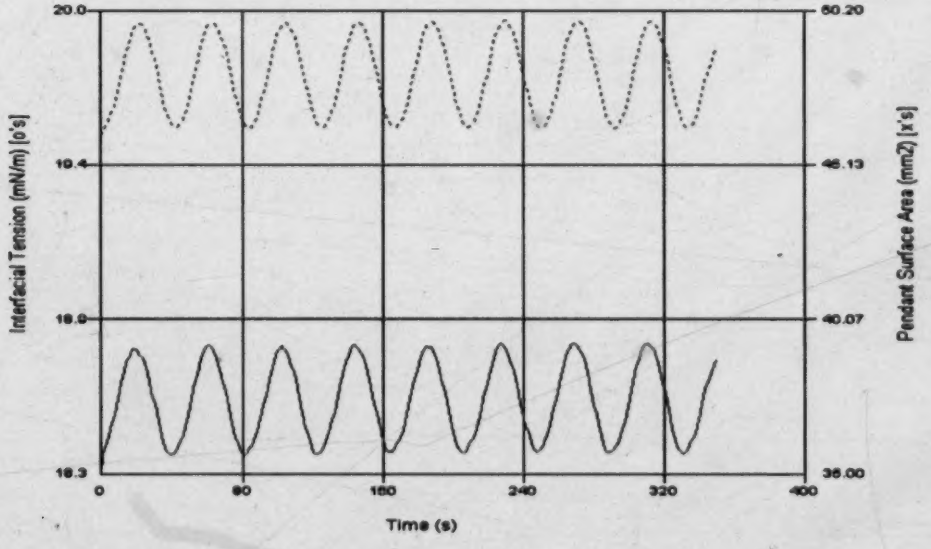

Figure 8-11 IFT (solid line) Response to Area Change (dash line), 10wt% DAB Solution, Period 40s (Age 1Day)

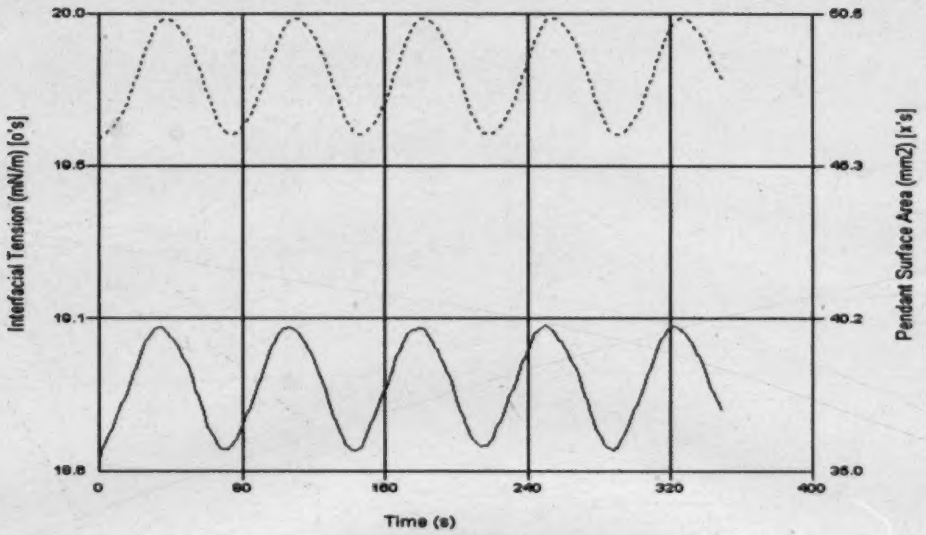

Figure 8-12 IFT (solid line) Response to Area Change (dash line), 10wt% DAB Solution, Period 80s (Age 1hr)

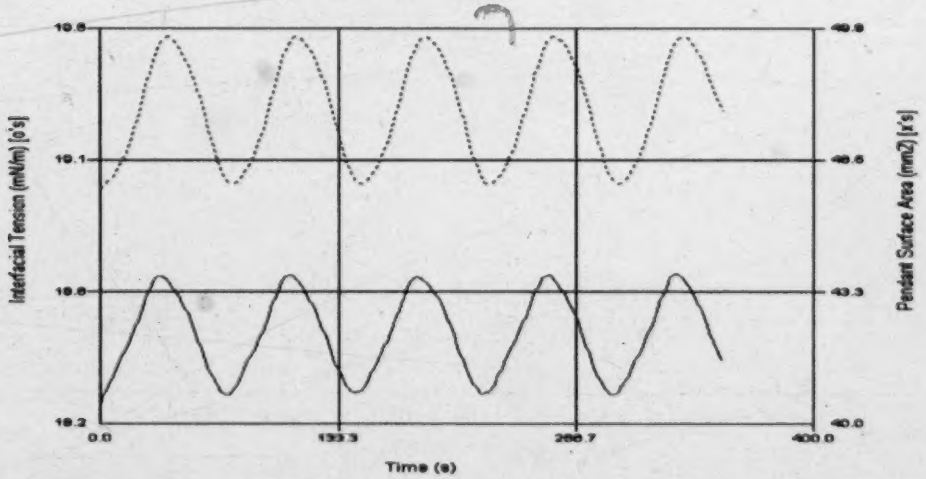

Figure 8-13 IFT (solid line) Response to Area Change (dash line), 10wt% DAB Solution, Period 80s (Age 1Day)

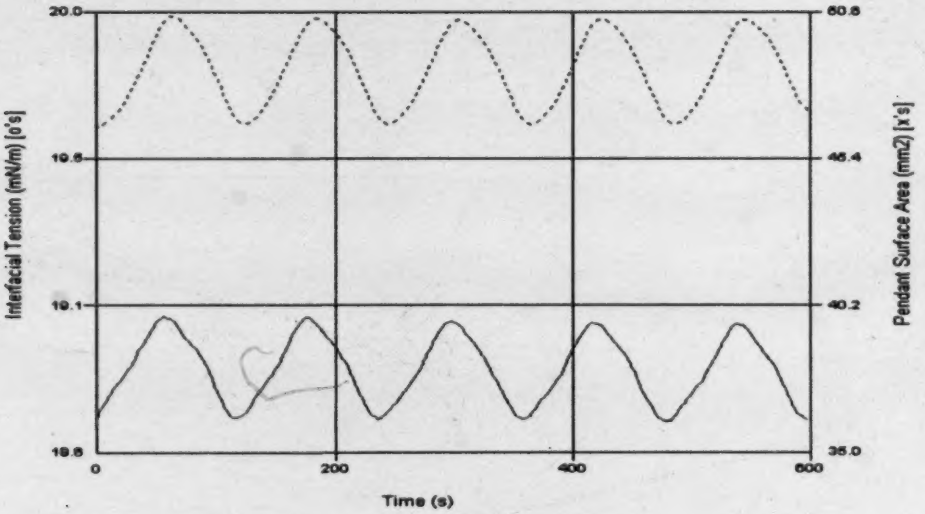

Figure 8-14 IFT (solid line) Response to Area Change (dash line), 10wt% DAB Solution, Period 160s (Age 1hr)

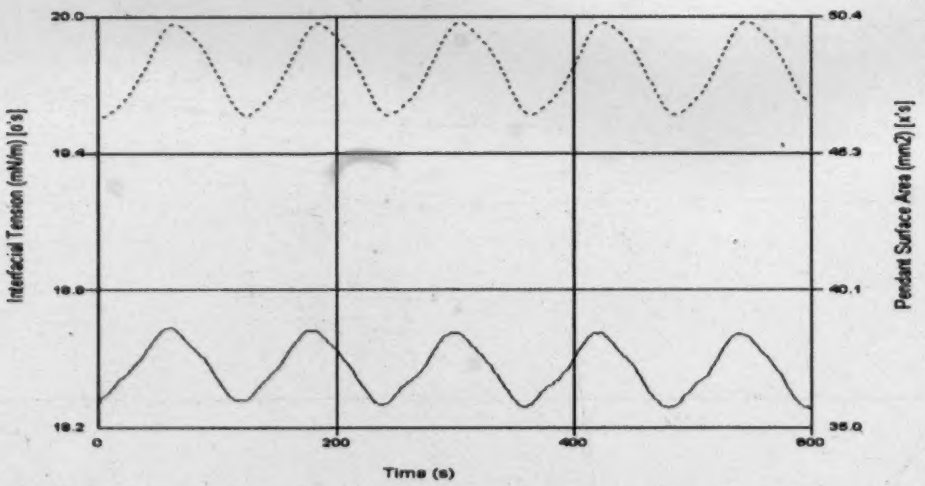

Figure 8-15 IFT (solid line) Response to Area Change (dash line), 10wt% DAB Solution, Period 160s (Age 1Day)

8.1.3 Graphs of IFT Response to Sinusoidal Area Input for 30wt% DAB Solution

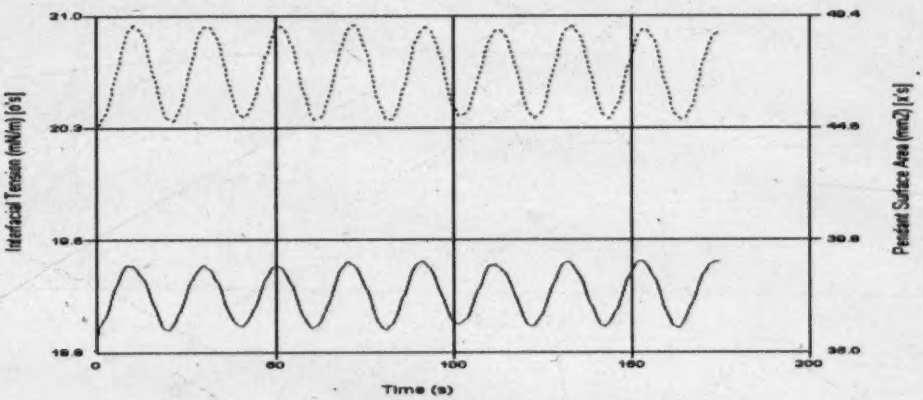

Figure 8-16 IFT (solid line) Response to Area Change (dash line), 30wt% DAB Solution, Period 20s (Age 1hr)

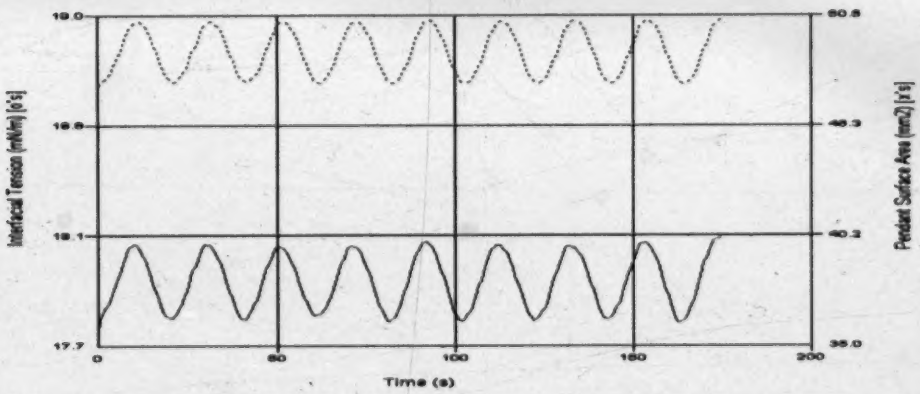

Figure 8-17 IFT (solid line) Response to Area Change (dash line), 30wt% DAB Solution, Period 20s (Age 1Day)

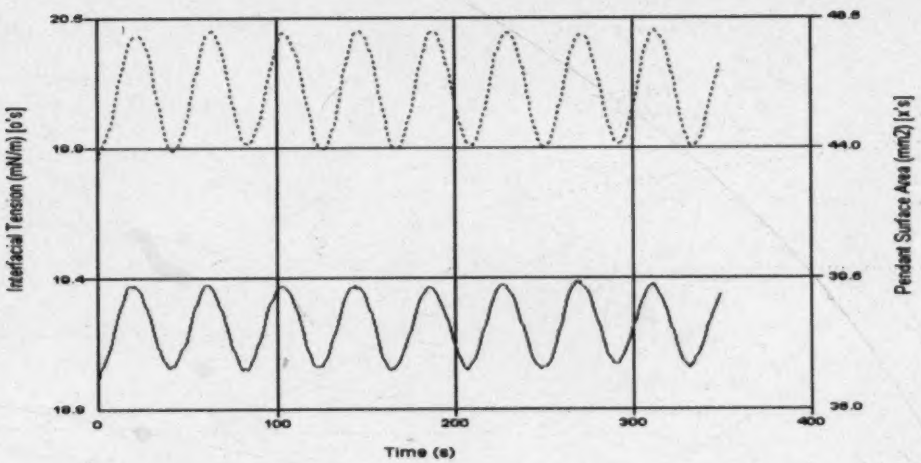

Figure 8-18 IFT (solid line) Response to Area Change (dash line), 30wt% DAB Solution, Period 40s (Age 1hr)

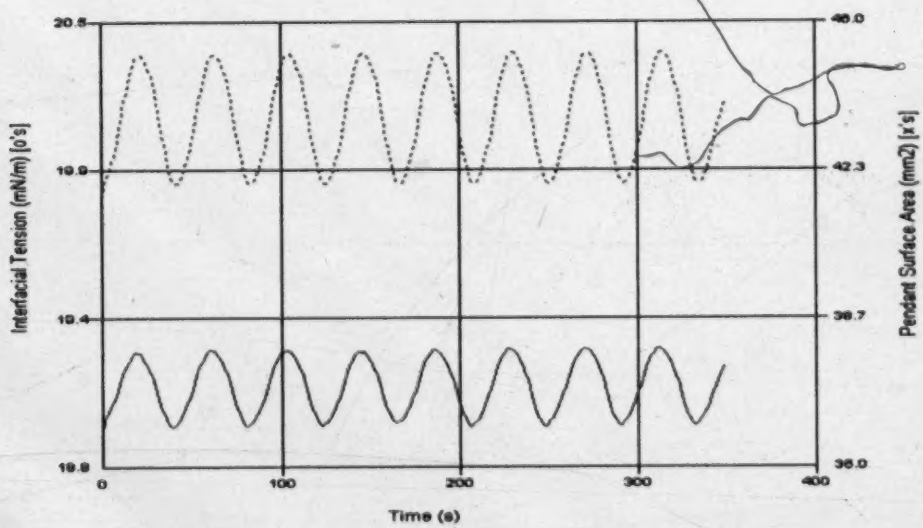

Figure 8-19 IFT (solid line) Response to Area Change (dash line), 30wt% DAB Solution, Period 40s (Age 1Day)

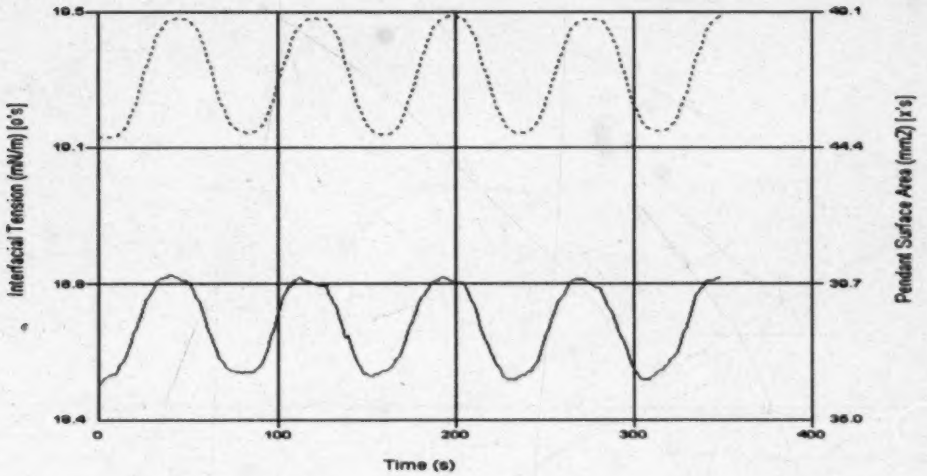

Figure 8-20 IFT (solid line) Response to Area Change (dash line), 30wt% DAB Solution, Period 80s (Age 1hr)

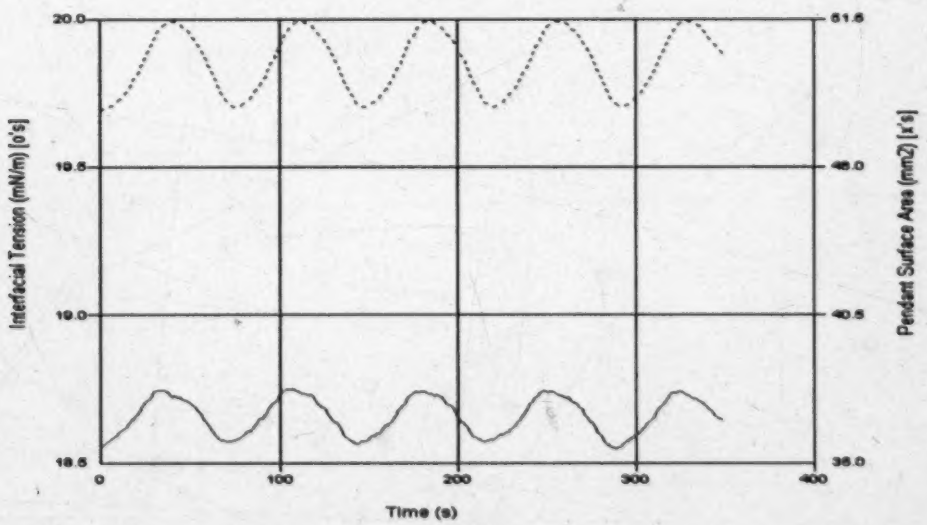

Figure 8-21 IFT (solid line) Response to Area Change (dash line), 30wt% DAB Solution, Period 80s (Age 1Day)

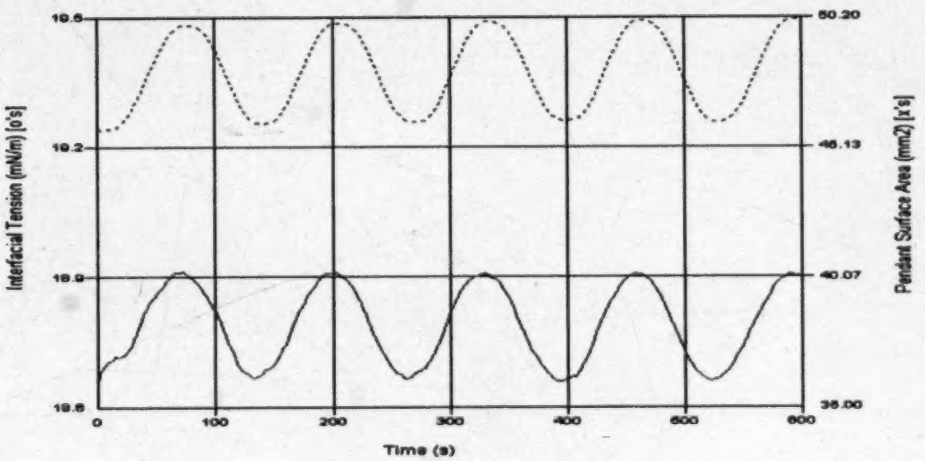

Figure 8-22 IFT (solid line) Response to Area Change (dash line), 30wt% DAB Solution, Period 160s (Age 1hr)

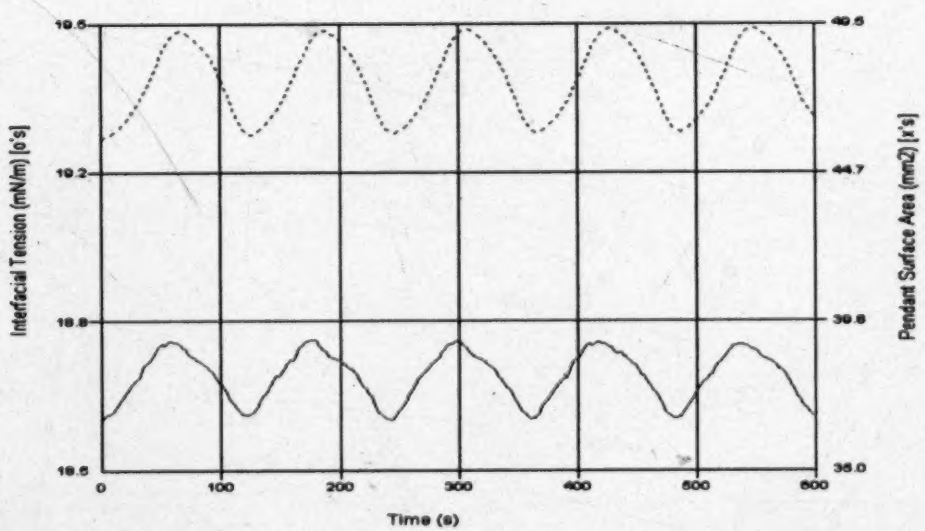

Figure 8-23 IFT (solid line) Response to Area Change (dash line), 30wt% DAB Solution, Period 160s (Age 1Day)

9. APPENDIX C

9.1 Asphaltenes

9.1.1 Graphs of IFT Response to Sinusoidal Area Input for 1wt% Asphaltenes Solution

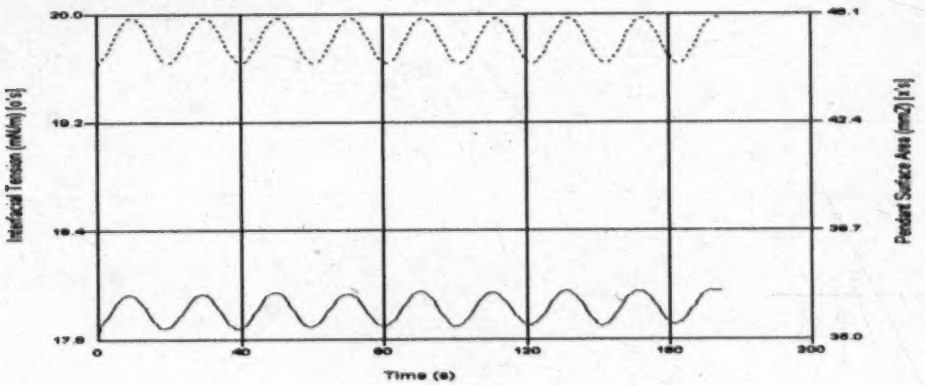

Figure 9-1 IFT (solid line) Response to Area Change (dash line), 1wt% Asphaltene Solution, Period 20s (Age 1hr)

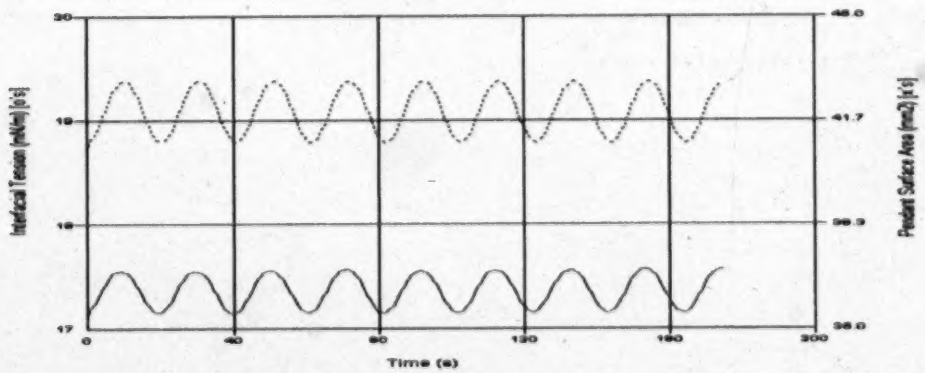

Figure 9-2 IFT (solid line) Response to Area Change (dash line), 1wt% Asphaltene Solution, Period 20s (Age 1Day)

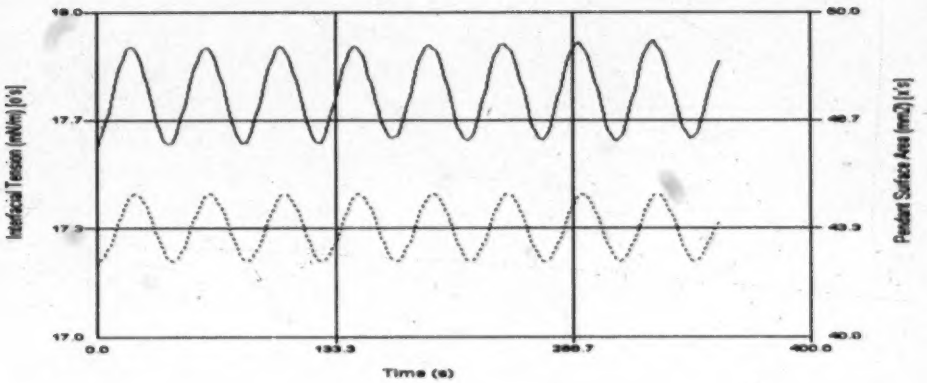

Figure 9-3 IFT (solid line) Response to Area Change (dash line), 1wt% Asphaltene Solution, Period 40s (Age 1hr)

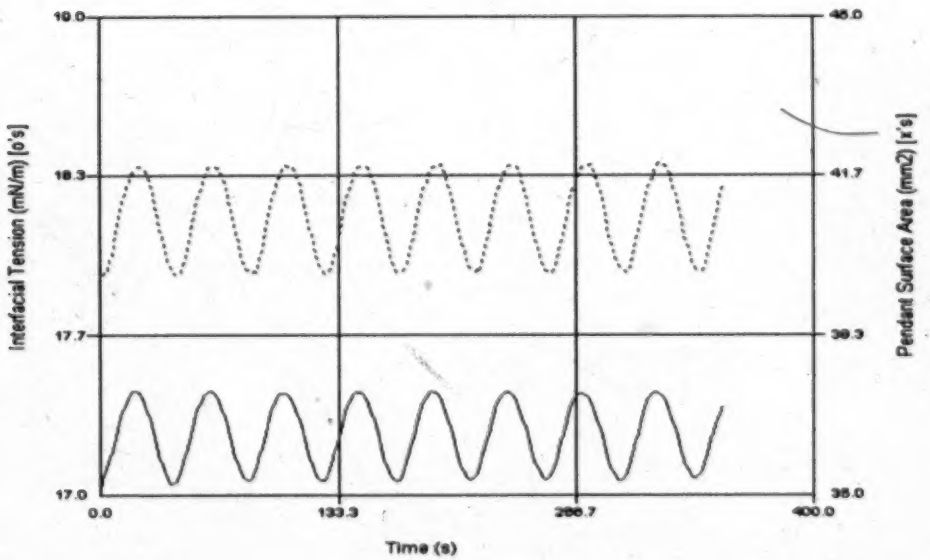

Figure 9-4 IFT (solid line) Response to Area Change (dash line), 1wt% Asphaltene Solution, Period 40s (Age 1Day)

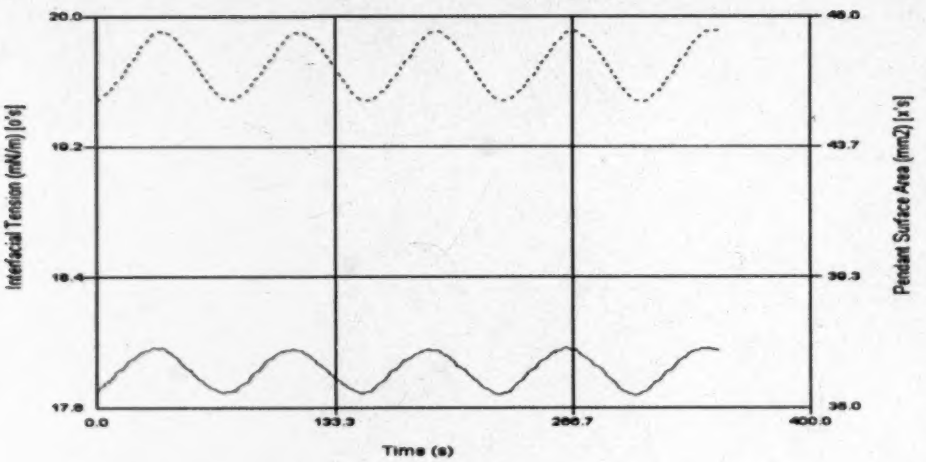

Figure 9-5 IFT (solid line) Response to Area Change (dash line), 1wt% Asphaltene Solution, Period 80s (Age 1hr)

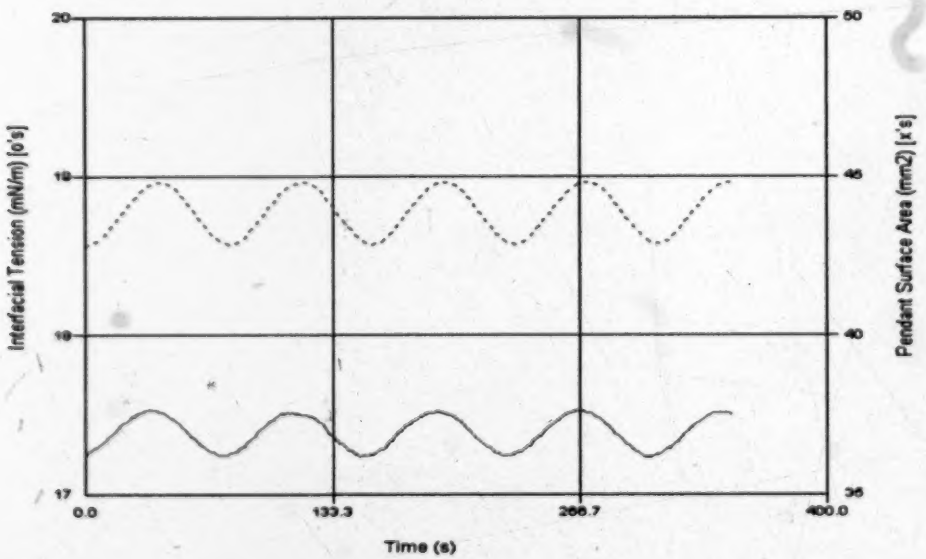

Figure 9-6 IFT (solid line) Response to Area Change (dash line), 1wt% Asphaltene Solution, Period 80s (Age 1Day)

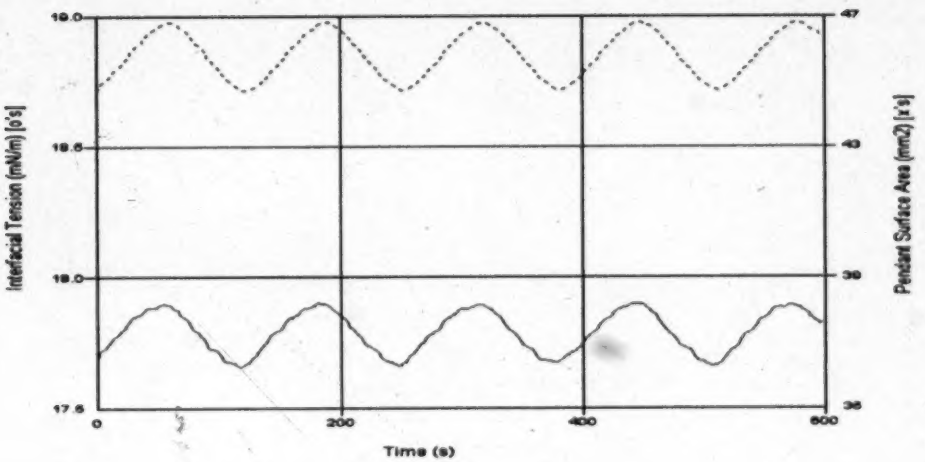

Figure 9-7 IFT (solid line) Response to Area Change (dash line), 1wt% Asphaltene Solution, Period 160s (Age 1hr)

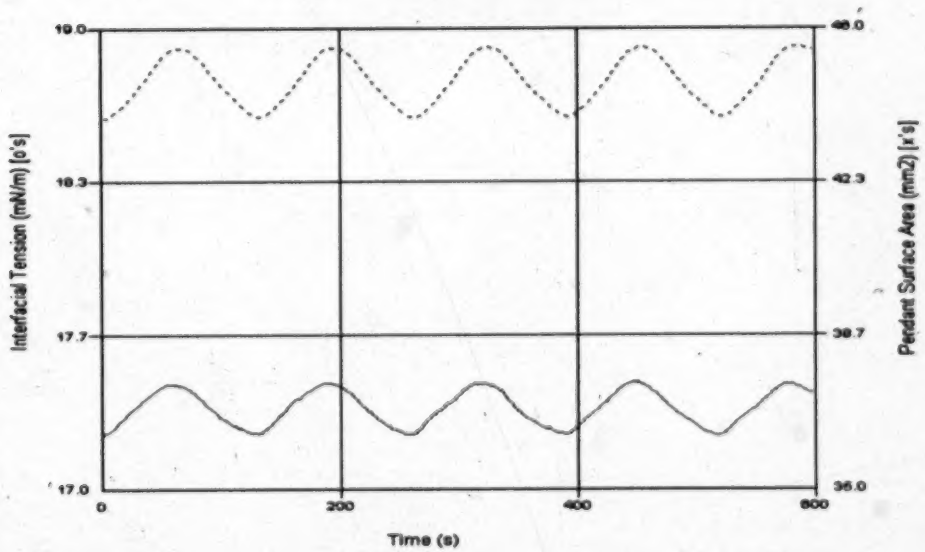

Figure 9-8 IFT (solid line) Response to Area Change (dash line), 1wt% Asphaltene Solution, Period 160s (Age 1Day)

9.1.2 Graphs of IFT Response to Sinusoidal Area Input for 10wt% Asphaltenes Solution

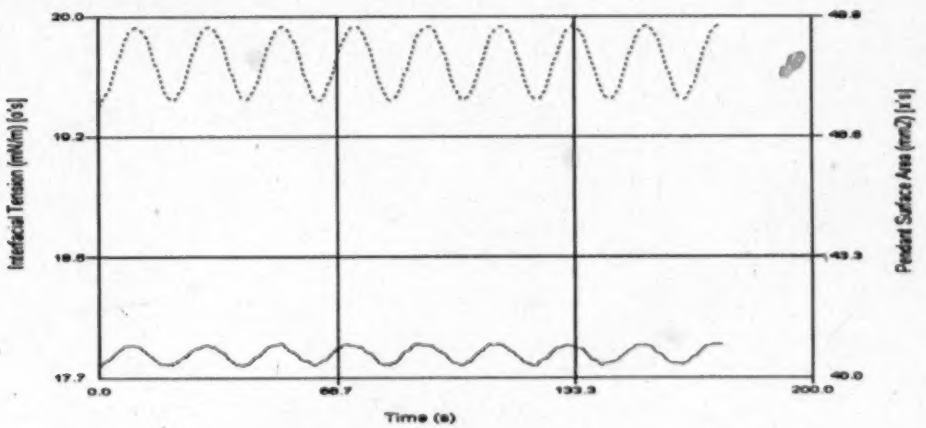

Figure 9-9 IFT (solid line) Response to Area Change (dash line), 10wt% Asphaltene Solution, Period 20s (Age 1hr)

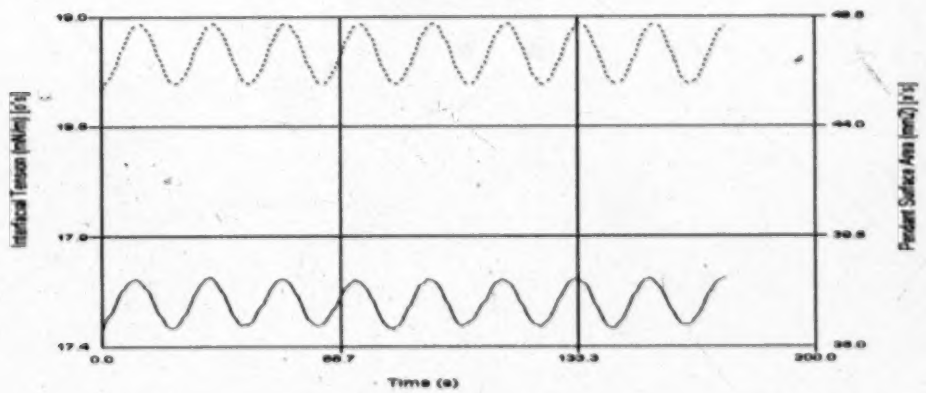

Figure 9-10 IFT (solid line) Response to Area Change (dash line), 10wt% Asphaltene Solution, Period 20s (Age 1Day)

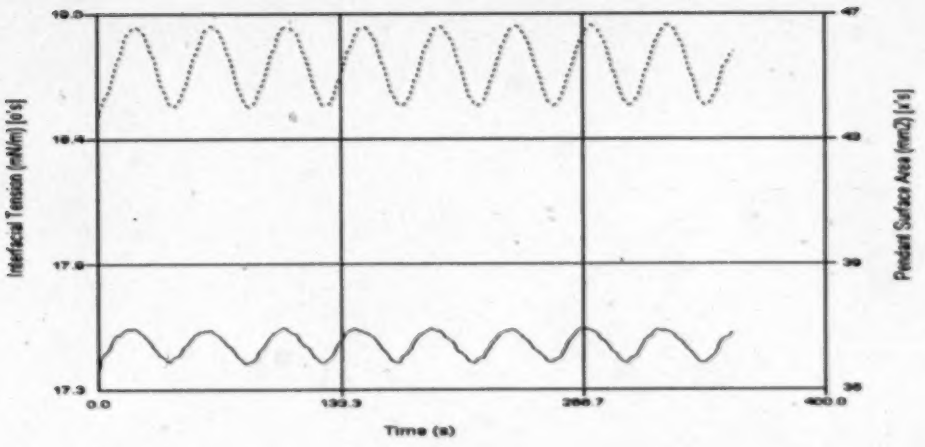

Figure 9-11 IFT (solid line) Response to Area Change (dash line), 10wt% Asphaltene Solution, Period 40s (Age 1hr)

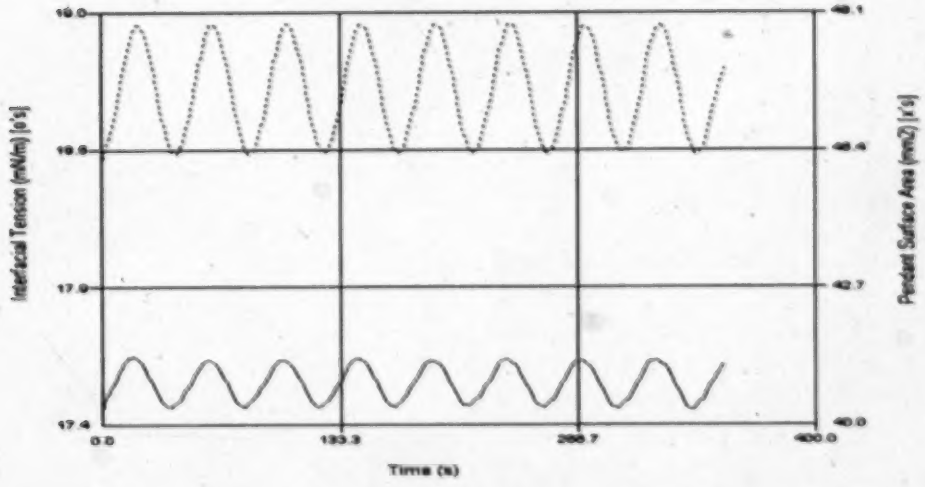

Figure 9-12 IFT (solid line) Response to Area Change (dash line), 10wt% Asphaltene Solution, Period 40s (Age 1Day)

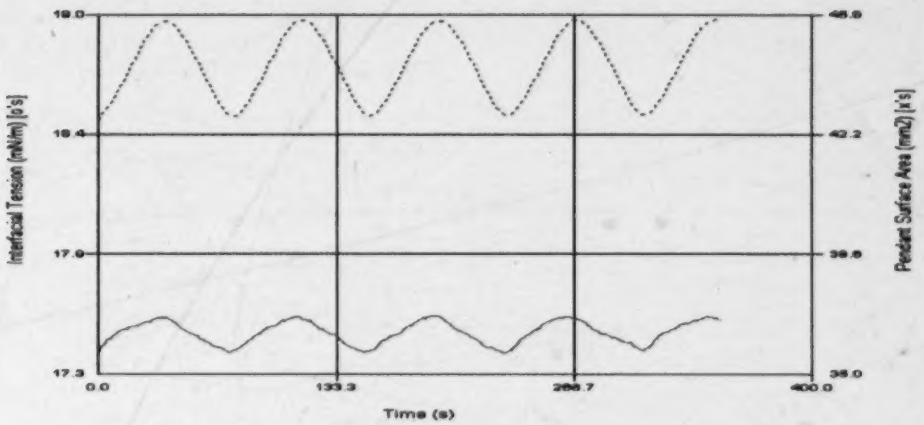

Figure 9-13 IFT (solid line) Response to Area Change (dash line), 10wt% Asphaltene Solution, Period 80s (Age 1hr)

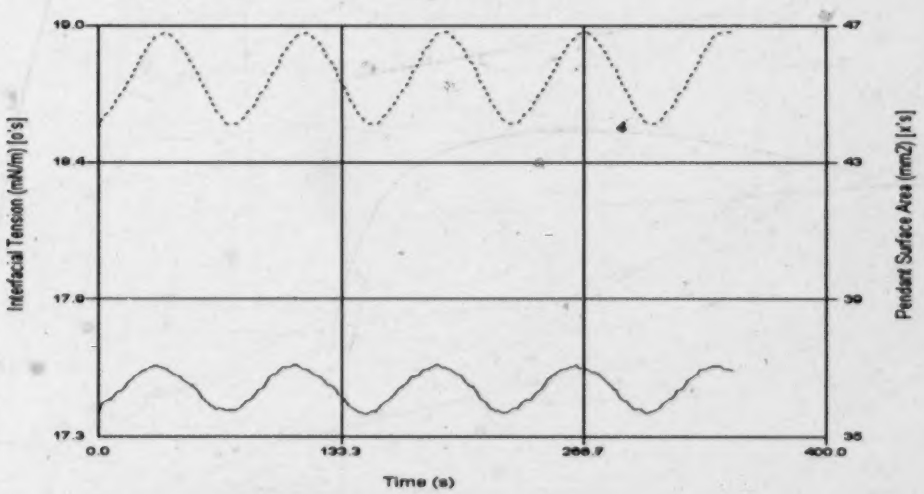

Figure 9-14 IFT (solid line) Response to Area Change (dash line), 10wt% Asphaltene Solution, Period 80s (Age 1Day)

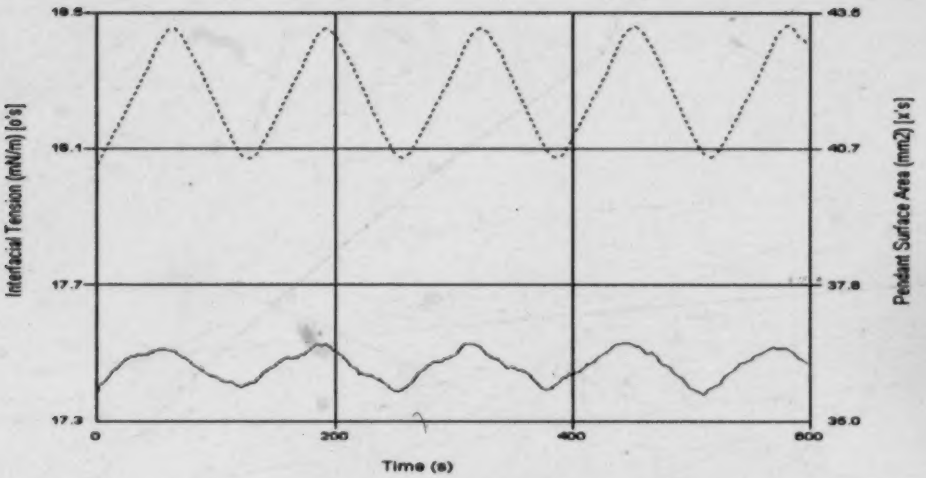

Figure 9-15 IFT (solid line) Response to Area Change (dash line), 10wt% Asphaltene Solution, Period 160s (Age 1hr)

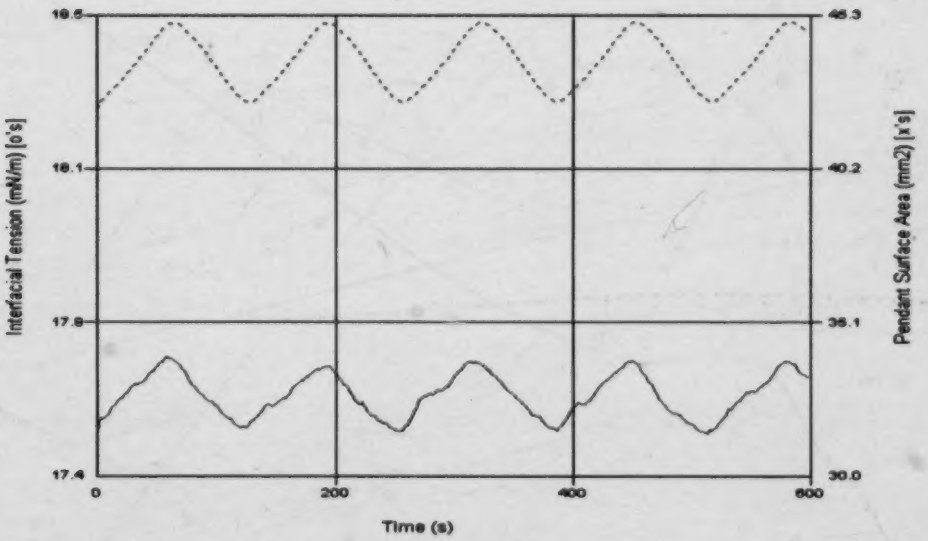

Figure 9-16 IFT (solid line) Response to Area Change (dash line), 10wt% Asphaltene Solution, Period 160s (Age 1Day)

9.1.3 Graphs of IFT Response to Sinusoidal Area Input for 20wt% Asphaltenes Solution

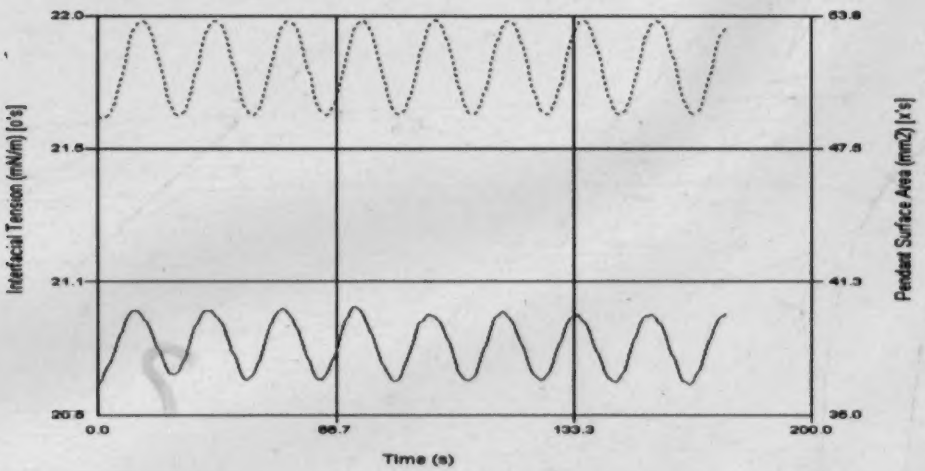

Figure 9-17 IFT (solid line) Response to Area Change (dash line), 20wt% Asphaltene Solution, Period 20s (Age 1hr)

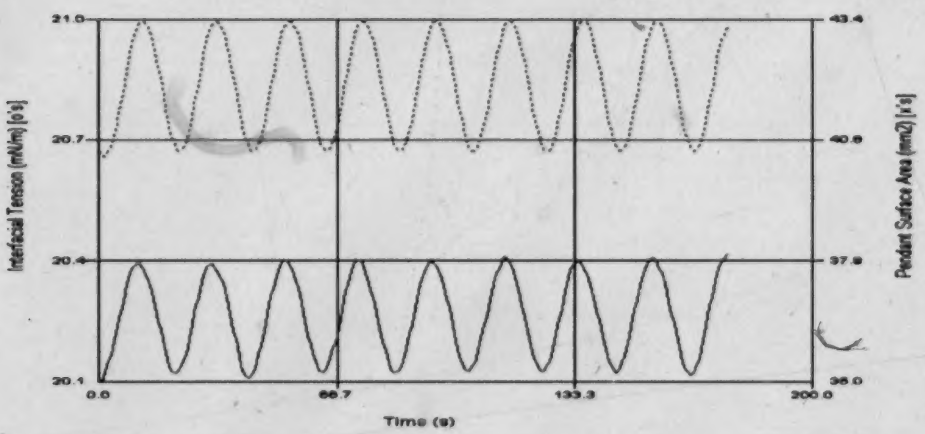

Figure 9-18 IFT (solid line) Response to Area Change (dash line), 20wt% Asphaltene Solution, Period 20s (Age 1Day)

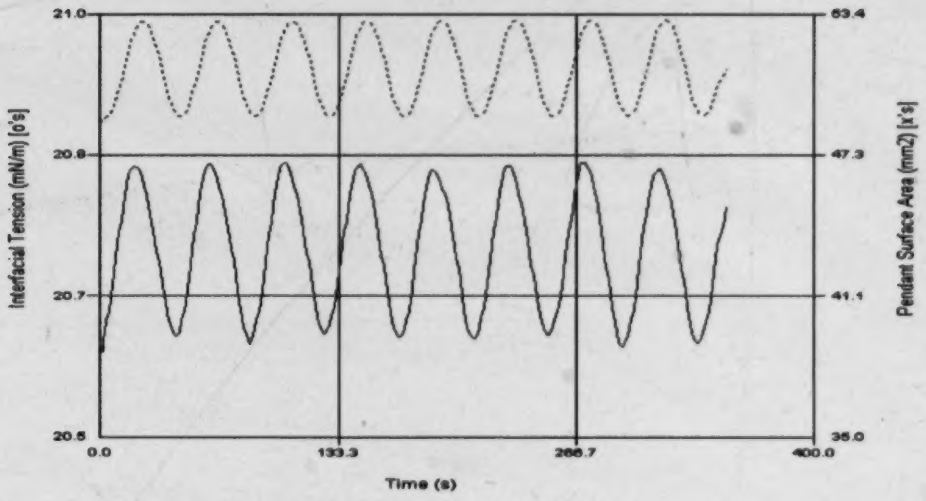

Figure 9-19 IFT (solid line) Response to Area Change (dash line), 20wt% Asphaltene Solution, Period 40s (Age 1hr)

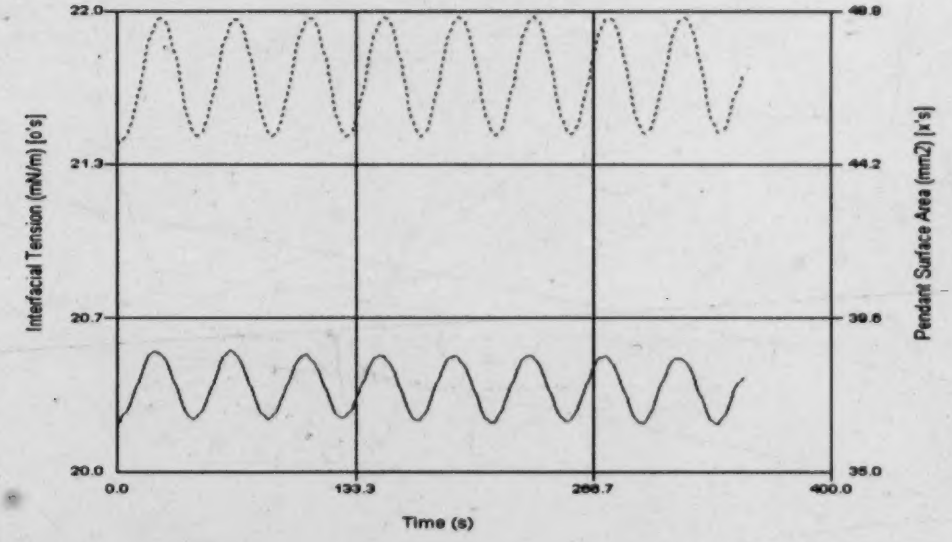

Figure 9-20 IFT (solid line) Response to Area Change (dash line), 20wt% Asphaltene Solution, Period 40s (Age 1Day)

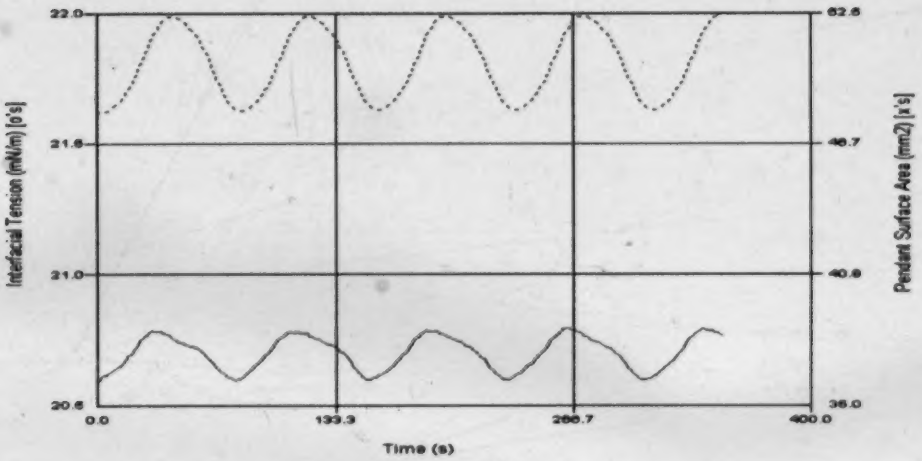

Figure 9-21 IFT (solid line) Response to Area Change (dash line), 20wt% Asphaltene Solution, Period 80s (Age 1hr)

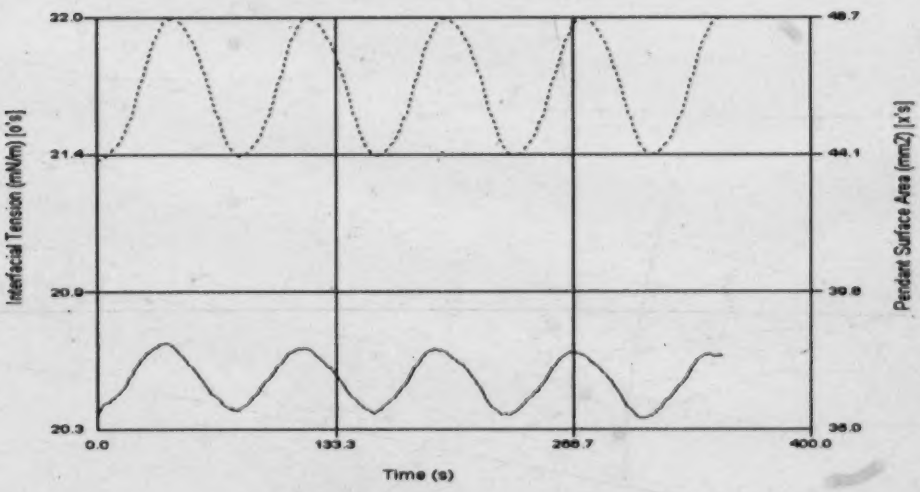

Figure 9-22 IFT (solid line) Response to Area Change (dash line), 20wt% Asphaltene Solution, Period 80s (Age 1Day)

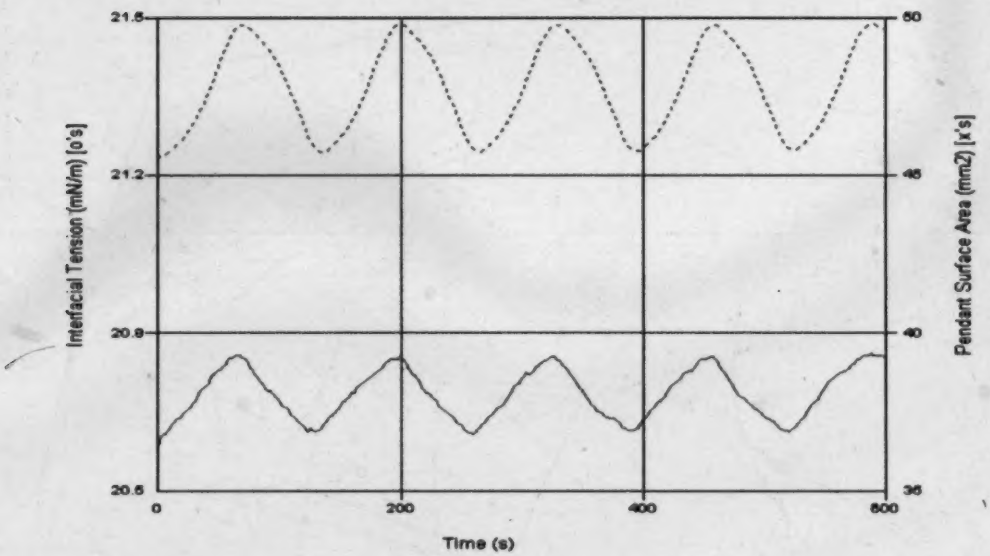

Figure 9-23 IFT (solid line) Response to Area Change (dash line), 20wt% Asphaltene Solution, Period 160s (Age 1hr)

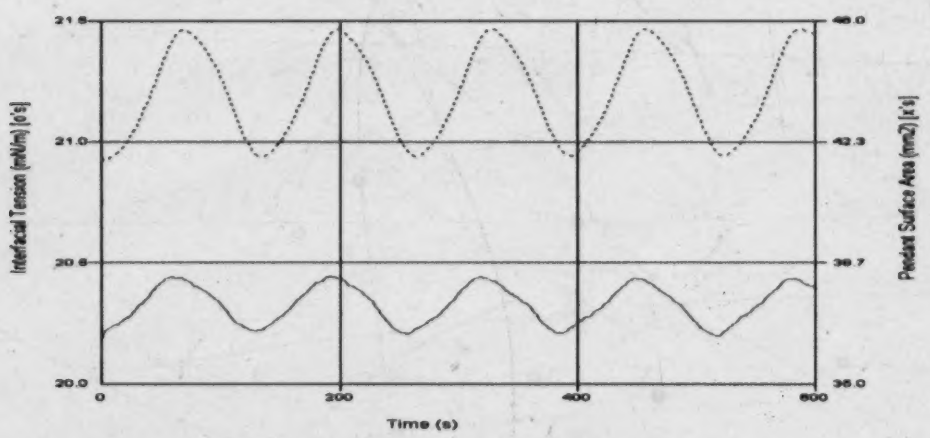

Figure 9-24 IFT (solid line) Response to Area Change (dash line), 20wt% Asphaltene Solution, Period 160s (Age 1Day)

10. APPENDIX D

10.1 Bitumen

10.1.1 Graphs of IFT Response to Sinusoidal Area Input for 5wt% Bitumen Solution

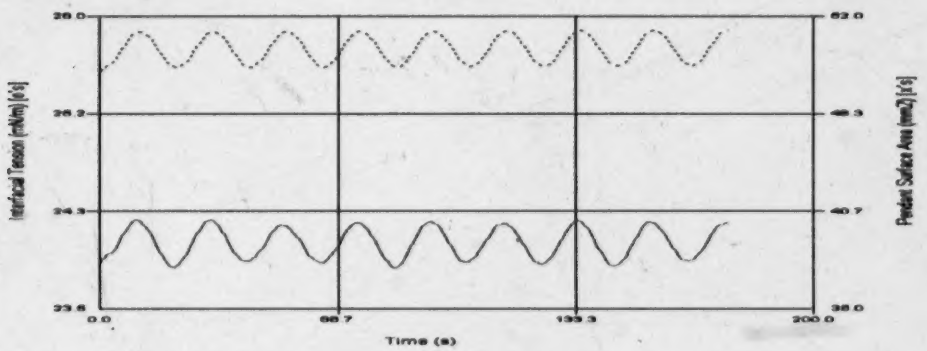

Figure 10-1 IFT (solid line) Response to Area Change (dash line), 5wt% Bitumen Solution, Period 20s (Age 1hr)

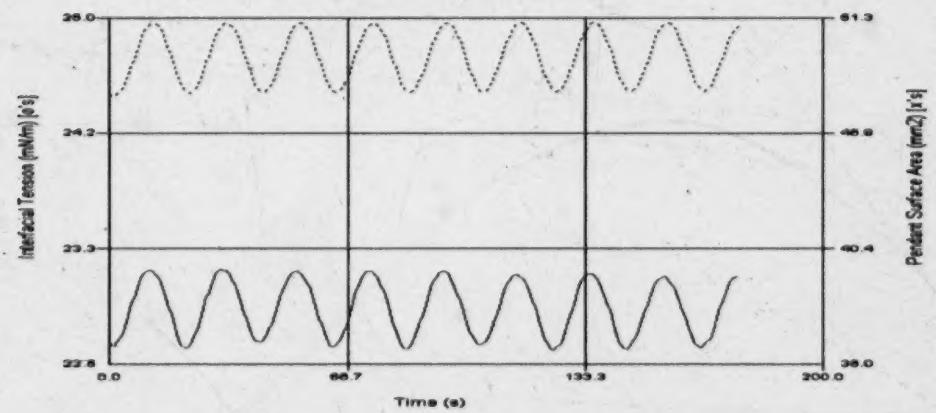

Figure 10-2 IFT (solid line) Response to Area Change (dash line), 5wt% Bitumen Solution, Period 20s (Age 1Day)

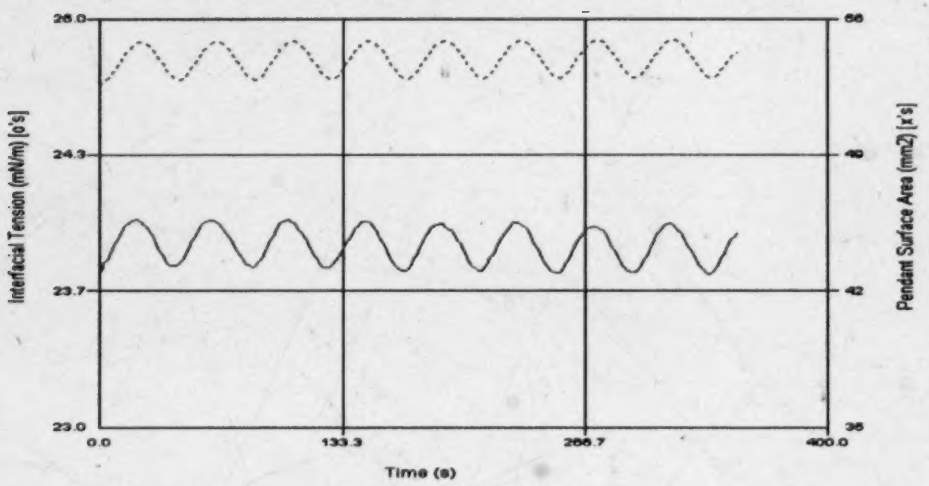

Figure 10-3 IFT (solid line) Response to Area Change (dash line), 5wt% Bitumen Solution, Period 40s (Age 1hr)

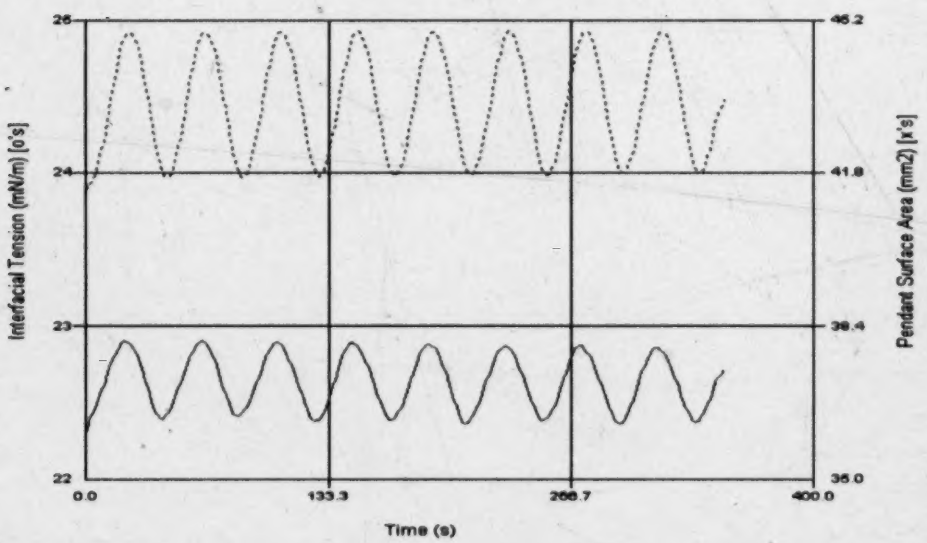

Figure 10-4 IFT (solid line) Response to Area Change (dash line), 5wt% Bitumen Solution, Period 40s (Age 1Day)

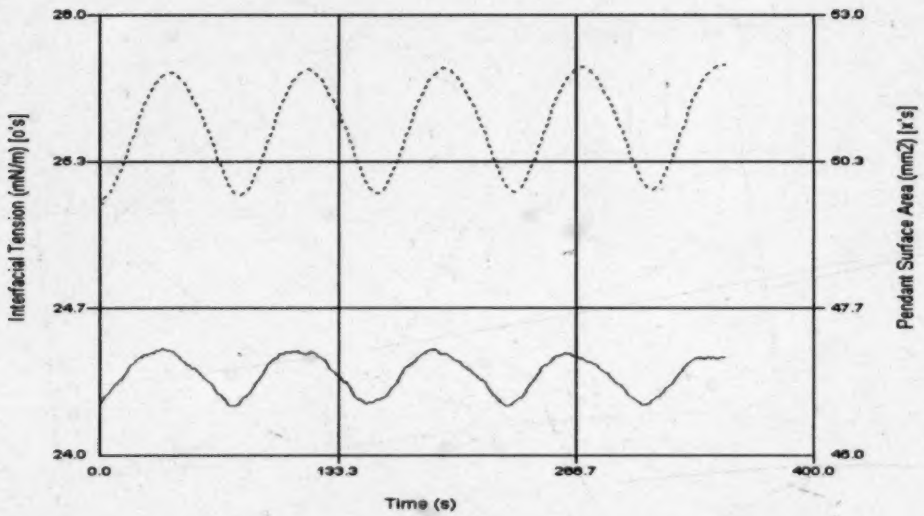

Figure 10-5 IFT (solid line) Response to Area Change (dash line), 5wt% Bitumen Solution, Period 80s (Age 1hr)

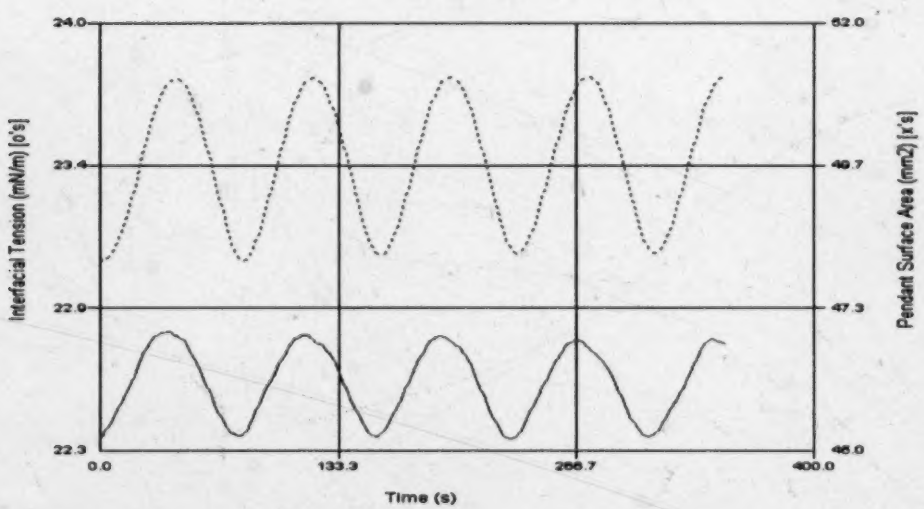

Figure 10-6 IFT (solid line) Response to Area Change (dash line), 5wt% Bitumen Solution, Period 80s (Age 1Day)

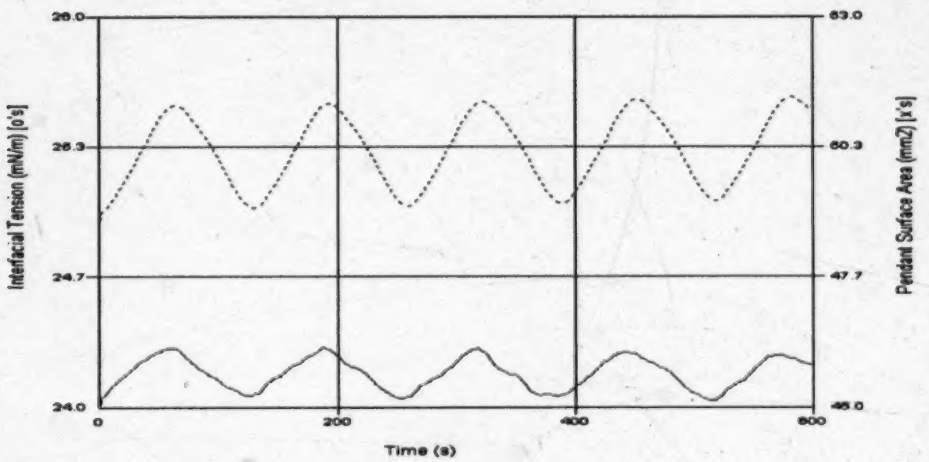

Figure 10-7 IFT (solid line) Response to Area Change (dash line), 5wt% Bitumen Solution, Period 160s (Age 1hr)

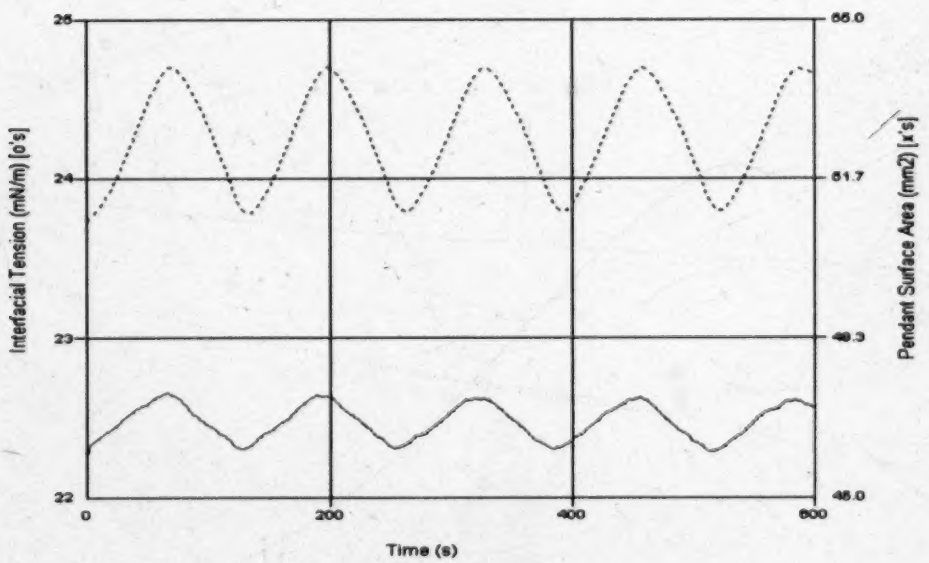

Figure 10-8 IFT (solid line) Response to Area Change (dash line), 5wt% Bitumen Solution, Period 160s (Age 1Day)

10.1.2 Graphs of IFT Response to Sinusoidal Area Input for 15wt% Bitumen Solution

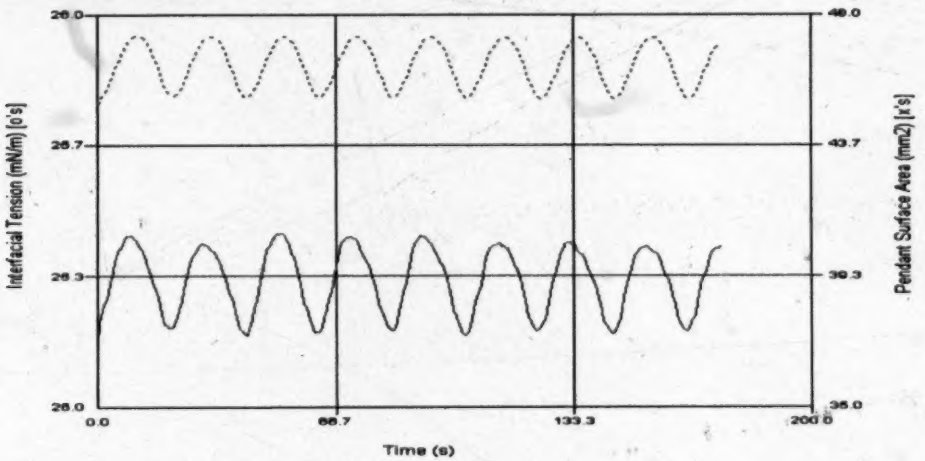

Figure 10-9 IFT (solid line) Response to Area Change (dash line), 15wt% Bitumen Solution, Period 20s (Age 1hr)

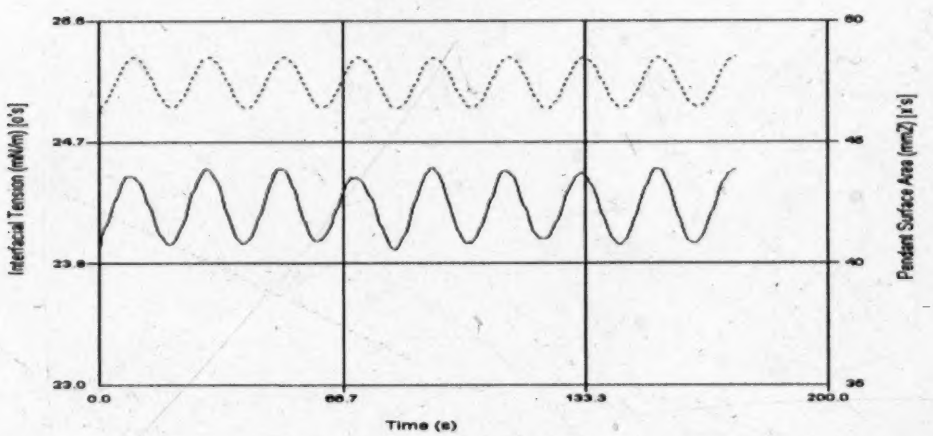

Figure 10-10 IFT (solid line) Response to Area Change (dash line), 15wt% Bitumen Solution, Period 20s (Age 1Day)

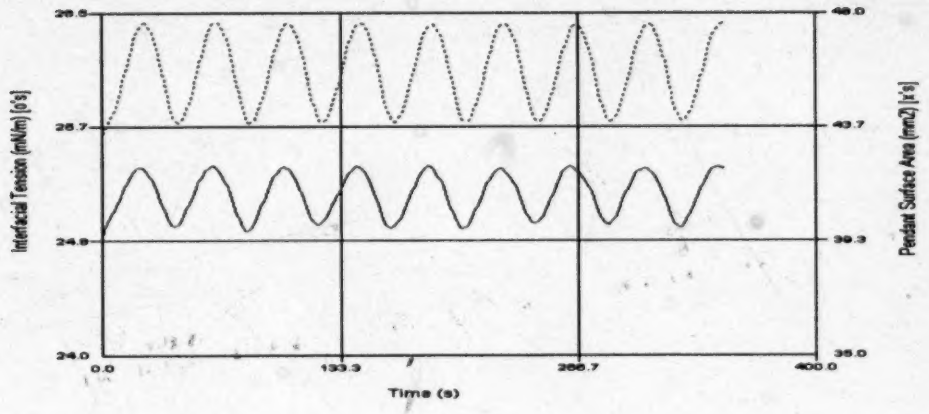

Figure 10-11 IFT (solid line) Response to Area Change (dash line), 15wt% Bitumen Solution, Period 40s (Age 1hr)

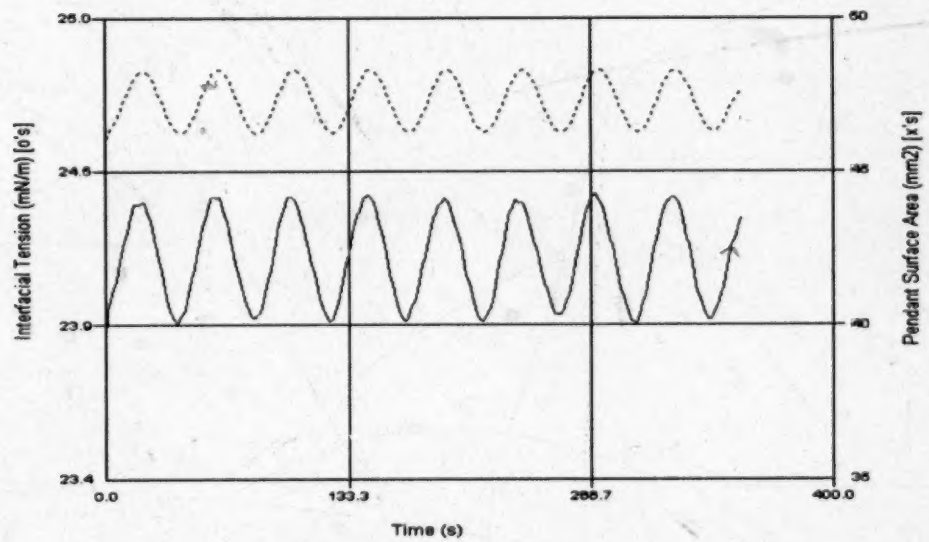

Figure 10-12 IFT (solid line) Response to Area Change (dash line), 15wt% Bitumen Solution, Period 40s (Age 1Day)

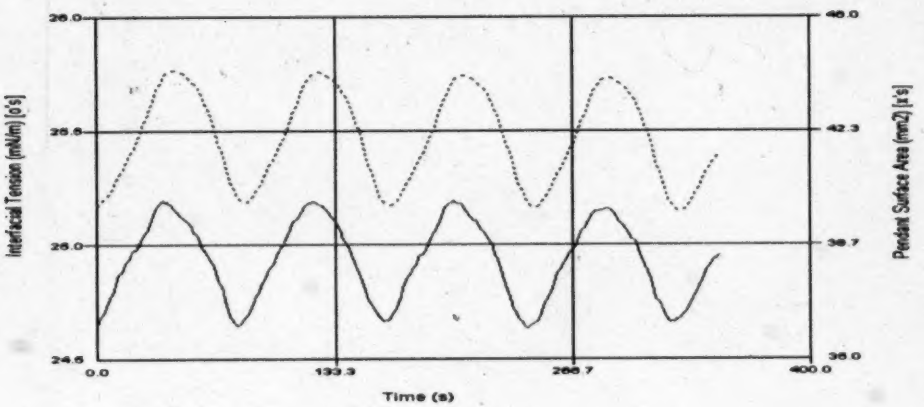

Figure 10-13 IFT (solid line) Response to Area Change (dash line), 15wt% Bitumen Solution, Period 80s (Age 1hr)

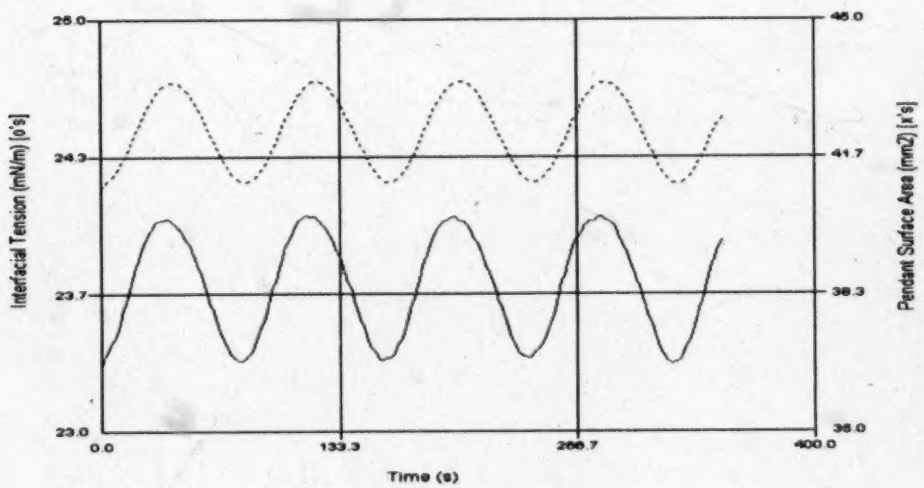

Figure 10-14 IFT (solid line) Response to Area Change (dash line), 15wt% Bitumen Solution, Period 80s (Age 1Day)

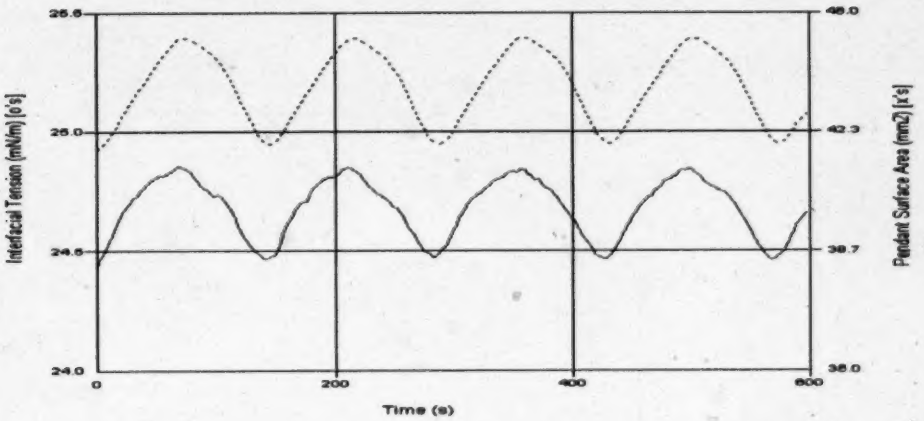

Figure 10-15 IFT (solid line) Response to Area Change (dash line), 15wt% Bitumen Solution, Period 160s (Age 1hr)

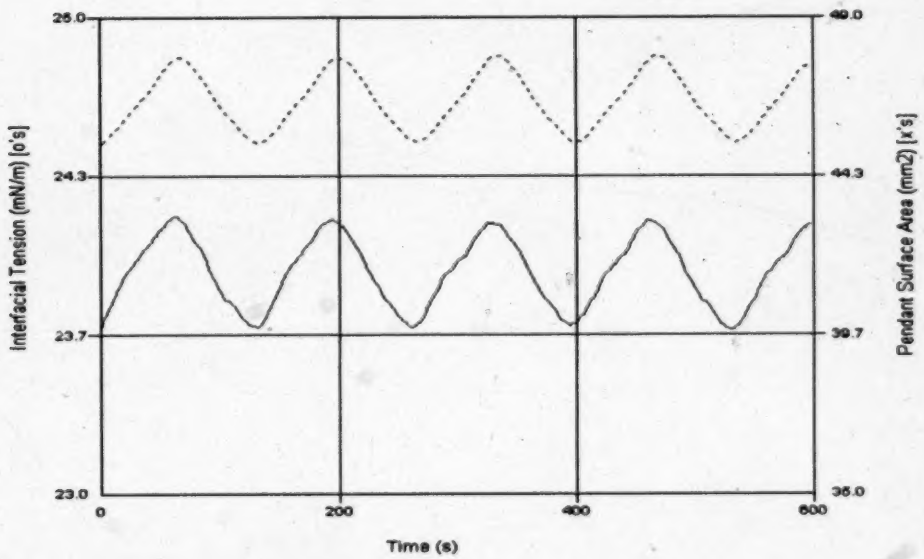

Figure 10-16 IFT (solid line) Response to Area Change (dash line), 15wt% Bitumen Solution, Period 160s (Age 1Day)

10.1.3 Graphs of IFT Response to Sinusoidal Area Input for 30wt% Bitumen Solution

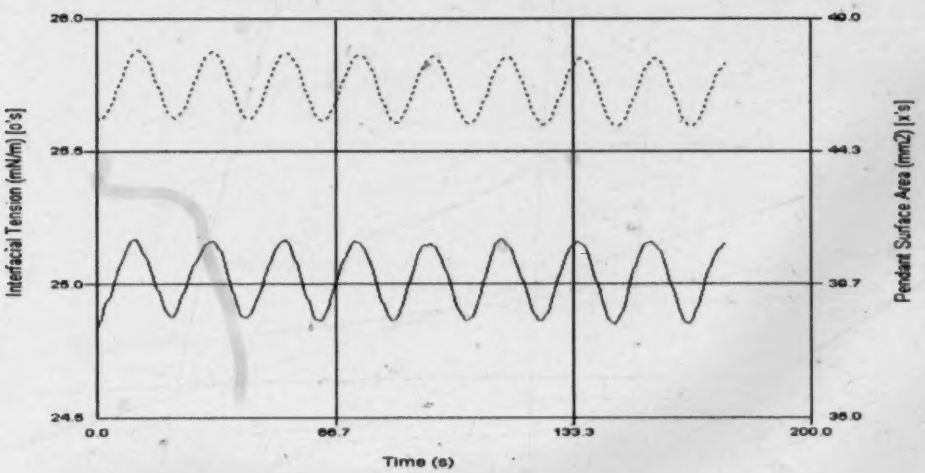

Figure 10-17 IFT (solid line) Response to Area Change (dash line), 30wt% Bitumen Solution, Period 20s (Age 1hr)

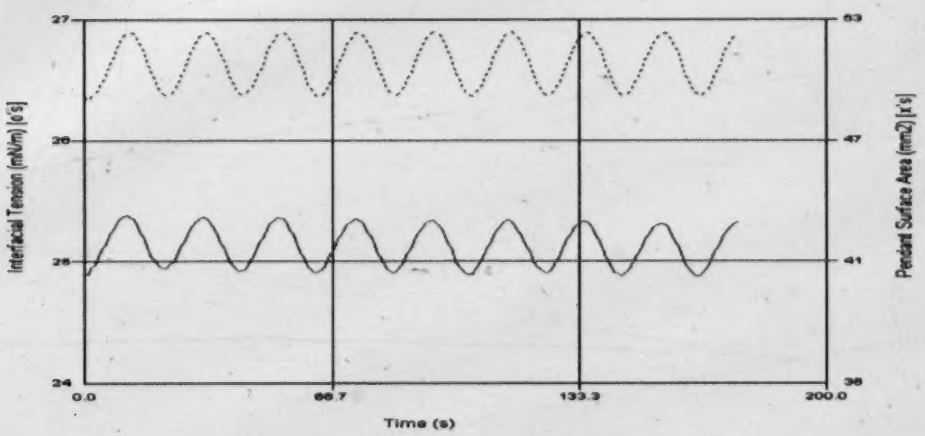

Figure 10-18 IFT (solid line) Response to Area Change (dash line), 30wt% Bitumen Solution, Period 20s (Age 1Day)

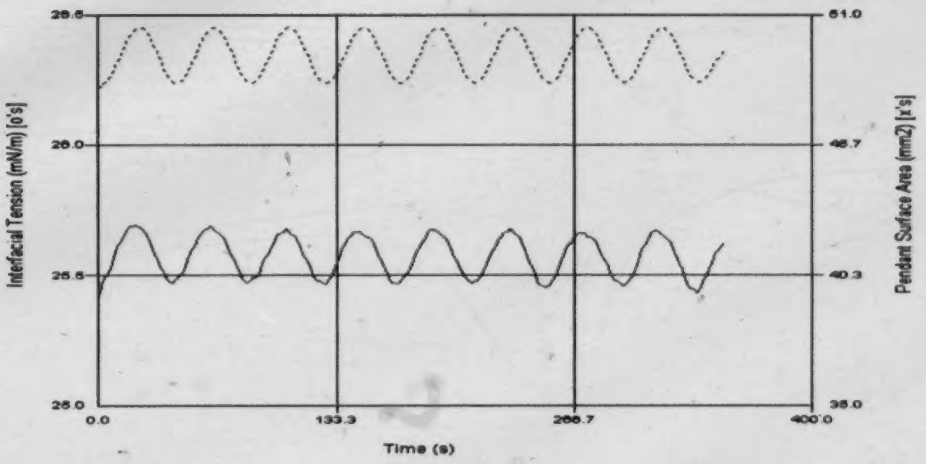

Figure 10-19 IFT (solid line) Response to Area Change (dash line), 30wt% Bitumen Solution, Period 40s (Age 1hr)

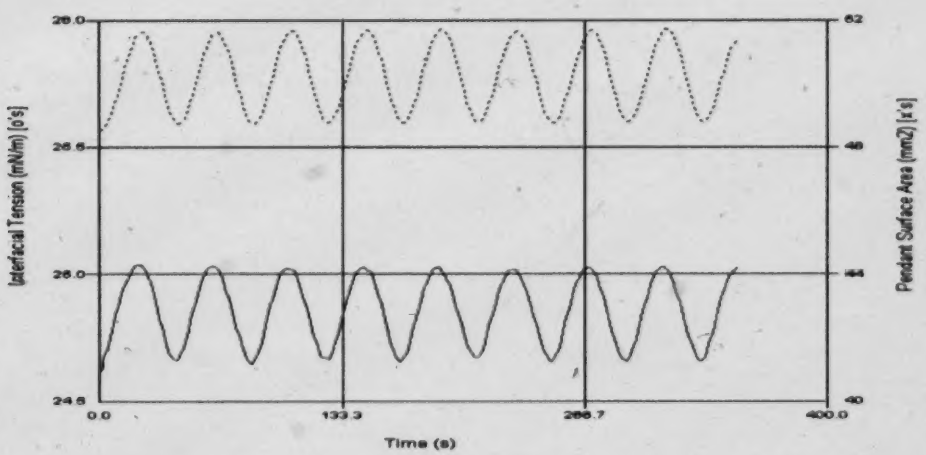

Figure 10-20 IFT (solid line) Response to Area Change (dash line), 30wt% Bitumen Solution, Period 40s (Age 1Day)

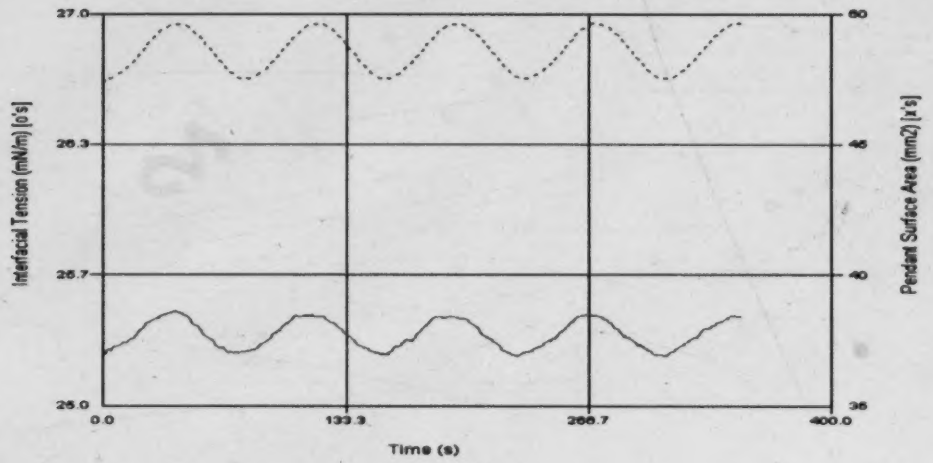

Figure 10-21 IFT (solid line) Response to Area Change (dash line), 30wt% Bitumen Solution, Period 80s (Age 1hr)

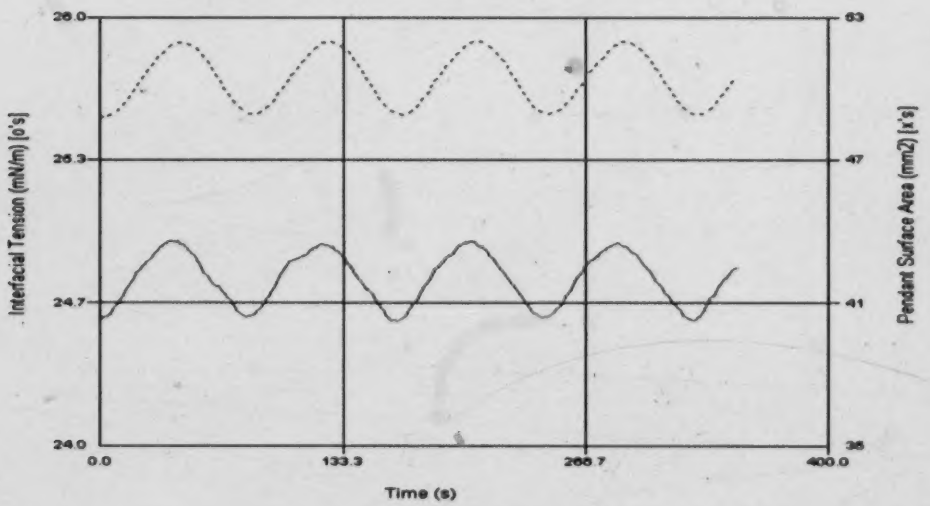

Figure 10-22 IFT (solid line) Response to Area Change (dash line), 30wt% Bitumen Solution, Period 80s (Age 1Day)

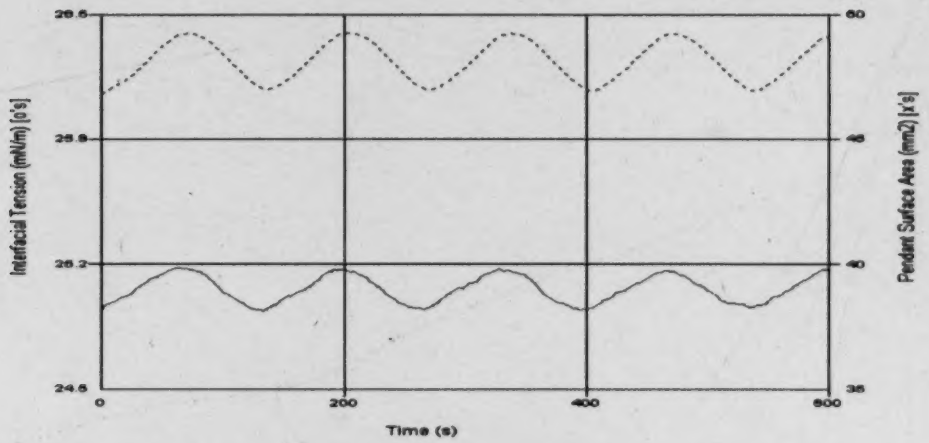

Figure 10-23 IFT (solid line) Response to Area Change (dash line), 30wt% Bitumen Solution, Period 160s (Age 1hr)

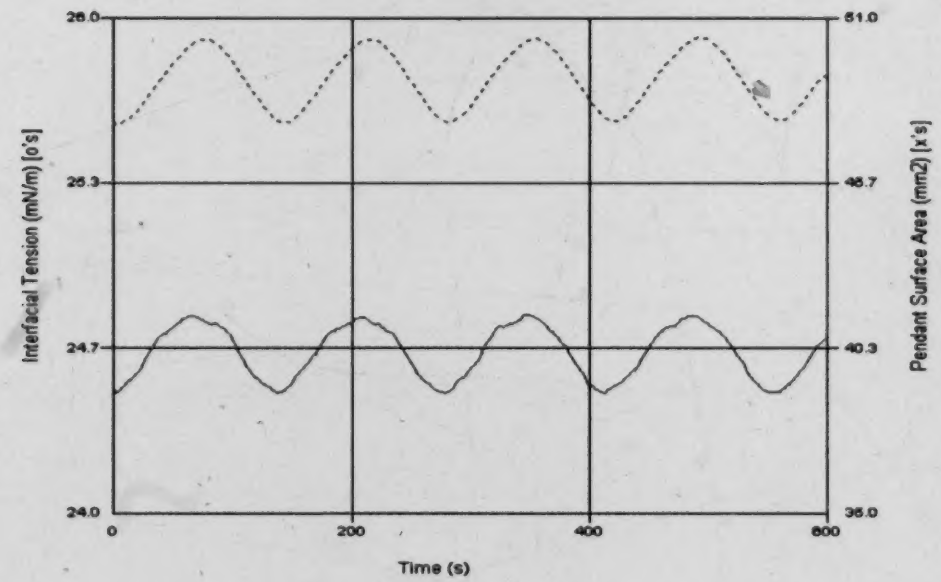

Figure 10-24 IFT (solid line) Response to Area Change (dash line), 30wt% Bitumen Solution, Period 160s (Age 1Day)